Structural evaluation of retinal ganglion cell damage: Fourier-domain optical coherence tomography and scanning laser polarimetry in glaucoma and acute optic neuritis

PhD Thesis

Anita Garas, MD

School of PhD Studies, Semmelweis University
Programme of Clinical Sciences
Ophthalmology

Supervisor: Gábor Holló, MD, PhD, DSc

Official reviewers: Zsuzsanna Récsán, MD, PhD
Pál Sziklai, MD, PhD

Chairman of Exam board: György Füst, MD, PhD, DSc
Members of Exam board: Ágnes Kerényi, MD, PhD
Antal Szabó, MD, PhD

Budapest, 2011

TABLE OF CONTENTS

1 ABBREVIATIONS USED IN THE THESIS

2D	=	2-dimensional
3D	=	3-dimensional
ACG	=	angle closure glaucoma
AMD	=	age-related macular degeneration
ARP	=	atypical retardation pattern
AUC	=	area under the receiver operating characteristic curve
BCVA	=	best corrected visual acuity
CCT	=	central corneal thickness
CI	=	confidence interval
CIS	=	clinically isolated syndrome
CNV	=	choroidal neovascularization
CV	=	coefficient of variation
D	=	diopters
FD-OCT	=	Fourier-domain optical coherence tomography
FLV	=	Focal Loss Volume
GCC	=	ganglion cell complex
GDx-ECC	=	scanning laser polarimetry with enhanced corneal compensation
GDx-NFA	=	scanning laser polarimetry - Nerve Fiber Analyzer
GDx-VCC	=	scanning laser polarimetry with variable corneal compensation
GLV	=	Global Loss Volume
i.e.	=	that is
ICC	=	intraclass correlation
ILM	=	internal limiting membrane
IOP	=	intraocular pressure
IPL	=	inner plexiform layer
IQR	=	interquartile range
LASIK	=	laser-assisted in situ keratomileusis
MD	=	mean defect value on the Octopus perimetry test
MS	=	multiple sclerosis
NA	=	not applicable

NFI	=	Nerve Fiber Indicator
NLR	=	negative likelihood ratio
NPV	=	negative predictive value
OAG	=	open-angle glaucoma
OCT	=	optical coherence tomography
OHT	=	ocular hypertension
ON	=	optic neuritis
ONH	=	optic nerve head
PLR	=	positive likelihood ratio
POAG	=	primary open-angle glaucoma
PPV	=	positive predictive value
RMS	=	Root Mean Square
RNFL	=	retinal nerve fiber layer
RNFLT	=	retinal nerve fiber layer thickness
RPE	=	retinal pigment epithelium
RTVue-100 OCT	=	RTVue-100 Fourier-domain optical coherence tomography
SD	=	standard deviation
SD-OCT	=	spectral-domain optical coherence tomography
SLP	=	scanning laser polarimetry
SSI	=	Signal Strength Index
TD-OCT	=	time-domain optical coherence tomography
TSNIT	=	temporal-superior-nasal-inferior-temporal
TSS	=	Typical Scan Score
USA	=	United States of America
VEGF	=	vascular endothelial growth factor
VF	=	visual field
vs.	=	versus

2 INTRODUCTION

Glaucoma is caused by progressive apoptotic loss of the retinal ganglion cells, which results in irreversible damage of the retinal nerve fiber layer (RNFL) and the optic nerve head (ONH).[1,2] It is one of the leading causes of severe visual impairment and blindness.[3-5] Since most forms of glaucoma develop without clinical symptoms, it is not surprising that 50 % of glaucoma sufferers remain undetected, even in the developed countries.[6,7] The prevalence of chronic open-angle glaucoma (OAG) is 1.5 to 3 % in Caucasians over 40 years of age, and increases up to approximately 7 % in advanced age.[3,8-12] According to epidemiological estimations, there will be 79.6 million people with OAG and angle closure glaucoma (ACG) in 2020, and of them 74 % will suffer from OAG. In 2020, 5.9 million people with OAG and 5.3 million people with ACG will suffer from bilateral blindness.[4]

In Caucasians, primary open-angle glaucoma (POAG) is the most common form of glaucoma.[4,7,11] Progression in this disease is relatively slow: several years are necessary to the development of clinically significant visual impairment, which is irreversible and severely decreases the quality of life. The asymptomatic progress and the irreversibility of damage make early diagnosis and careful follow-up crucial for effective treatment and management of glaucoma.[2,13-15]

In addition to the traditional diagnostic methods (e.g. Goldmann applanation tonometry, diurnal intraocular pressure [IOP] curve, ONH and RNFL photography) computerized structural investigation of the retinal nerve fiber thickness (RNFLT) has become an important part of modern glaucoma diagnostics. The new methods allow quantitative analysis of morphological alterations of the RNFL and the ONH, both of which are known to precede the development of clinically detectable visual field (VF) defects, in many cases.

Optical coherence tomography (OCT) [16-18] and scanning laser polarimetry (SLP) [19-21] are such structural diagnostic methods. In the last decade, time-domain optical coherence tomography (TD-OCT) became a standard method for glaucoma diagnostics. The recently developed Fourier-domain or spectral-domain OCT (FD-OCT) technology, however, provides several technical innovations compared to TD-OCT technology. SLP with variable cornea compensation (GDx-VCC) is also a well-established imaging method for detection of glaucoma.[22-27] The recently released enhanced cornea compensation

software (GDx-ECC) was developed to improve image quality in case of atypical retardation pattern (ARP), which is difficult to classify with the GDx-VCC software.[28-32]

The RTVue-100 Fourier-domain OCT (RTVue-100 OCT) is one of the new, commercially available FD-OCT instruments. The role of RTVue-100 OCT in glaucoma diagnostics was not evaluated in detail before I started my PhD period. Since in future both FD-OCT technology and SLP may be used to detect glaucoma, comparative evaluation of their diagnostic usefulness for real-life clinical decision making situations is of practical importance for ophthalmologists.

This thesis comprises six studies carried out between 2008 and 2010 for evaluation of the clinical usefulness of the RTVue-100 OCT and the GDx-VCC/ECC technologies. In these studies we investigated several aspects of reproducibility and diagnostic accuracy of the RTVue-100 OCT, and compared them to those of the GDx-VCC/ECC device. We also analyzed the influence of age-related macular degeneration (AMD) on the inner macular retinal thickness measurements. Finally, we examined the usefulness of the devices to detect thickness changes during the course of acute optic neuritis (ON) in multiple sclerosis (MS).

My personal involvement in all studies comprised in this thesis was significant. However, plural is used in the thesis to reflect the fact that this work is the result of team effort.

3 BACKGROUND

3.1 Optical coherence tomography

OCT was introduced in clinical practice in 1991 as a non-contact, non-invasive technique for in vivo imaging of the human retina.[33,34] This technique employs a low-coherence infrared light beam, which is directed through the ocular media to the retina to produce an interference pattern. This interference pattern is then processed into a signal, which is used to create a two-dimensional (2D) image of the retina, analogous to a cross-sectional histological section (*Figure 1*). OCT has many applications in clinical ophthalmology, including measurement of RNFLT.[35,36]

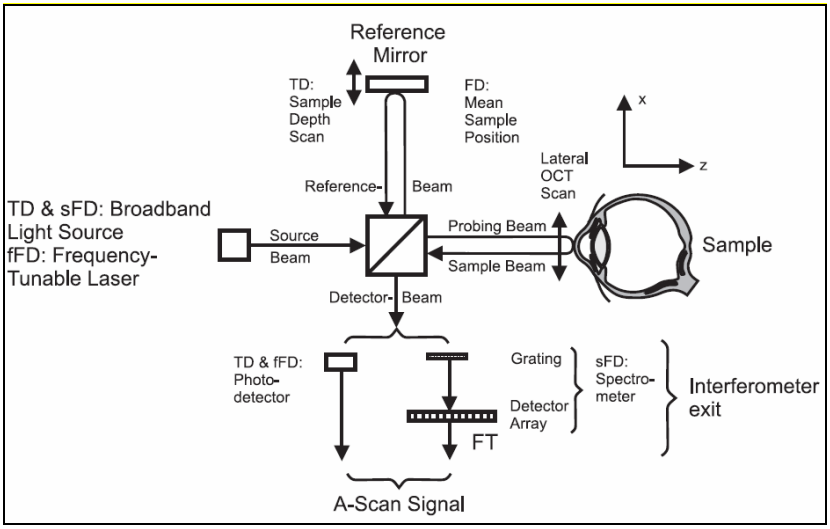

Figure 1. Standard TD-OCT and FD-OCT interferometer configurations [37]

The functions of the reference mirror and signal detection at the interferometer are different. FD-OCT techniques use either a broad-band light source (sFD) or a frequency-tunable laser (fFD) to produce an A-scan with Fourier transform (FT).

In the first generation of OCT devices time-domain technology was employed for image acquisition.[38] With this technique, near-infrared light is directed on the retina and is reflected from a reference mirror that is positioned at a known distance from each retinal layer. When light reflected from the retina combines with light reflected from the reference mirror, an interference pattern is formed that is interpreted as an A-scan signal by the OCT instrument. The reference mirror is then moved to different distances from the retina, thereby producing different signals for light reflected back from each respective retinal layer. Thus, time delay is used to form a different signal (A-scan) for each retinal layer at a

rate of 512 A-scans per 1.3 seconds. Multiple A-scans are combined to construct a 2D image (B-scan) displaying a different signal for each retinal layer.

TD-OCT with the third-generation Stratus OCT instrument (Carl Zeiss Meditec, Dublin, CA, USA) has become a widely used method for glaucoma diagnostics and research in the last decade.[39-44] Resolution of 8 to 10 μm in RNFLT measurements was attained. Previous studies with the Stratus OCT system have shown that reproducibility of the peripapillary RNFLT measurements is better in healthy eyes than in glaucomatous eyes: test-retest variability in RNFLT measurements (Mean, Mean Fast scan) ranges from 3.5 to 4.7 μm in normal eyes and 5.2 to 6.6 μm in glaucomatous eyes.[45] It is also known that pupil dilation [46,47] and variations of signal strength [48-59] influence the results and the reproducibility. RNFLT measurements for larger sectors are more reproducible than for narrower sectors: test-retest variability for quadrant measurements ranges from 6 to 16 μm, whereas for clock hours, test-retest variability approaches 20 μm between sessions in some sectors.[51,52] In general, the nasal sectors are the worst reproducible parameters. Incorrect alignment of the measurement area can alter the measured RNFLT values.[53-56] Though the reproducibility of the time-domain technology was found to be good for clinical purposes both in healthy and in glaucomatous eyes, in different studies, sensitivity and specificity of the Stratus OCT to detect glaucoma was found to be only moderate to high.[39-42] The inferior maximum parameter had the best combination of sensitivity and specificity, 75 % (95 % confidence interval [CI], 70.2 - 79.8 %) and 89.6 % (95 % CI, 82.6 - 96.6 %), respectively.[39]

Although OCT was originally designed to evaluate retinal thickness, software development has also permitted macular volume assessment.[57] However, studies comparing the ability of Stratus OCT to distinguish between normal and glaucomatous eyes using macular, RNFL, and ONH assessments found that the RNFLT and ONH parameters provided considerably better discrimination (inferior thickness, area under the receiver operating characteristic curve [AUC]=0.91; cup/disk area ratio, AUC=0.88) than total retinal thickness of the macula (inferior outer macular thickness, AUC=0.81).[58-61]

The recently developed FD-OCT technology provides considerable improvements in image acquisition speed and image resolution compared to the TD-OCT technology. In FD-OCT the reference mirror is stationary, and the OCT signal is acquired by using a spectrometer as detector or by varying the narrowband wavelength of the light source in time (*Figure 1*).[62] Mathematically, Fourier-transforms are used to extract the depth information. These characteristics allow increased image acquisition speed up to

18,000 - 40,000 A-scans per second, which reduces vulnerability to involuntary eye movement artifacts, and provides a denser sampling of the tissue. These features allow advanced three-dimensional (3D) reconstructions for improved definition of the topography of the ONH, RNFLT and other layers of the retina, such as the retinal ganglion cell layer (*Figure 2*).[63,64]

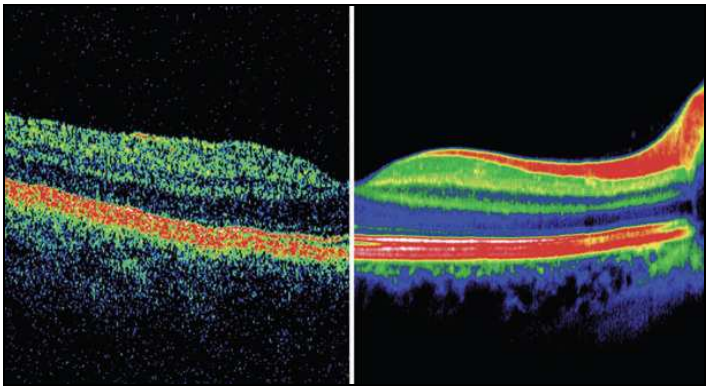

Figure 2. TD-OCT *(left)* and FD-OCT *(right)* images of the macula in the same subject; FD-OCT provides improved visualization of retinal layers [38]

Various investigations have shown that OCT instruments employing Fourier-domain technology (*Table 1*) have significantly higher image resolution and scan speed, easier clinical application and improved image segmentation compared to the TD-OCT.[63-67] This might increase the clinical usefulness of FD-OCT compared to TD-OCT,[68] however, published information on this new technology (e.g. reproducibility, diagnostic accuracy, influence of macular pathologies on the measured macular thickness parameters, etc.) is limited.[66,68-75]

Table 1. Basic parameters of various commercially available FD-OCT systems [38]

Manufacturer	Device	Axial resolution (µm)	Transverse resolution (um)	Scan speed (A-scans/s)	Additional features
Bioptigen, Inc, USA	3D SD-OCT	3-5	10	20,000	IR fundus, handheld, mouse, pediatric
Carl Zeiss Meditec, Inc, USA	Cirrus	5	25	27,000	LSLO, segmentation of the ILM and RPE
Heidelberg Engineering, GmbH, Germany	Spectralis HRA+OCT	3.5	14	40,000	CSLO, FA, ICG angiography, auto-fluorescence, eye tracking, automatic rescan, infrared imaging, red free imaging
Ophthalmic Technologies, Inc, Canada	OPKO Spectral OCT / SLO	5-6	15	27,000	SLO, microperimetry
Optopol Technology, SA, Poland	Copernicus	3	12-18	55,000	IR / red fundus detect RAPD, Doppler analysis of retinal blood flow
Optovue, Inc, USA	RTVue-100	5	15	26,000	IR fundus, segmentation of multiple retinal layers, anterior segment
Topcon Medical Systems, Inc, USA	3D-OCT - 1000	6	20	18,000	color fundus combined OCT with fundus camera

IR, infrared; LSLO, line-scanning laser ophthalmoscope; ILM, internal limiting membrane; RPE, retinal pigment epithel; HRA, Heidelberg retina angiograph; CSLO, confocal scanning laser ophthalmoscope; FA, fluorescein angiography; ICG, indocyanin green; SLO, scanning laser ophthalmoscope; RAPD, relative afferent pupillary defect

3.2 Scanning laser polarimetry

RNFLT measurement with SLP is based on retardation (slowing down) of the polarized illuminating laser light along one axis (“slow axis”) by the birefringent retinal ganglion cell axons of the RNFL.[76] The birefringent property of the axons is caused by the parallel organized intracellular organelles. When a retinal ganglion cell dies, the axon of the cell, together with its intracellular organelles and the related birefringence, also disappears. Thus, ganglion cell loss results in decrease of birefringence, which is measurable. This provides the bases of clinical application of polarimetry for glaucoma diagnostics.

The birefringent ocular structures cause retardation in the polarized light passing through them, and this retardation of the reflected light is measured automatically by the detector unit of the instrument (*Figure 3*). The automatic conversion of retardation to RNFLT data expressed in microns (μm) is based on the established linear relationship between retardation caused by the RNFL, and the histological thickness of this layer. Since other tissues (mainly the cornea and the crystalline lens) also cause retardation of the illuminating light, the influence of these structures on the measurement needs neutralization.

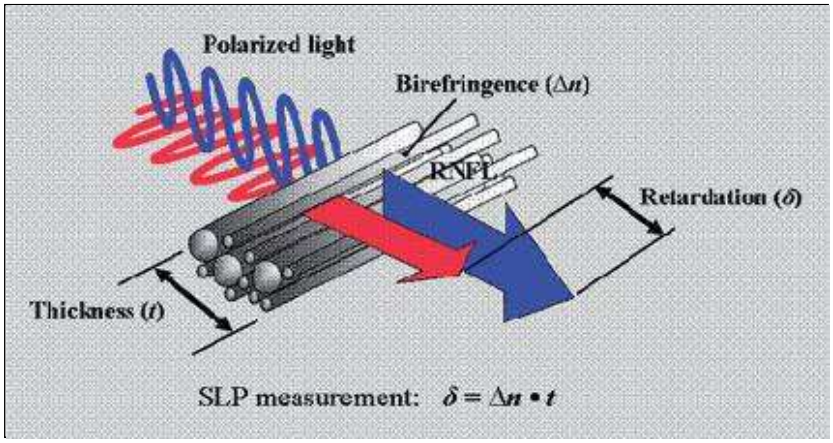

Figure 3. Basic principle of scanning laser polarimetry [77]

The GDx-Nerve Fiber Analyzer (GDx-NFA) was the first commercially available instrument for SLP.[20,78,79] In this version a built-in cornea compensator was used for neutralization of retardation caused by the cornea and the lens. The compensator had a fixed retardation capacity and a fixed angle, for the compensation of the corneal retardation.[78,79] Though this early instrument version contained sufficient normative database and provided favorable diagnostic accuracy,[80,81] its accuracy to neutralize anterior segment retardation was suboptimal.[82] The reason why any kind of fixed angle and magnitude cornea compensator is necessarily insufficient is the wide distribution of anterior segment retardation among eyes: it cannot be uniformly neutralized with a fixed compensator.[78,79] This problem became obvious when eyes undergoing laser-assisted in situ keratomileusis (LASIK) were investigated: the LASIK cut and the corneal healing process induced changes in the corneal retardation, which (due to its insufficient neutralization) led to measurement artifacts with this instrument version.[83-86]

The need for a better anterior segment compensation led to the development of GDx-VCC. The GDx-VCC instrument represents a new hardware compared to GDx-NFA, and

contains a major software innovation.[86-89] The compensation of anterior segment retardation with GDx-VCC is individual for each measurement, but since in eyes with no cornea disease the anterior segment retardation is stable,[90] in eyes with normal cornea the result can also be used to later measurements obtained during the follow-up. Using GDx-VCC image acquisition contains two steps: first a polarimetric image of the cornea and lens is obtained on the fovea area of the retina. Since there are no retinal ganglion cell axons in the centre of the macula, the retardation found in this area represents retardation caused by the anterior segment structures. In the second step, the peripapillary RNFL is imaged, and the software automatically corrects for the measured data with the retardation measured in the first step. Thus, the resulting image and report contain only corrected values i.e. true RNFLT data. The GDx-VCC instrument is now the standard device for SLP. Since it always compensates for the actual cornea retardation, changes of cornea retardation are easily and effectively neutralized. Using GDx-VCC both structure-function relationship (i.e. the relationship between RNFLT and the corresponding VF sensitivity) and diagnostic accuracy improved considerably compared to the GDx-NFA.[91-93] The sensitivity, at a specificity of 80 %, increased up to 89 %, and at a specificity of 95 % up to 91.7 %.[93-95] Of all GDx-VCC parameters, a Vector Support Machine generated parameter, the NFI performs consistently best for diagnostic accuracy.[96] In addition, it has been shown that in certain cases SLP can identify RNFL thinning before any VF deterioration can be seen. One signal-to-noise problem, however, was not solved with the GDx-VCC technique: the compensation for ARP required a further software innovation.

ARP is caused by poor signal-to-noise ratio. It is characterized by irregular patches of elevated retardation which does not match the expected retardation distribution based on the RNFL.[29,97,98] It is originated from behind the RNFL, and is frequent among myopic and glaucomatous eyes. The prevalence of ARP varies between 10 and 25 % in healthy eyes, and is up to 51 % in glaucomatous eyes.[29,97,98] Atypical retardation is quantified with a software-provided parameter, the Typical Scan Score (TSS): it ranges between 0 (maximally atypical image) and 100 (maximally typical image). A TSS value below 80 represents an atypical image. The most recent innovation, GDx-ECC was developed to remove or reduce ARP by improving the signal-to-noise ratio of the measurement.[25,29,30,98-101] In GDx-ECC, a known large birefringence bias is introduced into the measurement beam path to shift the measurement of total retardation into a higher value region. The birefringence bias is determined from the macular region of

each measurement and then, point by point, removed mathematically to yield the true RNFL retardation. GDx-ECC is effective in neutralization of ARP,[29,98] in addition, it improves the structure-function relationship between polarimetry and VF sensitivity.[30,98-100] On eyes with no ARP, GDx-ECC and GDx-VCC show very similar results and diagnostic accuracy.[25] In contrast, in case of eyes with ARP the diagnostic accuracy with GDx-VCC is reduced but with GDx-ECC remains high. Interestingly, when the RNFL defect is localized, the diagnostic accuracy of all compensation techniques remains below optimal.[102,103]

4 OBJECTIVES

4.1 Reproducibility of retinal nerve fiber layer and inner macular thickness measurements of the RTVue-100 Fourier-domain optical coherence tomograph

Based on its technical innovations, the RTVue-100 OCT seems to have the potential to increase the role of OCT devices in glaucoma diagnostics, but its clinical value has not yet been evaluated in detail. Therefore, the aims of our study were:

- to investigate intrasession and intersession reproducibility characterized by intraclass correlation (ICC), intrasession variability, and test-retest variability of the RNFLT and ganglion cell complex (GCC) measurements in normal and glaucomatous eyes;
- to investigate the role of several patient-related factors in measurement reproducibility: cooperation (previous patient experience in imaging examinations) and 3 factors with potential influence on the instrument's signal-to-noise ratio (glaucoma severity, pupil size, and age of the patients).

4.2 Comparison of repeatability of retinal nerve fiber layer thickness measurements made using the RTVue-100 Fourier-domain optical coherence tomograph and the GDx-VCC/ECC scanning laser polarimeter

In future both FD-OCT and SLP may be used in clinical practice. Thus, it is of clinical importance to compare the characteristics of these systems. In this study we aimed:

- to compare repeatability of RNFLT measurements made using the RTVue-100 OCT against repeatability of those made using GDx-VCC and GDx-ECC.

4.3 Diagnostic accuracy of retinal nerve fiber layer, inner macular thickness and optic disc measurements made with the RTVue-100 Fourier-domain optical coherence tomograph to detect glaucoma

As detection of glaucomatous ONH damage is frequently suboptimal, evaluation of the diagnostic accuracy of the different imaging devices is of clinical importance. To evaluate the diagnostic capability of the RTVue-100 OCT we used the software-provided classification, which is based on comparison between the measured values and the integrated normative database. Since reduction of macular thickness, especially of the inner retinal layers, is an important OCT finding associated with glaucoma, the GCC scan of the RTVue system may also have clinical importance. The aim of our study was:

- to evaluate the diagnostic accuracy of RNFLT, GCC and ONH measurements made with the RTVue-100 OCT to detect glaucoma in a Caucasian referral population.

4.4 Comparison of clinical diagnostic usefulness of retinal nerve fiber layer thickness measurements made using the RTVue-100 Fourier-domain optical coherence tomograph and the GDx-VCC/ECC scanning laser polarimeter

The evaluated techniques have different working principles and normative databases but comparable diagnostic reports, were recently developed, and will probably be used parallel for glaucoma detection in the following years. To compare the diagnostic value of the different methods, we used parameters which are indicated on both standard instrument reports, comparable between the methods, and easily available for the clinicians. The aims of the study were:

- to compare the diagnostic accuracy of the RTVue-100 OCT and the GDx-VCC and GDx-ECC to detect glaucoma.

4.5 Influence of age-related macular degeneration on inner macular thickness measurements made with RTVue-100 Fourier-domain optical coherence tomograph

AMD may potentially influence macular thickness measurements and their software-provided classification for glaucoma, even if all forms of AMD involve the outer retinal layers which are not investigated when inner macular retinal thickness is measured with the GCC scan of the RTVue-100 OCT. In the current study we investigated:

- whether early/intermediate AMD, untreated choroidal neovascularization (CNV) and CNV after intravitreal antiangiogenic treatment in fact influence the different average and pattern-based GCC parameters and their software-provided classification for detection of glaucoma, in non-glaucomatous eyes.

4.6 Nerve fiber layer and macular thinning measured with the RTVue-100 Fourier-domain optical coherence tomograph and the GDx-VCC/ECC scanning laser polarimeter during the course of acute optic neuritis

Though RNFLT and macular thickness following acute optic neuritis (ON) were previously investigated, to our knowledge no prospective follow-up study on eyes with acute ON in multiple sclerosis (MS) has been published. The primary goal of the current study was:

- to investigate the dynamics of RNFLT decrease and macular thinning, using different advanced imaging devices in acute ON in MS;
- to evaluate and compare the usefulness of the RTVue-100 OCT and GDx-VCC/ECC, for the detection of thickness changes during the follow-up.

5 METHODS

5.1 Instruments

5.1.1 Optical coherence tomography

OCT measurements were performed with the RTVue-100 OCT instrument (Optovue Inc, Fremont, CA, USA) with software versions 3.5 and 4.0 (*Figure 4*).[65,104] All measurements were performed by the same trained investigator (Anita Garas) using the same instrument. The RTVue-100 OCT uses a near-infrared light source with emission centered at 840 nm and a 50 nm bandwidth. The software version 3.5 contains a normative database for diagnostic classification consisting of more than 300 healthy eyes of mixed ethnicity with age ranging between 19 and 82 years,[105] whereas the normative database of software version 4.0 consists of 861 healthy eyes of mixed ethnicity subjects, with ages ranging between 19 and 82 years.[106] The RNFLT values have been found to correlate significantly with the age of subject, ethnicity and optic disc size, and adjustments for these effects (using multiple linear regression equations) are incorporated in the software to improve classification results.[105-107]

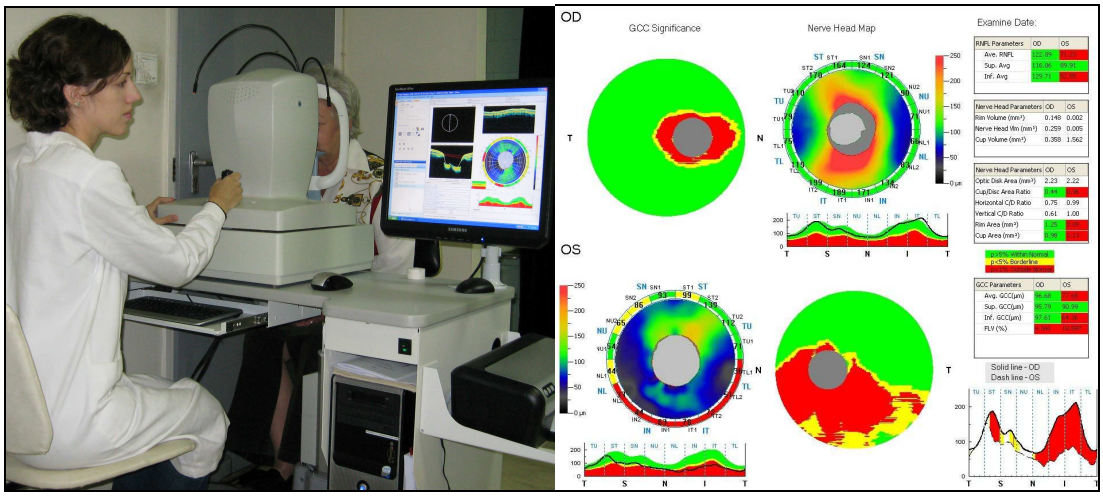

Figure 4. The RTVue-100 OCT device in clinical practice *(left)* and the color-coded Symmetry Report of its ONH scan *(right)*

The Symmetry report of the ONH scan contains from the left top, for each of the patient's eye: GCC significance map, which is a probability map indicating statistical significance of GCC loss. Next to it: RNFLT map and 16 sector RNFL analysis, where brighter colors (red and orange) represent thicker areas and cooler colors (blue and green) represent thinner areas. Local RNFLT values are compared to the normative database. Below the RNFLT map: TSNIT graph, showing the RNFLT profile around optic disc (black line), superimposed on normative database. On the right side: parameter tables and TSNIT symmetry analysis of the eyes.

For RNFLT, ONH and GCC measurements, the standard glaucoma protocol was used. This includes a "3D optic disc scan" for the definition of the disc margin based on computer-assisted determination of retinal pigment epithelium (RPE) endpoints; an "ONH scan" that measures the RNFLT in a zone with a diameter of 4 mm automatically centered on the predefined disc (this process is operator independent); and the standard "GCC scan" for the determination of the inner retinal thickness in the macula.

Each ONH scan consists of 12 radial lines and 6 concentric rings that are used to create an RNFLT map. The measuring circle (920 points) is derived from this map after the sample circle is adjusted to be centered on the optic disc. The GCC scan covers a 7x7 mm area centered 1 mm temporal to the fovea. Three average GCC thickness parameters (superior, inferior and average GCC) and three pattern-based GCC parameters (Focal Loss Volume [FLV], Global Loss Volume [GLV] and Root Mean Square [RMS], *Table 2*) are calculated by the software.[69] The GCC thickness parameters indicate thickness of all macular layers between the ILM and the inner plexiform layer (IPL) in the area above or below the horizontal meridian, or their average, respectively.

The measured parameters (*Table 2*) are automatically compared with the normative database for the total circle, the superior and inferior sectors, each of the 16 (22.5^{o}-sized) sectors of the measuring circle around the ONH, superior and inferior GCC, and several ONH parameters. For these software calculated parameters an instrument provided classification is indicated in a color-coded manner: sectors with "within normal limits" classification (i.e. sectors for which the probability of having no glaucomatous damage ≥5 %) are printed in green, sectors with "borderline" classification (p<5 % but ≥1 %) in yellow and sectors with "outside normal limits" classification (p<1 %) in red.

Image quality on the RTVue-100 OCT is determined by the Signal Strength Index (SSI) parameter. The SSI is a measure of the average signal strength across the scan. The stronger the OCT signal, the higher the SSI. Low signal strength can result in poor image resolution, lack of retinal detail, and an increase in segmentation errors, since there is little image structure for the algorithms to use in segmenting the various layers. The SSI can range from near 0 (no signal) to approximately 90 (very strong signal). The general guidelines from the manufacturer are as follows: SSI of <30 is a very poor quality scan that cannot be analyzed, SSI between 30 and 40 is a poor quality scan that can be analyzed but should be retaken to improve if possible, SSI between 40 and 50 is an adequate quality scan that can be analyzed but should be retaken to improve if possible, SSI between 50 and 60 is a good quality scan, and SSI of >60 is a very good quality scan.

Table 2. Definitions of the most important parameters of the RTVue-100 OCT, used in our studies

Parameter	Definition
RNFLT parameters	
Average	mean of RNFLT (µm) for the total 360º measuring circle of 3.45 mm diameter around the ONH centered on the disc
Superior	average RNFLT (µm) measured in the superior quadrant (90º) of the measuring circle
Inferior	average RNFLT (µm) measured in the inferior quadrant (90º) of the measuring circle
16 RNFL sectors	equally sized (22.5º), separate RNFLT sectors around the 360º measuring circle (TU; temporal upper, ST; superotemporal, SN; superonasal, NU; nasal upper, NL; nasal lower, IN; inferonasal, IT; inferotemporal, and TL; temporal lower)
ONH parameters	
Cup area, Cup/Disc area ratio, Rim area	automatically calculated parameters, with optic cup defined as the intersection points of the ONH inner boundary and a parallel line that is 150 µm above the connecting line of the RPE tips
GCC parameters	
Average	mean of software-provided superior and inferior GCC values
Superior	thickness of all macular layers between the ILM and the IPL in the area above the horizontal meridian
Inferior	thickness of all macular layers between the ILM and the IPL in the area below the horizontal meridian
Focal Loss Volume (FLV)	the total sum of statistically significant GCC volume loss divided by the GCC map area (%)
Global Loss Volume* (GLV)	sum of negative fractional deviation in the entire measurement area (%)
Root Mean Square* (RMS)	summary parameter showing fit of the fractional and pattern deviation maps to the normal pattern (the worse the fit, the higher the GCC RMS value)

* GCC GLV and RMS parameters are exported information which are not displayed on the printout

5.1.2 Scanning laser polarimetry

SLP was performed using the GDx instrument (Carl Zeiss Meditec Inc., Dublin, CA, USA) with software version 5.5.1 (*Figure 5*). All measurements were performed by the same trained investigator (Anita Garas) using the same instrument. This instrument can perform measurements both with VCC and ECC mode. The instrument projects a beam of 780 nm polarized laser light onto the retina through the pupil. The laser scans the fundus at a 40° x 20° scanning angle, and image acquisition takes approximately 0.7 seconds per trial. The birefringent ocular structures cause retardation in the polarized light passing through them, and this retardation is measured automatically. Because of the laser wavelength, mild to moderate cataract does not degrade the images in a clinically significant manner.[23]

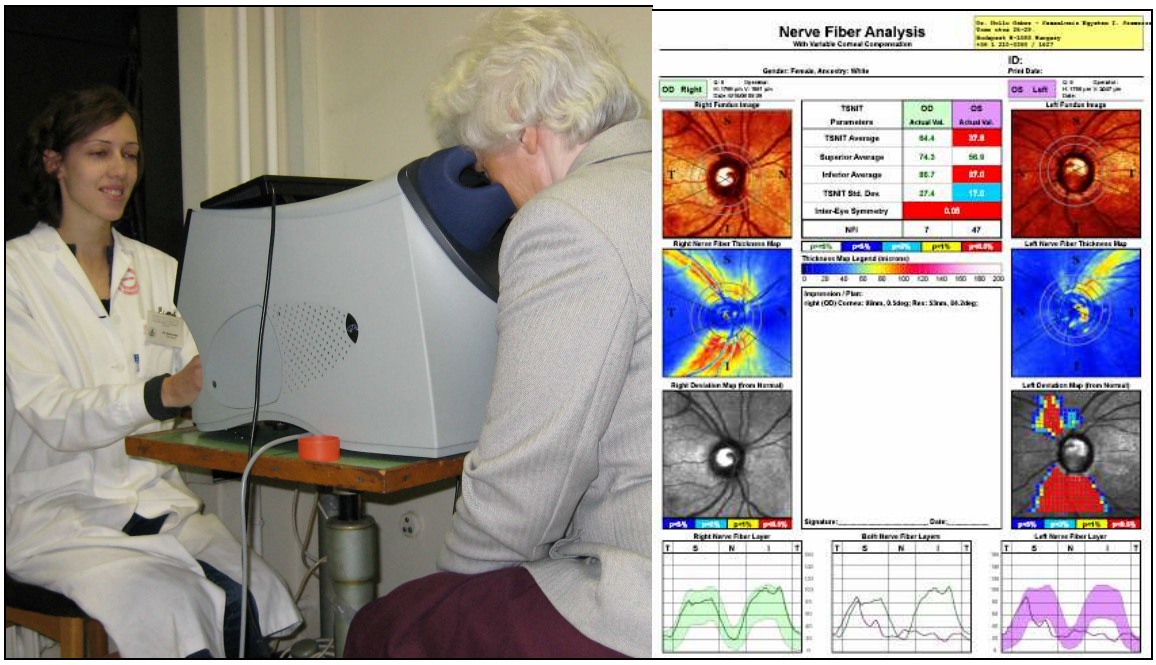

Figure 5. The GDx-VCC/ECC device in clinical practice *(left)* and its color-coded printout *(right)*

The printout of the GDx-VCC contains from top to bottom, for each of the patient's eye: a peripapillary fundus reflectance image, a polarimetric retardation image and a probability-of-normality image. At the bottom of the printout the patient's peripapillary RNFLT (double-hump line) is depicted against a normative database (green or purple band for right and left eye, respectively). Parameters for quantitative analysis are provided at the center-top of the printout.

In the VCC mode, as a first step the corneal polarimetric axis and magnitude values are calculated and then this information is used to correct the measured retardation around the ONH. In the ECC mode the compensator is adjusted so that it combines with the corneal retardation to produce a bias retardation of approximately 55 nm and a slow axis to be close to vertical. The software then measures a higher total retardation than the RNFL retardation alone, and the signal-to-noise ratio is improved as a result. The actual bias retardation and axis in each image are measured from the macular region and the actual RNFL retardation is derived mathematically. The actual bias is determined from each image, and removed from the final RNFL image.

The GDx-VCC features several parameters (*Table 3*), one of which, the NFI, has been trained specifically to discriminate between healthy and glaucomatous eyes. The NFI provides a single number (range, 1-100) representing the overall integrity of the RNFL.[108] The higher the score, the more likely the RNFL measurement represents a glaucomatous eye. The NFI has been trained on 540 healthy subjects and 271 glaucoma patients with varying degrees of disease severity.[108]

Table 3. Definitions of the most important parameters of the GDx-VCC/ECC, used in our studies

Parameter	Definition
TSNIT Average	average RNFLT (µm) measured in the total (temporal-superior-nasal-inferior-temporal) measuring circle
Superior Average	average RNFLT (µm) measured in the superior quadrant (120º) of the measuring circle
Inferior Average	average RNFLT (µm) measured in the inferior quadrant (120º) of the measuring circle
Nerve Fiber Indicator (NFI)	parameter indicating the probability of glaucomatous damage (range: 0-100, normal threshold ≤30)
Typical Scan Score (TSS)	parameter characterizing the typicality (regularity) of the retardation pattern

The GDx-VCC/ECC examination report provides color-coded information on the software-provided classification for temporal-superior-nasal-inferior-temporal (TSNIT) average RNFLT, superior RNFLT and inferior RNFLT. When a parameter is classified as "within normal limits" (i.e. the probability of having no glaucomatous damage is ≥5 %) the background color is white, when the probability of being statistically normal is <5 %, ≤2 %, ≤1 % and ≤0.5 %, the background color is blue, light blue, yellow or red, respectively.

5.2 Participants and protocols

The research protocols were approved by the Institutional Review Board for Human Research of Semmelweis University, Budapest, Hungary. Informed consent was obtained from all participants before enrollment.

5.2.1 Reproducibility of retinal nerve fiber layer and inner macular thickness measurements of the RTVue-100 Fourier-domain optical coherence tomograph

5.2.1.1 Participants

Between August and September 2008, 37 white individuals were enrolled in the study. These comprised 14 healthy and ocular hypertensive (OHT) subjects (group 1); 11 patients with glaucoma of moderate severity (group 2); and 12 patients with advanced glaucoma (group 3). All were experienced in imaging examinations. One eye per participant was selected for the investigation. For inclusion, all participants had to have, in the study eye, refractive error within ±7.0 diopters (D), clear optical media for optimal imaging, and

sufficient central vision (visual acuity better than 0.7) for optimal fixation. Additional inclusion criteria were that the normal and OHT participants had to have reliable and normal VF results with a mean defect (MD) of less than 2 dB and normal ONH and ophthalmic status for both eyes. The separation of normal and OHT eyes was based exclusively on IOP, which for the OHT eyes consistently was measured at more than 21 mmHg. The glaucoma patients, on at least the study eye, had to have reliable and reproducible VF defects typical for glaucoma (inferior and/or superior paracentral or arcuate scotomas; nasal step; hemifield defect; or generalized depression with MD higher than 2 dB) on the Octopus 101 (Interzeag AG, Schlieren, Switzerland) G2 normal threshold perimetry test, with MD either between 6 and 12 dB or higher than 15 dB, and glaucomatous ONH damage (diffuse or localized neuroretinal rim thinning, evaluated stereoscopically). The eyes were assigned to one of the 3 groups based on their classification and VF MD value, according to the following criteria: the normal and the OHT participants were assigned to group 1 (n=14), glaucoma patients with MD between 6 and 12 dB were assigned to group 2 (n=11), and glaucoma patients with MD higher than 15 dB were assigned to group 3 (n=12).

In November 2008, 40 consecutive unselected participants in a free glaucoma screening trial held in a non-hospital-based location were also enrolled in the study. All were white individuals with no previous experience in imaging tests. The screening trial prepublicity had invited attendance from persons with no diagnosed eye disease or major ocular symptoms, but with increased risk for glaucoma (age preferably older than 50 years, myopic refractive error, one or more close blood relatives with glaucoma). One eye per participant was selected randomly for the measurements, which were performed as a part of the screening. The 40 screening participants were classified as normal or glaucomatous based on the results of a detailed clinical investigation within 2 months. The demographics of all the participants are shown in *Table 4*.

Table 4. Demographic characteristics of participants in the study of investigating reproducibility of the RNFL and inner macular thickness measurements of the RTVue-100 OCT

	Hospital-based patients				Screening participants	p-value
	All patients	*Group 1*	*Group 2*	*Group 3*		
Number of participants	37	14	11	12	40	NA
Male/Female (n/n)	14/23	7/7	4/7	3/9	17/23	0.677*
Eye (right/left)	21/16	9/5	6/5	6/6	23/17	0.950*
Age (years) (mean±SD)	56.7±15.3	54.0±17.9	55.3±14.0	61.1±13.4	63.8±9.3	0.015†
MD (dB) (median)	9.1	-0.5	9.5	19.1	NA	NA
BCVA (mean±SD)	1.0±0.1	1.0±0.1	1.0±0.1	0.9±0.2	1.0±0.1	0.504‡
Refractive error (D) (mean±SD)	-0.6±2.3	-1.1±2.0	-0.7±3.4	0.2±1.1	+1.1±1.9	0.001†
Lens status (phakic/ pseudophakic)	35/2	14/0	9/2	12/0	38/2	0.940*

BCVA, best corrected visual acuity; * Pearson's chi-square test; † unpaired t-test, 2-tailed, equal variances not assumed; ‡ Mann-Whitney U-test; NA, not applicable

5.2.1.2 Protocol

Each participant completed the measurements for determination of intrasession variability and the measurements via dilated pupil on the same day. For determination of intersession reproducibility, 34 of the 37 hospital-based patients repeated the measurement series at 3 months after the initial examination. The following protocol in each measurement session was used. First, standard visual acuity testing with determination of best refractive correction was performed. Image acquisition was started by obtaining 1 high-quality ONH image using the 3D scan. Then, 5 high-quality ONH scans and 5 high-quality GCC scans were obtained. During the image acquisition procedure, the head of the participant was moved from the headrest after each image was obtained and the head was repositioned for the following measurement. During the first visit, for the 37 participants with experience in imaging, pupil dilation was performed after the first measurement series. Two drops of 0.5 % tropicamide eye drops (Chauvin Ankerpharm GmbH, Berlin, Germany) were instilled in the study eye, with a 15-minute interval between the first and second drop. Thirty minutes later, the diameter of the dilated pupil was measured, and all previous measurements were repeated. The screening participants underwent the same intrasession measurements series, but without pupil dilation.

The RTVue-100 OCT measurements were performed with software version 3.5. Of the several items of structural information of the ONH report only 1 was used in the current study: namely, RNFLT determined for different areas of the 360° measuring circle of

3.45 mm in diameter centered on the disc. The RNFLT values for each of 16 individual sectors of the measuring circle around the ONH were numbered for reference purposes in sequence from the temporal side of the horizontal meridian (clockwise for the right, and anticlockwise for the left eye).

The following software-provided parameters were evaluated: 1) average RNFLT for the total 360° around the ONH; 2) superior quadrant RNFLT; 3) inferior quadrant RNFLT; 4) temporal quadrant RNFLT; 5) nasal quadrant RNFLT; 6) all 16 separate RNFLT sectors, 7) superior GCC; and 8) inferior GCC. Only images with SSI >45 were used.

5.2.1.3 Statistics

The SPSS program package version 15.0 (SPSS, Inc., Chicago, IL, USA) was used for statistical analysis. Intrasession and intersession reproducibility were characterized by the corresponding ICC and coefficient of variation (CV), intratest variability (1.96 times intrasession standard deviation [SD], in micrometers) and test-retest variability (1.96 times intersession SD, in micrometers). Calculation of these parameters was based on variance components calculated using the mixed model analysis. The ratio of intrasession to intersession CV was determined, and also that of intratest to test-retest variability. Statistical comparisons of the parameters were based on individually calculated estimations, as follows. A one-way analysis of variance with linear trend analysis was used to compare the mean values, and the Kruskall-Wallis test with the Jonckheere-Terpstra test for trend was used to compare the intrasession CV values between the severity groups. The paired t-test was used to compare the corresponding mean values, and the Wilcoxon signed-rank test was used to compare the corresponding CV and intratest variability values. The Pearson's chi-square test, the unpaired t-test, and the Mann-Whitney U-test were used to compare the 2 study populations. For comparison of pupil size, the mean thickness values and SSI determined via undilated and dilated pupil, respectively, the paired t-test was used. The Spearman correlation was used to investigate the influence of age on measurement reproducibility in the healthy screening trial participants. P-values of less than 0.05 were considered to be statistically significant.

5.2.2 Comparison of repeatability of retinal nerve fiber layer thickness measurements made using the RTVue-100 Fourier-domain optical coherence tomograph and the GDx-VCC/ECC scanning laser polarimeter

5.2.2.1 Participants

The same 37 individuals, who participated in the study described in detail in *chapter 5.2.1* participated in the current study. The same eyes and groups were used (*Table 4*).

5.2.2.2 Protocol

Each participant completed the study within one day. All measurements were performed according to the following protocol. First standard visual acuity testing was performed, with determination of best refractive correction. Then the RTVue-100 OCT imaging was performed; image acquisition was started by obtaining one high quality ONH image using the 3D scan. Then 5 high-quality ONH scans were obtained. Subsequently, 5 separate GDx measurements were taken in the VCC mode, followed by 5 separate GDx measurements in the ECC mode. For all procedures, the participant's head was moved from the headrest after each image was obtained, and repositioned for the following measurement.

To compare corresponding sectors of RNFL around the ONH, we defined 8 sectors of interest, as follows: (1) the average of the total 360º around ONH (this corresponds to the software-provided RNFLT average from the RTVue-100 OCT, and the TSNIT average from the GDx-VCC and GDx-ECC); (2) superior quadrant (45 to 135°); (3) inferior quadrant (225 to 315°); (4) temporal quadrant (315 to 45°); (5) nasal quadrant (135 to 225°); (6) inferotemporal sector (270 to 303.7°); (7) superotemporal sector (56.3 to 90°); and (8) papillomacular sector (343.1 to 16.8°). All angles are increments measured from the horizontal meridian on the temporal side (0º). The exact extent of the narrower sectors (sectors 6, 7, and 8), approximately 30º, was chosen to permit comparability between measurements from the 2 instruments.

All eyes were classified with all the 3 methods investigated. For GDx-VCC and GDx-ECC the NFI and the standard RNFLT sectors indicated on the reports were used for classification. We used the generally accepted cutoff value of 30 (as suggested by the manufacturer). The GDx classification was considered as "normal" if NFI was ≤30 and all standard RNFLT sectors were classified as within normal limits; and as "glaucomatous" if NFI was >30 and/or at least one standard RNFLT sector was classified as borderline or

outside normal limits. With the RTVue-100 OCT the standard RNFLT report was used for classification, as follows. If all RNFLT values were within the statistical normal limits, the eye was classified as “normal”. When at least one of the RNFLT parameters was labeled as borderline or outside normal limits, the eye was classified as “glaucomatous”.

The RTVue-100 OCT measurements were performed with software version 3.5. In all cases image quality was carefully checked after each image acquisition, and all images with insufficient quality or with any artifact were rejected and reacquired. Only images with SSI >45 were used.

For GDx measurements one corneal image per eye was obtained for all RNFLT measurements. All RNFLT measurements were based on a fixed-size measurement circle of diameter 3.2 mm centered on the operator-placed ellipse. Images of inadequate quality (quality score <8) were reacquired.

5.2.2.3 Statistics

The SPSS 15.0 program package was used for statistical analysis. Repeatability was characterized by using the calculated CV, which was calculated individually and averaged, to enable correct statistical comparisons of correlated estimates. Repeated measures analysis of variance with the contrast was used to compare the mean values of the 5 repeated RTVue-100 OCT measurements to the corresponding values determined with GDx-VCC and GDx-ECC. The Kruskall-Wallis test with the Jonckheere-Terpstra test for trend was used for comparison of the CV values within subject groups. The Wilcoxon signed-rank test was used for comparison of the corresponding CV values between the methods. The p-values of <0.01 were considered statistically significant.

5.2.3 Diagnostic accuracy of retinal nerve fiber layer, inner macular thickness and optic disc measurements made with the RTVue-100 Fourier-domain optical coherence tomograph to detect glaucoma

5.2.3.1 Participants

One randomly selected eye of each of 316 consecutive Caucasian individuals referred for detection of glaucoma by their family doctors, optometrists or local ophthalmologists in the Glaucoma Center of the Semmelweis University in Budapest, who all underwent RNFLT measurements made with the RTVue-100 OCT between 1st January and 30th November 2009, was enrolled in the study.

Table 5. Demographic characteristics of the participants and eyes analyzed in the study of investigating diagnostic accuracy of RNFL, inner macular thickness and ONH measurements made with the RTVue-100 OCT to detect glaucoma

Race (n)	Caucasian (100 %)
Number of eyes involved in statistical analysis (n)	286 (100 %)
Male/Female (n/n)	126/160
BCVA (mean ± SD)	0.9 ± 0.2
Refractive error (D) (mean ± SD, range)	-0.7 ± 2.9 (-14.00 - +8.00)
Prevalence of healthy eyes	93/286 (32.5 %)
Prevalence of OHT eyes	36/286 (12.6 %)
Prevalence of glaucoma eyes	157/286 (54.9 %)
- *preperimetric*	46/157 (29.3 %)
- *perimetric*	111/157 (70.7 %)
Type of glaucoma	
- *POAG*	103/157 (65.6 %)
- *juvenile OAG*	11/157 (7.0 %)
- *normal pressure glaucoma*	12/157 (7.6 %)
- *chronic ACG*	11/157 (7.0 %)
- *pseudoexfoliative glaucoma*	7/157 (4.5 %)
- *pigment glaucoma*	9/157 (5.7 %)
- *other secondary glaucomas*	3/157 (1.9 %)
- *congenital glaucoma*	1/157 (0.6 %)
Mean defect (dB) (mean ± SD)	
- *healthy eyes*	0.3 ± 1.4
- *OHT eyes*	-0.1 ± 1.2
- *preperimetric glaucoma eyes*	0.1 ± 1.8
- *perimetric glaucoma eyes*	9.8 ± 7.8
Distribution of disease severity in the perimetric glaucoma group*	
- *stage 1*	26/111 (23.4 %)
- *stage 2*	34/111 (30.6 %)
- *stage 3*	21/111 (18.9 %)
- *stage 4*	24/111 (21.6 %)
- *stage 5*	6/111 (5.4 %)
Age (years) (mean ± SD)	
- *healthy eyes*	54.9 ± 15.9
- *OHT eyes*	51.5 ± 16.5
- *preperimetric glaucoma eyes*	57.6 ± 11.8
- *perimetric glaucoma eyes*	62.2 ± 14.7
Untreated maximal IOP of the OHT eyes (mmHg) (mean ± SD)	29.1 ± 8.7

* Classified according to the Modified Bascom Palmer glaucoma staging system [109]

For inclusion, all participants had to have, in the study eye, sufficient central vision for optimal fixation, image quality sufficient for optimal evaluation, no macular pathology except for a small number of hard drusen on stereoscopic evaluation. Of the 316 referred

patients 30 were excluded from the study because of severe degenerative fundus changes in high (>14.0 D) myopia (n=14), AMD, diabetic retinopathy and scar formation after vitreoretinal surgery (n=7), non-glaucomatous optic neuropathies (n=7) and cornea degeneration (n=2).

The patient population comprised of 93 healthy subjects with no ONH damage, reliable and reproducible normal VF tests with normal MD (MD less than 2 dB), and IOP consistently below 21 mmHg, based on daytime phasing (five measurements between 7.45 and 16.00 hours); 36 OHT subjects with normal ONH, VF with MD less than 2 dB and untreated IOP consistently above 21 mmHg; 46 preperimetric glaucoma patients characterized with definite glaucomatous neuroretinal rim loss (diffuse or localized neuroretinal rim thinning) and reliable and reproducible normal VF with MD less than 2 dB; and 111 perimetric glaucoma patients characterized with glaucomatous neuroretinal rim loss and reliable and reproducible VF defect typical for glaucoma (*chapter 5.2.1.1*). Severity of glaucomatous VF damage was classified according to the Modified Bascom Palmer glaucoma staging system.[109] The demographics of the participants are shown in *Table 5*.

5.2.3.2 Protocol

All patients underwent the same diagnostic protocol, which comprised a detailed slit-lamp evaluation, stereoscopic ONH photography and evaluation, stereoscopic evaluation of the macula, repeated Octopus normal or dynamic G2 threshold VF testing, and daytime IOP phasing made with Goldman applanation tonometry within 2 months from the RTVue-100 OCT imaging. The final clinical classification based on the results of these tests was made by the head of the glaucoma team. The RTVue-100 OCT examinations were not used for the clinical classification of the patients.

OCT measurements were performed via undilated pupil with the RTVue-100 OCT with software version 4.0. In the current investigation the following software-provided parameters were evaluated: 1) average RNFLT for the total 360^{o} around the ONH; 2) superior quadrant RNFLT; 3) inferior quadrant RNFLT; 4) all 16 separate RNFLT sectors; 5) superior GCC; 6) inferior GCC; 7) average GCC; 8) GCC FLV; 9) cup area; 10) cup/disc area ratio; and 11) rim area. To be included in the analysis, images had to have a SSI >40.

5.2.3.3 Statistics

The SPSS 15.0 program package was used for statistical analysis. ANOVA with the Tukey post hoc tests was used to compare age and the measured parameter values between the patient groups. Sensitivity, specificity, positive predictive value (PPV), negative predictive value (NPV), positive likelihood ratio (PLR) and negative likelihood ratio (NLR) of the software-provided classification results were determined. P-values of <0.05 were considered as statistically significant.

5.2.4 Comparison of clinical diagnostic usefulness of retinal nerve fiber layer thickness measurements made using the RTVue-100 Fourier-domain optical coherence tomograph and the GDx-VCC/ECC scanning laser polarimeter

5.2.4.1 Participants

One randomly selected eye of each of 177 consecutive Caucasian individuals referred for detection of glaucoma by their family doctors, optometrists or local ophthalmologists in the Glaucoma Center of the Semmelweis University in Budapest, who all underwent RNFLT measurements made with the RTVue-100 OCT, GDx-VCC and GDx-ECC between 1st January and 31st October 2009, was enrolled in the study. For inclusion, all participants had to have, in the study eye, refractive error within ± 10.0 D, sufficient central vision for optimal fixation, and image quality sufficient for optimal evaluation (SSI >40 for the RTVue-100 OCT measurements and quality score >8 for the GDx-VCC/ECC measurements). All patients underwent the same diagnostic protocol which comprised a detailed slit lamp evaluation, stereoscopic ONH photography and evaluation, repeated Octopus Normal or Dynamic G2 threshold VF testing (minimum 2 examinations), ultrasonic pachymetry, and daytime IOP phasing made with Goldmann applanation tonometry. The final clinical classification based on the results of these tests was made by the head of the glaucoma team. The RTVue-100 OCT and GDx-VCC/ECC examinations were not used for the clinical classification of the patients.

The patient population comprised 50 healthy subjects with no ONH damage, reliable and reproducible normal VF tests with MD less than 2 dB, and IOP consistently below 21 mmHg; 28 OHT subjects with normal ONH and VF with MD less than 2 dB and untreated IOP consistently above 21 mmHg; 33 preperimetric glaucoma patients characterized with glaucomatous neuroretinal rim loss (diffuse or localized neuroretinal

rim thinning) and reliable and reproducible normal VF with MD less than 2 dB; and 66 perimetric glaucoma patients characterized with glaucomatous neuroretinal rim loss and reliable and reproducible VF defect typical for glaucoma (*chapter 5.2.1.1*). The glaucoma groups comprised both OAG and ACG cases.

The demographics of the participants are shown in *Table 6*. For cross-sectional clinical classification, the healthy and OHT eyes were considered as eyes with no structural and functional damage (currently normal eyes with or without increased risk for future development of glaucoma), while the preperimetric and perimetric glaucoma eyes were considered as diseased (eyes with manifest structural damage with or without currently detectable functional consequences).

5.2.4.2 Protocol

For each instrument, the software-provided automatic comparison with the corresponding age-corrected normative database was used for classification. Five RNFLT parameters and their combinations were analyzed. Three parameters were directly provided by the instruments' software: 1) 360^{o} average RNFLT around the ONH; 2) superior RNFLT; and 3) inferior RNFLT. In order to detect localized superotemporal and inferotemporal nerve fiber bundle defects, two easily recognizable new parameters, comparable between the RTVue-100 OCT and GDx-VCC/ECC systems were generated. For the RTVue-100 OCT measurements, the two 22.5^{o}-sized superotemporal sectors (ST1 and ST2) and inferotemporal sectors (IT1 and IT2) were analyzed in combination, respectively. In cases where at least one of the sectors was labeled as "outside normal limits" or "borderline" the combined sector was considered as damaged. Since for GDx-VCC and GDx-ECC no narrow sectors are automatically classified, localized nerve fiber bundle type thinning on the deviation map was used as the indicator of localized RNFL damage. A localized nerve fiber bundle type thinning was defined as a one disc-diameter or longer arcuate group of continuous superpixels, with probability <5 % of being normal, this group being adjacent to the superotemporal or inferotemporal edge of the ONH (*Figure 6*).[110,111]

Table 6. Demographic characteristics of the participants and eyes analyzed by comparing the clinical diagnostic usefulness of RNFLT measurements made using the RTVue-100 OCT and the GDx-VCC/ECC

Race (n)	Caucasian: 177
Number of eyes involved in statistical analysis (n)	177 (100 %)
Prevalence of healthy eyes	50 (28.3 %)
Prevalence of OHT eyes	28 (15.8 %)
Prevalence of preperimetric glaucoma eyes	33 (18.6 %)
Prevalence of perimetric glaucoma eyes	66 (37.3 %)
Number of eyes with TSS<80 on GDx-VCC	50 (28.3 %)
Healthy eyes	
- male/female (n/n)	22/28
- age (years) (mean ± SD, range)	50.2 ± 17.3 (20 - 78)
- BCVA (mean ± SD)	1.00 ± 0.00
- refractive error (D) (mean ± SD, range)	0.1 ± 2.0 (-5.5 - +5.0)
- MD (dB) (mean ± SD)	0.1 ± 1.4
- CCT (µm ± SD)	549.4 ± 38.9
OHT eyes	
- male/female (n/n)	13/15
- age (years) (mean ± SD, range)	50.8 ± 15.6 (23 - 72)
- BCVA (mean ± SD)	0.97 ± 0.11
- refractive error (D) (mean ± SD, range)	-1.5 ± 2.4 (-8.0 - +2.25)
- MD (dB) (mean ± SD)	-0.3 ± 1.1
- CCT (µm ± SD)	554.6 ± 35.0
Preperimetric glaucoma eyes	
- male/female (n/n)	16/17
- age (years) (mean ± SD, range)	56.2 ± 12.1 (29 - 75)
- BCVA (mean ± SD)	0.99 ± 0.04
- refractive error (D) (mean ± SD, range)	-0.1 ± 2.3 (-8.5 - +3.0)
- MD (dB) (mean ± SD)	0.3 ± 1.7
- CCT (µm ± SD)	546.0 ± 37.9
Perimetric glaucoma eyes	
- male/female (n/n)	24/42
- age (years) (mean ± SD, range)	64.3 ± 12.9 (32 - 88)
- BCVA (mean ± SD)	0.87 ± 0.23
- refractive error (D) (mean ± SD, range)	-0.8 ± 2.5 (-9.5 - +4.5)
- MD (dB) (mean ± SD)	9.6 ± 6.8 (-1.5 - 24.6)
- CCT (µm ± SD)	531.6 ± 45.4
- distribution of disease severity in the perimetric glaucoma group	
MD <6.0 dB	26 (39.4 %)
MD 6.0 - 12.0 dB	19 (28.8 %)
MD >12.0 dB	21 (31.8 %)

CCT, central corneal thickness

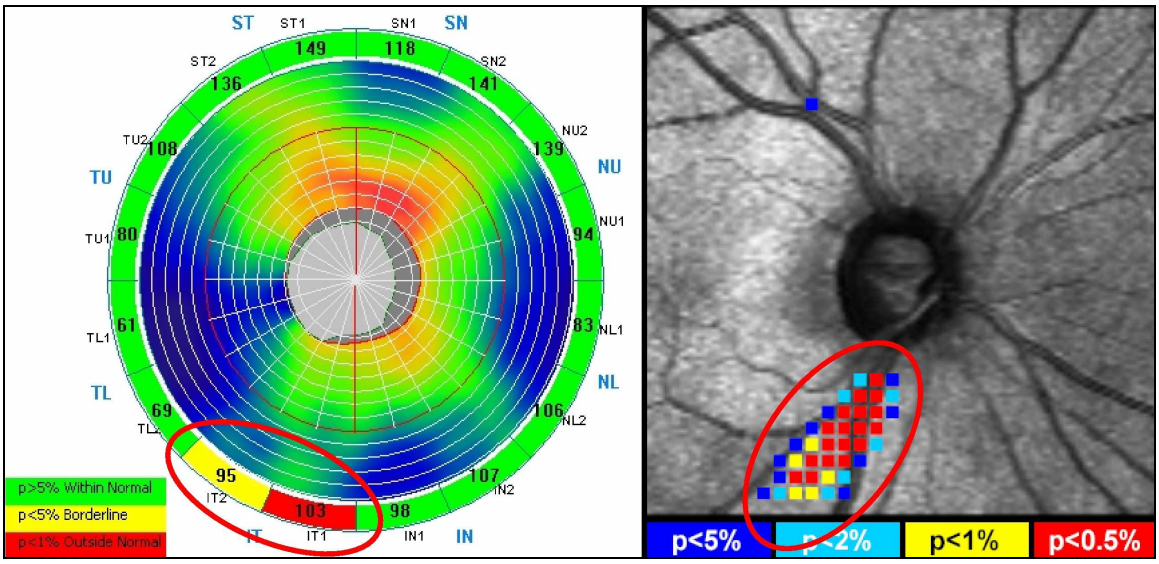

Figure 6. Presentation of the same inferotemporal retinal nerve fiber bundle defect on the ONH scan report of RTVue-100 OCT *(left)* and the GDx-VCC/ECC deviation map *(right)*

The GDx-VCC/ECC examination report provides color-coded information on the software-provided classification for TSNIT average RNFLT, superior RNFLT and inferior RNFLT. In the current investigation a probability <5 % but ≥2 % (color code: blue) was considered as a borderline classification. NFI values >30 were considered as pathological. An ARP was defined with TSS <80 on GDx-VCC examination.

5.2.4.3 Statistics

The SPSS 15.0 program package was used for statistical analysis. Sensitivity and specificity were calculated for each criterion and method, respectively, and were compared between RTVue-100 OCT and each of the GDx methods using McNemar's test. The kappa statistic was used to study the level of diagnostic agreement between the average RNFLT of the RTVue-100 OCT and the NFI of the GDx-VCC/ECC. P-values less than 0.01 were considered as statistically significant.

5.2.5 Influence of age-related macular degeneration on inner macular thickness measurements made with RTVue-100 Fourier-domain optical coherence tomograph

5.2.5.1 Participants

AMD was defined and classified according to the Age-Related Eye Disease Study Research Group report No 8 (AREDS report 8).[112] Between April and June 2010, 79 consecutive Caucasian persons with no glaucoma and diabetes mellitus in their history

were enrolled in the study (one eye of each participant). Of these, 25 eyes had no AMD (age-matched healthy controls), 19 eyes suffered from early or intermediate AMD (drusen group) with mild RPE abnormalities but without other pathology (e.g. geographic atrophy), 16 eyes had untreated subfoveal CNV scheduled for intravitreal antiangiogenic treatment (CNV group), and 19 eyes had juxtafoveal or subfoveal CNV previously treated with at least one intravitreal antiangiogenic injection (all vascular endothelial growth factor [VEGF] blocking agents included; CNV-anti-VEGF group). All CNV membranes were caused by AMD. The examination protocol comprised stereoscopic evaluation, digital photography, OCT measurements and fluorescein angiography of the macula.

For inclusion, all participants had to have clear optical media and sufficient fixation for optimal imaging, normal ONH, normal ophthalmic status and IOP less than 22 mmHg with Goldmann applanation tonometry, for both eyes. In addition, the healthy control subjects had to have reliable and normal VF on the Octopus G2 threshold perimetry test, for both eyes. Glaucomatous structural damage was defined with diffuse or localized neuroretinal rim thinning, evaluated stereoscopically, and a RNFL defect on stereoscopic evaluation in red-free light illumination, via dilated pupil. Participants with glaucomatous structural damage in at least one eye were to be excluded from the study, but no such case was observed. The RTVue-100 OCT examinations were not used for the clinical classification of the patients. The demographics of the participants are shown in *Table 7*.

To be included in the analysis, all images had to have a SSI >40. Image segmentation was reviewed for each completed GCC image, and the presence or absence of segmentation errors was recorded.

5.2.5.2 Statistics

The SPSS 15.0 program package was used for statistical analysis. Normal distribution fitting was checked with the Kolmogorov-Smirnov Goodness of Fit-test. Change of best corrected visual acuity (BCVA) in the CNV-anti-VEGF group after intravitreal antiangiogenic treatment was analyzed with the Wilcoxon signed-rank test. ANOVA with the Dunnet post hoc tests or the Kruskall-Wallis test with the Mann-Whitney U-test (as appropriate) was used to compare the measured parameter values between the healthy controls and each AMD group, respectively. Pearson's chi-square test was used to compare the distribution of the software-provided classification results and image segmentation errors between the control group and each of the AMD groups. Bonferroni correction was made for all comparisons. P-values of <0.05 were considered as statistically significant.

Table 7. Demographics of the participants in the study of investigating the influence of AMD on inner macular thickness measurements made with RTVue-100 OCT

	Control (0)	Drusen (1)	CNV (2)	CNV-anti-VEGF (3)	p-value
Participants (n)	25	19	16	19	
Age (mean ± SD)	72.6±7.1	74.3±7.6	72.4±9.1	74.2±7.8	0.796*
Gender (male/female)	7/18	4/15	4/12	6/13	0.598† (0 vs. 1) 0.833† (0 vs. 2) 0.797† (0 vs. 3)
BCVA (median (IQR))	1.00 (1.00-1.00)	0.70 (0.40-0.80)	0.10 (0.04-0.38)	0.25 (0.10-0.60)	<0.001‡ (0 vs. 1) <0.001‡ (0 vs. 2) <0.001‡ (0 vs. 3)
BCVA before anti-VEGF treatment (median (IQR))	NA	NA	NA	0.20 (0.10-0.40)	0.183#
Pseudophakic eyes (n)	2	3	3	6	0.420† (0 vs. 1) 0.305† (0 vs. 2) 0.135† (0 vs. 3)

IQR, interquartile range; *ANOVA; † Pearson's chi-square test with Bonferroni correction; ‡ Mann-Whitney U-test; # Wilcoxon signed-rank test for comparison of BCVA before and after intravitreal antiangiogenic treatment

5.2.6 Nerve fiber layer and macular thinning measured with the RTVue-100 Fourier-domain optical coherence tomograph and the GDx-VCC/ECC scanning laser polarimeter during the course of acute optic neuritis

5.2.6.1 Participants

Between August 2008 and August 2009, 9 eyes of 7 individuals experiencing the first episode of acute ON as the first sign of MS were enrolled in the study within 2 weeks from the onset of the acute visual deterioration. MS was diagnosed according to the standard clinical and neuroimaging methods, and treated according to the international standards (1000 mg methylprednisolone per day intravenously for 3 days) in all cases.[113] If a second episode of acute ON developed in the same eye, data collection was stopped. As a result, the length of follow-up was 12 months for 6 eyes, 9 months for 1 eye, and 6 months for 2 eyes. A control group (9 randomly selected healthy eyes of 9 healthy participants with age similar to that of the patients with MS) was followed for 12 to 19 months, to identify disease-independent measurement variability.

5.2.6.2 Protocol

The following investigations were performed once a week during the first month, biweekly during the second and third months, once per month between the third and sixth months, and then once every third month until the end of follow-up in the ON group, and every sixth month in the control group: determination of BCVA, peripapillary RNFLT measurement and GCC measurement with the RTVue-100 OCT, peripapillary RNFLT measurement with the GDx-VCC and GDx-ECC methods, detailed stereoscopic fundus and ONH evaluation, and automatic threshold perimetry with the Octopus 101 perimeter. ONH stereophotography was performed during the initial visit and at least 2 times during the follow-up. Of the several parameters of the Octopus perimetry report, MD was used to characterize the functional deficit. The demographics of the patients are shown in *Table 8*.

For the determination of the inner retinal thickness in the macula the standard GCC scan was used. In order to avoid incorrect delineation of the ONH border due to optic disc edema in the early phase of ON, the disc margin was defined when it became clearly visible during the follow-up (between the first and third month of follow-up). Then, for RNFLT measurements, the ONH contour line was applied for all images obtained both previously and later during the follow-up, using the software-provided function.

ONH is not determined in SLP, thus optic disc edema does not influence image centering. The software-provided TSS, which automatically calculates the degree of typicality of the retardation pattern, was used to identify ARP. ARP was defined with a TSS value ≤80 on GDx-VCC examination.[28,29] No statistical analysis was performed.

Table 8. Demographics of the participants in the study of investigating RNFL and macular thinning measured with the RTVue-100 OCT and the GDx-VCC/ECC during the course of acute ON

	No 1	**No 2**	**No 3**	**No 4**	**No 5**	**No 6**	**No 7**	**No 8**	**No 9**
ON eyes									
Gender	female	female	female	female	female	female	female	female	female
Age (years)	25	30	30	37	29	32	30	30	47
Eye	left	right	left	right	left	right	left	right	left
MS classification	CIS	CIS	CIS	CIS	ON	CIS	CIS	CIS	CIS
Anterior optic nerve involvement on MRI	yes	no	no	yes	no	yes	no	no	yes
Optic disc edema at initial visit	diffuse	nasal	no	diffuse	no	nasal	no	nasal	diffuse
Time to optic disc decoloration (weeks)	6	8	16	22	12	3	35	no decolo-ration	4
Time between the onset of visual symptoms and initial visit (days)	5	11	7	4	4	4	14	5	11
Length of follow-up (months)	12	12	12	6	12	12	12	6	9
BCVA, first visit	<0.02	0.1	1.0	0.5	0.08	0.02	0.02	0.4	<0.02
BCVA, last visit	0.7	1.0	1.0	0.9	1.0	1.0	1.0	1.0	0.3
VF MD, initial visit (dB)	29.5	9.7	11.6	23.0	12.8	16.2	2.2	2.7	28.0
VF MD, last visit (dB)	1.7	0.9	1.0	0.4	0.9	-0.1	-0.1	-0.1	6.9
GDx-VCC TSS	100	96	94	82	81	80	88	98	85
GDx-ECC TSS	83	100	100	84	91	100	100	100	88
Healthy control eyes									
Gender	male	female	female	female	male	female	male	male	male
Age (years)	18	32	34	47	32	45	34	40	54
Eye	left	right	right	left	right	right	left	left	right
Length of follow-up (months)	19	13	15	12	15	12	16	12	15
BCVA	1.0	1.0	1.0	1.0	1.0	1.0	1.0	1.0	0.9
GDx-VCC TSS	86	100	100	96	91	78	85	100	100
GDx-ECC TSS	97	95	99	100	88	90	100	100	100
VF MD (dB)	-0.3	-1.6	-1.2	-0.3	-1.2	-1.2	-0.5	0.6	1.0

CIS, clinically isolated syndrome

6 RESULTS

6.1 Reproducibility of retinal nerve fiber layer and inner macular thickness measurements of the RTVue-100 Fourier-domain optical coherence tomograph

Image acquisition was successful and image quality met the preset criteria in all 77 eyes. For the 37 hospital-based participants, the diameter of the pupil (mean ± SD) was 2.5 ± 1.0 mm before dilation and 6.1 ± 1.7 mm under pharmacologic mydriasis ($p<0.001$, paired t-test). The mean and SD of the RNFLT and GCC values, intrasession ICC, intratest variability, and intrasession CV for this group are shown in *Table 9*. for undilated and dilated pupil, respectively.

Table 9 shows that before pupil dilation, intrasession CV was 2.20 % for average RNFLT, and the figures for the different quadrants varied between 3.61 % (inferior RNFLT) and 5.69 % (nasal RNFLT). The CV values of the 16 peripapillary sectors varied between 4.90 % (sector 13; inferotemporal) and 11.66 % (sector 15; temporal). The CV values for the superior and inferior GCC were 2.36 % and 1.95 %, respectively. Intrasession ICC varied between 81.2 % (sector 16; temporal) and 99.0 % (average RNFLT and inferior GCC). For average RNFLT and the quadrant RNFLT parameters, intratest variability varied between 3.65 µm (average RNFLT) and 9.13 µm (superior RNFLT). When the measurement series was repeated via dilated pupil, only average RNFLT and sector 9 (nasal) RFNLT increased to a statistically significantly degree (mean change, 0.5 µm [0.6 %] and 0.8 µm [1.5 %], respectively). The other thickness values, the intratest variability, and the CV did not change because of pupil dilation.

When the 3 glaucoma severity groups were analyzed separately, all thickness values, intratest variability, and CV figures were unchanged after pupil dilation, except for superior RNFLT in group 1 (detailed data not shown). The change for superior RNFLT in group 1 was 1.5 µm (1.2 %; $p=0.027$, paired t-test). The SSI for the ONH and GCC scans was 57.0 ± 8.4 and 68.0 ± 7.1 before pupil dilation and 55.7 ± 8.0 and 66.9 ± 6.3 after pupil dilation, respectively ($p=0.052$ and $p=0.058$, paired t-test). Relationship of RNFLT, GCC thickness and measurement reproducibility for the 3 severity groups are shown for each parameter in *Table 10*.

Table 9. Reproducibility of the RTVue-100 OCT measurements calculated for the 37 hospital-based patients and the influence of pupil dilation on the values

Measurements (µm)	Undilated pupil				Dilated pupil				p-value		
	Mean ± SD (µm)	*ICC (%)*	*Intratest variability (µm)*	*CV (%)*	*Mean ± SD (µm)*	*ICC (%)*	*Intratest variability (µm)*	*CV (%)*	*Mean**	*Intratest variability†*	*CV†*
Average RNFLT	84.8±19.0	99.0	3.65	2.20	85.3±19.0	98.9	3.92	2.34	0.017	0.402	0.551
Temporal RNFLT	65.1±16.6	96.1	6.48	5.09	65.3±16.5	96.1	6.53	5.09	0.679	0.446	0.502
Superior RNFLT	103.7±23.3	96.1	9.13	4.50	104.5±23.9	96.6	8.72	4.25	0.107	0.281	0.242
Nasal RNFLT	64.7±14.5	93.9	7.21	5.69	65.3±15.0	95.1	6.66	5.19	0.100	0.815	0.678
Inferior RNFLT	105.6±26.9	98.0	7.43	3.61	106.1±26.3	97.9	7.62	3.66	0.209	0.656	0.769
Sector 1	57.3±19.0	94.3	9.09	8.11	56.9±19.0	95.1	8.43	7.53	0.282	0.982	0.656
Sector 2	79.4±21.4	93.0	11.40	7.34	79.2±21.1	93.6	10.70	6.88	0.689	0.411	0.411
Sector 3	107.9±28.5	96.1	11.14	5.28	108.2±29.2	96.6	10.68	5.03	0.634	0.982	0.815
Sector 4	109.1±27.4	95.3	11.87	5.56	109.9±28.0	94.8	12.78	5.92	0.295	0.815	0.839
Sector 5	96.1±21.3	89.9	13.83	7.35	97.1±21.2	89.9	13.77	7.23	0.138	0.561	0.386
Sector 6	102.1±22.2	91.3	13.31	6.66	102.6±23.3	93.4	12.08	6.00	0.413	0.982	0.946
Sector 7	80.7±20.3	90.2	13.01	8.22	80.7±21.8	92.3	12.27	7.74	0.907	0.521	0.592
Sector 8	55.4±14.4	91.5	8.54	7.86	56.0±14.9	93.5	7.62	6.93	0.141	0.288	0.182
Sector 9	53.4±11.8	92.2	6.68	6.39	54.2±12.1	91.0	7.36	6.91	0.026	0.141	0.288
Sector 10	69.5±14.7	87.5	10.72	7.88	70.4±14.1	89.0	9.59	6.94	0.105	0.723	0.624
Sector 11	98.0±20.2	93.3	10.50	5.48	98.3±19.5	90.7	12.13	6.29	0.671	0.197	0.197
Sector 12	104.8±29.3	96.0	11.60	5.66	105.6±29.2	96.0	11.68	5.63	0.128	0.769	0.700
Sector 13	114.8±35.0	97.5	10.97	4.90	115.6±34.3	97.0	11.82	5.20	0.099	0.667	0.946
Sector 14	104.3±30.6	96.4	11.52	5.66	104.9±30.7	96.6	11.20	5.44	0.386	0.512	0.757
Sector 15	70.5±18.5	83.1	16.06	11.66	71.4±19.2	93.7	9.66	6.90	0.088	0.474	0.446
Sector 16	52.9±12.7	81.2	11.66	11.29	53.5±12.5	91.8	7.23	6.88	0.128	0.757	0.757
Superior GCC	83.4±15.7	98.4	3.87	2.36	83.4±15.4	98.3	3.95	2.41	0.991	0.946	0.934
Inferior GCC	81.3±16.1	99.0	3.11	1.95	81.2±16.3	98.9	3.42	2.15	0.655	0.492	0.361

* Paired t-test; † Wilcoxon signed-rank test

Table 10. Relationship of RNFLT, GCC thickness and measurement reproducibility of the RTVue-100 OCT with different severity of glaucoma

Measurements (µm)	Mean ± SD (µm)			Intratest variability (µm)			CV (%)			p-value		
	Group 1	*Group 2*	*Group 3*	*Group 1*	*Group 2*	*Group 3*	*Group 1*	*Group 2*	*Group 3*	*Mean**	*Intratest variability*†	*CV*†
Average RNFLT	106.7±7.5	75.0±9.4	68.2±4.6	2.91	3.51	4.41	1.39	2.38	3.30	<0.001	0.302	0.006
Temporal RNFLT	81.4±7.8	60.6±12.8	50.3±9.0	5.72	5.09	8.14	3.58	4.27	8.25	<0.001	0.105	0.000
Superior RNFLT	128.8±12.8	94.2±14.0	83.1±7.0	7.01	8.16	11.64	2.76	4.42	7.14	<0.001	0.118	0.000
Nasal RNFLT	80.1±9.1	58.7±9.0	52.3±3.5	7.42	6.95	7.21	4.69	6.03	7.04	<0.001	0.889	0.070
Inferior RNFLT	136.6±12.7	86.5±11.9	86.9±8.6	6.91	7.48	7.90	2.58	4.42	4.64	<0.001	0.780	0.007
Sector 1	73.5±7.3	55.6±16.1	40.1±15.0	9.77	7.50	9.61	6.77	6.89	12.23	<0.001	0.074	0.001
Sector 2	96.9±9.2	74.3±22.1	63.7±16.4	9.26	11.40	13.41	4.86	7.83	10.74	<0.001	0.016	0.000
Sector 3	136.3±12.4	96.5±25.3	85.3±13.4	11.50	9.88	11.80	4.29	5.22	7.06	<0.001	0.230	0.209
Sector 4	139.5±16.5	96.3±12.2	85.4±6.7	10.64	11.03	13.79	3.88	5.84	8.24	<0.001	1.000	0.021
Sector 5	115.1±17.7	89.9±15.3	79.5±9.6	9.72	13.44	17.60	4.30	7.63	11.30	<0.001	0.012	0.000
Sector 6	123.9±14.1	94.6±18.4	83.5±5.2	7.97	15.39	15.81	3.27	8.30	9.66	<0.001	0.026	0.001
Sector 7	101.7±14.0	71.0±13.9	65.2±4.9	11.79	14.57	12.80	5.88	10.47	10.02	<0.001	0.402	0.007
Sector 8	69.4±10.2	51.5±9.6	42.6±5.4	9.70	7.97	7.61	7.08	7.90	9.12	<0.001	0.845	0.065
Sector 9	64.8±8.5	49.9±8.3	43.3±4.6	6.75	6.53	6.75	5.29	6.69	7.95	<0.001	0.435	0.005
Sector 10	84.5±10.2	63.2±9.9	57.9±4.6	9.93	10.92	11.38	5.98	8.81	10.03	<0.001	0.738	0.036
Sector 11	117.6±16.7	83.9±12.9	87.9±7.3	8.94	7.90	13.71	3.88	4.80	7.96	<0.001	0.219	0.002
Sector 12	134.1±22.7	85.6±18.5	88.1±10.9	10.59	9.29	14.28	4.02	5.54	8.27	<0.001	0.451	0.011
Sector 13	155.0±16.3	91.2±15.8	89.3±12.2	11.30	10.95	10.61	3.72	6.12	6.06	<0.001	0.372	0.058
Sector 14	139.0±17.5	84.7±12.3	81.7±9.7	11.92	12.42	10.12	4.38	7.48	6.32	<0.001	0.577	0.079
Sector 15	88.5±16.3	62.1±10.6	57.0±5.2	20.77	9.04	14.95	11.97	7.42	13.38	<0.001	0.112	0.002
Sector 16	65.0±8.1	50.4±8.5	41.0±5.8	15.48	7.55	9.56	12.18	7.65	11.90	<0.001	0.539	0.019
Superior GCC	97.8±5.2	81.5±14.5	68.5±8.8	3.45	4.22	4.00	1.80	2.62	2.98	<0.001	0.615	0.058
Inferior GCC	98.4±5.8	76.0±11.8	66.3±6.3	3.11	3.42	2.83	1.61	2.28	2.18	<0.001	0.867	0.048

* Trend analysis; † Jonckheere-Terpstra test

A significant trend was found for increased CV values in increasing disease severity for most RNFLT and GCC parameters, and a non-significant trend for all but one of the remaining RNFLT and GCC parameters was found. The trend was similar after pupil dilation (detailed data not shown). However, the intrasession CV for average RNFLT was only 3.30 %, and the quadrant RNFLT figures did not exceed 8.25 %, even in the advanced glaucoma group. In contrast, for intratest variability, no similar trend was seen except for 3 of the 16 RNFLT sectors. For average RNFLT, intratest variability was 2.91 µm, 3.51 µm, and 4.41 µm in groups 1, 2, and 3, respectively. For the quadrant RNFLT parameters, the corresponding figures varied between 5.72 and 7.42 µm, 5.09 and 8.16 µm, and 7.21 and 11.64 µm for the respective groups. Intratest variability in the 16 peripapillary sectors ranged between 6.75 and 20.77 µm in group 1, 6.53 and 15.39 µm in group 2, and 6.75 and 17.60 µm in group 3. For the GCC parameters, intratest variability did not exceed 3.45, 4.22, and 4.00 µm in the 3 groups, respectively.

The 40 unselected screening trial participants lacking experience in imaging tests were significantly older than the 37 hospital-based patients with such experience (mean age difference, 7.1 years), but the visual acuity and lens status showed no difference between these 2 groups (*Table 4*). All screening participants were classified as normal based on the result of a detailed clinical examination, including stereoscopic ONH evaluation via dilated pupil. The average and quadrant RNFLT, the GCC, and the intrasession CV values calculated for this healthy group are shown in *Table 11*. The CV values for average, superior, and inferior RNFLT were 1.65 %, 3.18 %, and 2.63 %, respectively.

Table 11. Comparison of thickness and measurement reproducibility of the screening trial participants with the normal and OHT subgroup of the hospital-based patients

Measurement	Screening participants (n=40)		Hospital-based patients (Group 1; n=14)		p-value	
	Mean±SD (µm)	*CV (%)*	*Mean±SD (µm)*	*CV (%)*	*Thickness**	*CV†*
Average RNFLT	103.3±9.6	1.65	106.7±7.5	1.39	0.186	0.836
Temporal RNFLT	76.8±10.8	5.04	81.4±7.8	3.58	0.099	0.567
Superior RNFLT	124.0±13.7	3.18	128.8±12.8	2.76	0.240	0.760
Nasal RNFLT	77.8±10.6	6.09	80.1±9.1	4.69	0.440	0.221
Inferior RNFLT	134.5±14.4	2.63	136.6±12.7	2.58	0.623	0.875
Superior GCC	94.8±8.1	1.84	97.8±5.2	1.80	0.120	0.984
Inferior GCC	96.8±7.3	1.68	98.4±5.8	1.61	0.397	0.920

* Unpaired t-test (equal variances not assumed); † Mann-Whitney U-test

Table 11 also shows that when the 40 screening participants and the normal and OHT subpopulation of the hospital-based patients (group 1) were compared, no statistically significant difference was seen either for the mean thickness values or for the CV values. No influence of age was found on the measurement reproducibility in the healthy screening trial participants (age range, 26 - 79 years; $p>0.05$ for all parameters, Spearman correlation).

Thirty-four of the 37 hospital-based patients returned for a second examination 3 months later. Intersession reproducibility calculated for these patients is shown in *Table 12*. Intratest variability and intrasession CV represented 79.1 % to 98.6 % and 77.1 % to 95.0 % of test-retest variability and intersession CV, respectively. The test-retest variability and the intersession CV were 4.25 µm and 2.64 % for average RNFLT and varied between 6.57 µm and 9.57 µm and 4.06 % and 6.26 % for the RNFLT quadrants, respectively. The corresponding figures for the inferior GCC were 3.93 µm and 2.53 %; and 4.51 µm and 2.81 %, respectively, for the superior GCC.

Table 12. Relationship of within-visit and between-visit reproducibility of the RTVue-100 OCT

Measurement	**Intervisit reproducibility (n=34)**			**Portion of intravisit variability in test-retest variability (%)**	**Portion of intrasession CV in intersession CV (%)**
	ICC (%)	*Test-retest variability (µm)*	*CV (%)*		
Average RNFLT	98.5	4.25	2.64	85.9	83.3
Temporal RNFLT	95.4	6.57	5.36	98.6	95.0
Superior RNFLT	94.9	9.57	4.84	95.4	93.0
Nasal RNFLT	92.6	7.78	6.26	92.7	90.9
Inferior RNFLT	97.1	8.14	4.06	91.3	88.9
Superior GCC	97.9	4.51	2.81	85.8	84.0
Inferior GCC	98.4	3.93	2.53	79.1	77.1

6.2 Comparison of repeatability of retinal nerve fiber layer thickness measurements made using the RTVue-100 Fourier-domain optical coherence tomograph and the GDx-VCC/ECC scanning laser polarimeter

In all 37 eyes image acquisition was successful, and with all methods image quality met the predetermined quality criteria. Mean RNFLT determined with RTVue-100 OCT for the total 360º measuring circle, for the 4 quadrants and for the superotemporal, inferotemporal, and papillomacular sectors was consistently different from that measured with either GDx technique (repeated measures analysis of variance with contrast, $p<0.011$ for all parameters; detailed data not shown). For most RTVue-100 OCT and GDx parameters the SD of RNFLT increased with increasing disease severity. For the RTVue-100 OCT RNFLT measurements, a significant trend for increased CV with increasing disease severity was seen for the 360º average RNFLT, and the superior, inferior and temporal quadrant RNFLT (Jonckheere-Terpstra test, $p<0.007$ for all parameters), but not for the nasal quadrant RNFLT ($p=0.070$) or for the 3 narrower sectors ($p>0.079$ for all sectors). CV calculated for the ONH scan of the RTVue-100 OCT, GDx-VCC and GDx-ECC are shown in *Table 13* to *Table 15*.

Table 13. Repeatability (CV) of the RNFLT measurements with the RTVue-100 OCT, GDx-VCC and GDx-ECC, for the total 360º measuring circle

Total 360º measuring circle	CV (%)			p value*	
	RTVue-100 OCT (1)	*GDx-VCC (2)*	*GDx-ECC (3)*	*1 vs. 2*	*1 vs. 3*
All participants (n=37)	2.11	3.04	3.22	0.044	0.008
Group 1 (n=14)	1.36	1.92	1.68	0.096	0.084
Group 2 (n=11)	2.29	3.76	3.06	0.082	0.075
Group 3 (n=12)	2.84	3.68	5.16	0.583	0.082

* Wilcoxon signed-rank test; p values incorporate Bonferroni correction

Table 13 shows that the mean CV for the RTVue-100 OCT total 360º circle was 2.11 % for all participants, and varied between 1.36 % (mean for group 1: no VF damage) and 2.84 % (mean for group 3: severe glaucoma). *Table 13* also shows that for all participants the CV calculated for the total 360º measuring circle was significantly smaller with RTVue-100 OCT than with GDx-ECC.

Table 14. Repeatability (CV) of RNFLT measurements with RTVue-100 OCT, GDx-VCC and GDx-ECC, for the four peripapillary retina quadrants

Quadrants	CV (%)			p-value*	
	RTVue-100 OCT (1)	*GDx-VCC (2)*	*GDx-ECC (3)*	*1 vs. 2*	*1 vs. 3*
Temporal					
All participants (n=37)	4.88	6.81	7.40	0.022	0.008
Group 1 (n=14)	3.30	5.80	5.88	0.032	0.008
Group 2 (n=11)	4.25	6.96	7.55	0.131	0.082
Group 3 (n=12)	7.29	7.84	9.04	0.583	0.754
Superior					
All participants (n=37)	4.49	4.68	4.94	0.792	0.354
Group 1 (n=14)	2.78	3.30	3.28	0.331	0.221
Group 2 (n=11)	4.26	5.60	4.79	0.286	0.657
Group 3 (n=12)	6.70	5.46	7.00	0.272	0.814
Nasal					
All participants (n=37)	5.33	5.27	6.30	0.613	0.420
Group 1 (n=14)	4.19	4.55	3.76	0.778	0.510
Group 2 (n=11)	5.58	7.06	6.71	0.424	0.248
Group 3 (n=12)	6.43	4.45	8.89	0.071	0.388
Inferior					
All participants (n=37)	3.49	5.20	4.08	0.004	0.331
Group 1 (n=14)	2.37	3.14	2.40	0.198	0.925
Group 2 (n=11)	4.03	6.33	3.73	0.066	0.859
Group 3 (n=12)	4.30	6.56	6.35	0.060	0.071

*Wilcoxon signed-rank test; p values incorporate Bonferroni correction

Table 15. Repeatability (CV) of RNFLT measurements with RTVue-100 OCT, GDx-VCC and GDx-ECC, for the superotemporal, inferotemporal and papillomacular sectors

Sectors	CV (%)			p-value*	
	RTVue-100 OCT (1)	*GDx-VCC (2)*	*GDx-ECC (3)*	*1 vs. 2*	*1 vs. 3*
Superotemporal					
All participants (n=37)	7.39	7.06	6.44	0.331	0.757
Group 1 (n=14)	7.19	4.95	4.30	0.778	0.638
Group 2 (n=11)	6.52	9.16	6.30	0.091	0.722
Group 3 (n=12)	8.41	7.59	9.06	0.937	0.695
Inferotemporal					
All participants (n=37)	7.81	5.74	4.88	0.208	0.099
Group 1 (n=14)	8.70	3.20	2.90	0.041	0.112
Group 2 (n=11)	7.32	7.34	4.40	0.657	0.091
Group 3 (n=12)	7.23	7.24	7.63	0.530	0.638
Papillomacular					
All participants (n=37)	9.53	8.56	10.24	0.712	0.288
Group 1 (n=14)	6.70	7.75	10.05	0.177	0.124
Group 2 (n=11)	10.58	9.27	9.21	0.790	0.657
Group 3 (n=12)	11.88	8.86	11.40	0.638	0.530

* Wilcoxon signed-rank test; p values incorporate Bonferroni correction

Table 14 illustrates that for all participants together, and for group 1, the CV for the temporal quadrant was significantly smaller with RTVue-100 OCT than with GDx-ECC, and tended to be smaller than with GDx-VCC. For all participants, repeatability for the inferior quadrant was also significantly better with RTVue-100 OCT than with GDx-VCC. For the other quadrants no difference for measurement repeatability was seen between RTVue-100 OCT and GDx-VCC or GDx-ECC.

The CV values calculated for the 3 smaller sectors of clinical interest are presented in *Table 15*. No significant difference was seen for these sectors when comparing figures calculated for RTVue-100 OCT and either GDx method.

Classification of the study eyes ("normal" vs. "glaucomatous") was in agreement using all methods for eyes in group 1 ("normal" in 14 of 14 eyes) and in group 3 ("glaucomatous" in 12 of 12 eyes), and for all but 1 eye in group 2 ("glaucomatous" in 10 of 11 eyes). The remaining eye in group 2 was classified as "normal" with both GDx compensation techniques, but as "glaucomatous" with RTVue-100 OCT ("borderline" RNFLT in the inferior quadrant and inferotemporal sector). In this eye, clinically a localized inferotemporal glaucomatous neuroretinal rim thinning with a corresponding, isolated, retinal nerve fiber bundle defect was seen.

6.3 Diagnostic accuracy of retinal nerve fiber layer, inner macular thickness and optic disc measurements made with the RTVue-100 Fourier-domain optical coherence tomograph to detect glaucoma

The age of the perimetric glaucoma group was higher than that of the healthy participants and OHT group (*Table 5*, ANOVA, $p<0.01$, Tukey post hoc test, $p<0.003$ for both comparisons). For the other comparisons no significant age difference was seen. All images met the pre-defined SSI criterion and were analyzed.

Comparison of the different RNFLT, GCC and ONH values between the patient groups is shown in *Table 16*. Superior RNFLT and RNFLT sector ST1 were significantly thinner for the OHT eyes than for the healthy eyes. For the other group comparisons most RNFLT, GCC and ONH parameters differed significantly between the groups, showing decreasing RNFLT, GCC thickness and rim area values, and increasing cup area and cup/disc area ratio with increasing disease severity categories.

Diagnostic performance of the software-provided classification is shown in *Table 17*, for each disease category and parameter, respectively. When “borderline” and “outside normal limits” classifications were grouped together (both considered abnormal), specificity was high (94.6 - 100 %) for most RNFLT and GCC parameters, and low (72.0 - 76.3 %) for the ONH parameters, in all analyses. For all parameters, sensitivity did not exceed 27.8 % when discrimination of OHT and healthy eyes was investigated. Sensitivity for detection of preperimetric glaucoma varied between 73.9 and 76.1 % for the ONH parameters, but only between 6.5 % (RNFLT sector NL1 and superior GCC) and 37.0 % (superior RNFLT and RNFLT sector ST2) for the other parameters. For detection of perimetric glaucoma, GCC FLV showed the best sensitivity (92.8 %). Sensitivity of average RNFLT was 83.8 %. When discrimination of all preperimetric and perimetric glaucoma eyes from healthy eyes was evaluated, sensitivity varied between 66.2 and 69.4 % for average RNFLT and the RNFLT quadrants, 17.2 and 71.3 % for the RNFLT sectors, 52.2 and 72.0 % for the GCC parameters, and 82.2 and 84.1 % for the ONH parameters.

Considering the whole population (*Table 18*), the sensitivity values did not exceed 73.6 % for the ONH parameters, and 62.7 % for the other parameters. PPV varied between 84.5 and 86.3 % for the ONH parameters whereas 92.4 and 100 % for the RNFLT and GCC parameters. The highest NPV value (56.8 %) was found for the ONH parameters. PLR was higher than 10 for average, inferior and superior RNFLT (25.5 to infinite), 12 of the 16 RNFLT sectors (12.6 to infinite), and three of the four GCC parameters (40.0 - 48.6). No ONH parameter had a PLR higher than 3.0. The NLR values varied between 0.4 and 0.9. When “borderline” and “within normal limits” classifications were grouped together (all considered normal), specificity was similar to that in the other grouping, but sensitivity was considerably lower (detailed data are not shown).

Table 16. Comparison of the different RNFLT, GCC and ONH parameters of the RTVue-100 OCT between the patient groups

	Healthy (0)		**OHT (1)**		**Preperimetric glaucoma (2)**		**Perimetric glaucoma (3)**		**p-values***					
	Mean	*SD*	*Mean*	*SD*	*Mean*	*SD*	*Mean*	*SD*	*0 vs. 1*	*0 vs. 2*	*0 vs. 3*	*1 vs. 2*	*1 vs. 3*	*2 vs. 3*
Main RNFLT parameters (µm)														
Average	106.5	9.1	102.0	10.7	94.9	12.3	74.9	12.0	0.173	<0.001	<0.001	0.021	<0.001	<0.001
Temporal	77.9	10.4	76.8	10.2	69.9	9.7	55.8	13.4	0.964	0.001	<0.001	0.039	<0.001	<0.001
Superior	132.8	15.1	123.5	15.8	114.3	19.5	91.8	16.7	0.023	<0.001	<0.001	0.062	<0.001	<0.001
Nasal	80.0	10.2	77.1	13.3	75.3	11.5	60.1	11.9	0.572	0.107	<0.001	0.895	<0.001	<0.001
Inferior	135.1	14.5	130.7	19.9	120.2	18.6	92.1	15.9	0.518	<0.001	<0.001	0.024	<0.001	<0.001
RNFLT sectors (µm)														
TU1	69.1	10.0	68.8	8.3	63.0	9.3	48.6	16.0	0.999	0.034	<0.001	0.164	<0.001	<0.001
TU2	95.1	15.3	91.0	12.0	81.6	15.4	65.0	18.5	0.590	<0.001	<0.001	0.046	<0.001	<0.001
ST2	134.5	21.2	125.3	17.6	113.4	24.2	88.6	21.4	0.128	<0.001	<0.001	0.062	<0.001	<0.001
ST1	148.0	21.0	133.9	24.6	126.8	21.0	95.4	20.2	0.004	<0.001	<0.001	0.428	<0.001	<0.001
SN1	123.8	19.0	116.6	24.1	107.0	23.9	89.4	18.1	0.270	<0.001	<0.001	0.143	<0.001	<0.001
SN2	124.9	17.8	118.1	15.6	109.8	21.6	93.6	18.3	0.244	<0.001	<0.001	0.179	<0.001	<0.001
NU2	97.2	13.6	92.0	19.0	90.7	14.9	71.0	15.2	0.309	0.084	<0.001	0.978	<0.001	<0.001
NU1	69.8	9.5	67.8	14.7	65.3	13.7	51.4	11.7	0.809	0.147	<0.001	0.786	<0.001	<0.001
NL1	66.9	9.7	64.2	13.0	63.0	10.8	50.6	11.0	0.601	0.192	<0.001	0.954	<0.001	<0.001
NL2	86.3	14.1	84.5	13.6	82.4	13.6	67.6	14.1	0.918	0.415	<0.001	0.904	<0.001	<0.001
IN2	117.8	18.3	114.6	18.6	107.1	20.5	92.3	16.4	0.802	0.006	<0.001	0.244	<0.001	<0.001
IN1	135.8	21.7	130.7	27.9	121.0	24.9	94.7	20.5	0.655	0.002	<0.001	0.220	<0.001	<0.001
IT1	152.7	18.9	145.6	30.3	134.2	24.0	95.0	22.5	0.397	<0.001	<0.001	0.113	<0.001	<0.001
IT2	134.1	21.1	131.7	23.0	118.5	24.6	86.4	16.8	0.931	<0.001	<0.001	0.021	<0.001	<0.001
TL2	85.6	16.4	85.1	17.4	77.4	14.3	62.1	13.8	0.997	0.016	<0.001	0.111	<0.001	<0.001
TL1	61.6	8.6	62.3	10.4	57.6	7.1	47.6	13.2	0.988	0.160	<0.001	0.199	<0.001	<0.001
GCC parameters														
Average (µm)	97.9	6.7	95.3	7.0	91.8	7.0	75.0	12.8	0.817	0.536	<0.001	0.989	<0.001	<0.001
Superior (µm)	98.3	7.2	95.3	8.9	92.0	8.4	74.3	14.9	0.521	0.010	<0.001	0.546	<0.001	<0.001
Inferior (µm)	97.5	6.7	95.2	6.4	91.5	6.8	75.6	13.7	0.665	0.006	<0.001	0.348	<0.001	<0.001
FLV (%)	1.0	1.6	1.9	2.8	1.4	1.4	7.9	4.3	0.369	0.826	<0.001	0.884	<0.001	<0.001
ONH parameters														
Cup area (mm2)	0.842	0.540	0.801	0.530	1.486	0.493	1.603	0.556	0.980	<0.001	<0.001	<0.001	<0.001	0.600
Cup/disc area ratio	0.416	0.233	0.417	0.214	0.696	0.121	0.819	0.177	1.000	<0.001	<0.001	<0.001	<0.001	0.002
Rim area (mm2)	1.113	0.468	0.962	0.304	0.627	0.265	0.334	0.314	0.150	<0.001	<0.001	<0.001	<0.001	<0.001

* Tukey post hoc test (ANOVA<0.01 for all parameters)

Table 17. Sensitivity and specificity of the software-provided classification of the RTVue-100 OCT for detection of the different disease categories, for each parameter, respectively; for the analysis "borderline" and "outside normal limits" classifications were grouped together as abnormal results

	Normal vs. OHT		**Normal vs. Preperimetric glaucoma**		**Normal vs. Perimetric glaucoma**		**Normal vs. Preperimetric and Perimetric glaucoma**	
	Sensitivity (%) (95 % CI)	*Specificity (%) (95 % CI)*	*Sensitivity (%) (95 % CI)*	*Specificity (%) (95 % CI)*	*Sensitivity (%) (95 % CI)*	*Specificity (%) (95 % CI)*	*Sensitivity (%) (95 % CI)*	*Specificity (%) (95 % CI)*
Main RNFLT parameters (µm)								
Average	8.3 (0.5-63.0)	100.0 (96.0-100.0)	34.8 (16.6-58.9)	100.0 (96.0-100.0)	83.8 (75.0-89.9)	100.0 (96.0-100.0)	69.4 (60.2-77.3)	100.0 (96.0-100.0)
Superior	8.3 (0.5-63.0)	100.0 (96.0-100.0)	37.0 (18.5-60.2)	100.0 (96.0-100.0)	78.4 (68.6-85.7)	100.0 (96.0-100.0)	66.2 (56.7-74.6)	100.0 (96.0-100.0)
Inferior	5.6 (0.2-69.4)	97.8 (92.4-99.4)	23.9 (7.9-53.4)	97.8 (92.4-99.4)	83.8 (75.0-89.9)	97.8 (92.4-99.4)	66.2 (56.7-74.6)	97.8 (92.4-99.4)
RNFLT sectors (µm)								
TU1	2.8 (0.0-80.5)	94.6 (87.8-97.7)	13.0 (2.0-53.0)	94.6 (87.8-97.7)	67.6 (56.3-77.1)	94.6 (87.8-97.7)	51.6 (40.9-62.2)	94.6 (87.8-97.7)
TU2	5.6 (0.2-69.4)	96.8 (90.8-98.9)	32.6 (14.7-57.6)	96.8 (90.8-98.9)	74.8 (64.5-82.9)	96.8 (90.8-98.9)	62.4 (52.5-71.4)	96.8 (90.8-98.9)
ST2	8.3 (0.5-63.0)	95.7 (89.3-98.3)	37.0 (18.5-60.2)	95.7 (89.3-98.3)	76.6 (66.5-84.3)	95.7 (89.3-98.3)	65.0 (55.3-73.5)	95.7 (89.3-98.3)
ST1	5.6 (0.2-69.4)	96.8 (90.8-98.9)	17.4 (3.9-52.0)	96.8 (90.8-98.9)	65.8 (54.3-75.6)	96.8 (90.8-98.9)	51.6 (40.9-62.2)	96.8 (90.8-98.9)
SN1	2.8 (0.0-80.5)	100.0 (96.0-100.0)	19.6 (5.1-52.2)	100.0 (96.0-100.0)	31.5 (18.6-48.1)	100.0 (96.0-100.0)	28.0 (16.9-42.6)	100.0 (96.0-100.0)
SN2	0.0 (0.0-9.7)	100.0 (96.0-100.0)	15.2 (2.9-52.2)	100.0 (96.0-100.0)	40.5 (27.5-55.1)	100.0 (96.0-100.0)	33.1 (21.9-46.7)	100.0 (96.0-100.0)
NU2	2.8 (0.0-80.5)	100.0 (96.0-100.0)	8.7 (0.7-57.2)	100.0 (96.0-100.0)	35.1 (22.1-50.8)	100.0 (96.0-100.0)	27.4 (16.3-42.1)	100.0 (96.0-100.0)
NU1	0.0 (0.0-9.7)	100.0 (96.0-100.0)	10.9 (1.2-54.5)	100.0 (96.0-100.0)	39.6 (26.6-54.4)	100.0 (96.0-100.0)	31.2 (20.0-45.1)	100.0 (96.0-100.0)
NL1	0.0 (0.0-9.7)	100.0 (96.0-100.0)	6.5 (0.3-61.6)	100.0 (96.0-100.0)	39.6 (26.6-54.4)	100.0 (96.0-100.0)	29.9 (18.8-44.1)	100.0 (96.0-100.0)
NL2	0.0 (0.0-9.7)	97.8 (92.4-99.4)	8.7 (0.7-57.2)	97.8 (92.4-99.4)	27.0 (14.4-44.8)	97.8 (92.4-99.4)	21.7 (11.1-38.0)	97.8 (92.4-99.4)
IN2	0.0 (0.0-9.7)	98.9 (94.1-99.8)	10.9 (1.2-54.5)	98.9 (94.1-99.8)	19.8 (8.3-40.3)	98.9 (94.1-99.8)	17.2 (7.4-35.2)	98.9 (94.1-99.8)
IN1	8.3 (0.5-63.0)	98.9 (94.1-99.8)	15.2 (2.9-52.2)	98.9 (94.1-99.8)	46.8 (34.0-60.2)	98.9 (94.1-99.8)	37.6 (26.3-50.3)	98.9 (94.1-99.8)
IT1	19.4 (4.3-56.2)	97.8 (92.4-99.4)	30.4 (12.9-56.4)	97.8 (92.4-99.4)	88.3 (80.4-93.3)	97.8 (92.4-99.4)	71.3 (62.4-78.9)	97.8 (92.4-99.4)
IT2	8.3 (0.5-63.0)	95.7 (89.3-98.3)	32.6 (14.7-57.6)	95.7 (89.3-98.3)	79.3 (69.7-86.4)	95.7 (89.3-98.3)	65.6 (56.0-74.1)	95.7 (89.3-98.3)
TL2	2.8 (0.0-80.5)	95.7 (89.3-98.3)	10.9 (1.2-54.5)	95.7 (89.3-98.3)	47.7 (34.9-60.9)	95.7 (89.3-98.3)	36.9 (25.7-49.8)	95.7 (89.3-98.3)
TL1	5.6 (0.2-69.4)	94.6 (87.8-97.7)	8.7 (0.7-57.2)	94.6 (87.8-97.7)	51.4 (38.7-63.8)	94.6 (87.8-97.7)	38.9 (27.6-51.4)	94.6 (87.8-97.7)
GCC parameters								
Average (µm)	8.3 (0.5-63.0)	98.9 (94.1-99.8)	15.2 (2.9-52.2)	98.9 (94.1-99.8)	74.8 (64.5-82.9)	98.9 (94.1-99.8)	57.3 (47.0-67.0)	98.9 (94.1-99.8)
Superior (µm)	5.6 (0.2-69.4)	98.9 (94.1-99.8)	6.5 (0.3-61.6)	98.9 (94.1-99.8)	71.2 (60.4-80.0)	98.9 (94.1-99.8)	52.2 (41.6-62.7)	98.9 (94.1-99.8)
Inferior (µm)	13.9 (1.9-57.3)	98.9 (94.1-99.8)	17.4 (3.9-52.0)	98.9 (94.1-99.8)	80.2 (70.7-87.1)	98.9 (94.1-99.8)	61.8 (51.8-70.8)	98.9 (94.1-99.8)
FLV (%)	22.2 (5.9-56.6)	89.1 (80.6-94.2)	21.7 (6.5-52.7)	89.1 (80.6-94.2)	92.8 (86.1-96.4)	89.1 (80.6-94.2)	72.0 (63.1-79.4)	89.1 (80.6-94.2)
ONH parameters								
Cup area (mm2)	27.8 (9.6-58.3)	76.3 (65.3-84.7)	73.9 (57.3-85.7)	76.3 (65.3-84.7)	85.6 (77.1-91.3)	76.3 (65.3-84.7)	82.2 (74.7-87.8)	76.3 (65.3-84.7)
Cup/disc area ratio	27.8 (9.6-58.3)	72.0 (60.3-81.4)	76.1 (59.8-87.2)	72.0 (60.3-81.4)	87.4 (79.3-92.6)	72.0 (60.3-81.4)	84.1 (76.9-89.3)	72.0 (60.3-81.4)
Rim area (mm2)	27.8 (9.6-58.3)	76.3 (65.3-84.7)	73.9 (57.3-85.7)	76.3 (65.3-84.7)	85.6 (77.1-91.3)	76.3 (65.3-84.7)	82.2 (74.7-87.8)	76.3 (65.3-84.7)

Table 18. Sensitivity, specificity, PPV, NPV, PLR and NLR of the software-provided classification of the RTVue-100 OCT for detection of glaucoma in the total study population (n=286), for each parameter, respectively; for the analysis "borderline" and "outside normal limits" classifications were grouped together as abnormal results

	Normal vs. OHT, Preperimetric and Perimetric glaucoma					
	Sensitivity (%) (95 % CI)	*Specificity (%) (95 % CI)*	*PPV (%) (95 % CI)*	*NPV (%) (95 % CI)*	*PLR (95 % CI)*	*NLR (95 % CI)*
Main RNFLT parameters (µm)						
Average	58.0 (48.8-66.8)	100.0 (96.0-100.0)	100.0 (96.7-100.0)	53.4 (43.4-63.2)	Infinite	0.4 (0.3-0.5)
Superior	55.4 (46.0-64.5)	100.0 (96.0-100.0)	100.0 (96.5-100.0)	52.0 (41.9-61.8)	Infinite	0.4 (0.4-0.6)
Inferior	54.9 (45.4-64.1)	97.8 (92.4-99.4)	98.1 (93.4-99.5)	51.1 (41.0-61.1)	25.5 (6.3-103.2)	0.5 (0.4-0.6)
RNFLT sectors (µm)						
TU1	42.5 (32.4-53.3)	94.6 (87.8-97.7)	94.3 (87.0-97.6)	44.2 (34.3-54.6)	7.9 (3.2-19.7)	0.6 (0.5-0.7)
TU2	51.8 (42.1-61.4)	96.8 (90.8-98.9)	97.1 (91.7-99.0)	49.2 (39.1-59.3)	16.1 (5.1-50.6)	0.5 (0.4-0.6)
ST2	54.4 (44.9-63.6)	95.7 (89.3-98.3)	96.3 (90.8-98.6)	50.3 (40.1-60.4)	12.6 (4.7-34.2)	0.5 (0.4-0.6)
ST1	43.0 (32.9-53.7)	96.8 (90.8-98.9)	96.5 (90.1-98.8)	45.0 (35.1-55.3)	13.3 (4.2-42.5)	0.6 (0.5-0.7)
SN1	23.3 (13.4-37.5)	100.0 (96.0-100.0)	100.0 (92.1-100.0)	38.6 (29.3-48.7)	Infinite	0.8 (0.7-0.9)
SN2	26.9 (16.8-40.3)	100.0 (96.0-100.0)	100.0 (93.1-100.0)	39.7 (30.4-49.9)	Infinite	0.7 (0.6-0.9)
NU2	22.8 (12.9-37.1)	100.0 (96.0-100.0)	100.0 (92.0-100.0)	38.4 (29.2-48.6)	Infinite	0.8 (0.7-0.9)
NU1	25.4 (15.3-39.0)	100.0 (96.0-100.0)	100.0 (92.7-100.0)	39.2 (29.9-49.4)	Infinite	0.7 (0.6-0.9)
NL1	24.4 (14.3-38.2)	100.0 (96.0-100.0)	100.0 (92.4-100.0)	38.9 (29.6-49.1)	Infinite	0.8 (0.6-0.9)
NL2	17.6 (8.3-33.5)	97.8 (92.4-99.4)	94.4 (81.4-98.5)	36.4 (27.3-46.7)	8.2 (1.7-39.2)	0.8 (0.7-1.0)
IN2	14.0 (5.4-31.5)	98.9 (94.1-99.8)	96.4 (81.9-99.4)	35.7 (26.6-45.8)	13.0 (1.5-114.1)	0.9 (0.7-1.0)
IN1	32.1 (21.8-44.5)	98.9 (94.1-99.8)	98.4 (91.5-99.7)	41.3 (31.7-51.5)	29.9 (4.1-219.2)	0.7 (0.6-0.8)
IT1	61.7 (52.7-69.9)	97.8 (92.4-99.4)	98.3 (94.1-99.5)	55.2 (44.9-65.0)	28.7 (7.1-115.5)	0.4 (0.3-0.5)
IT2	54.9 (45.4-64.1)	95.7 (89.3-98.3)	96.4 (90.9-98.6)	50.6 (40.4-60.7)	12.8 (4.7-34.5)	0.5 (0.4-0.6)
TL2	30.6 (20.3-43.2)	95.7 (89.3-98.3)	93.7 (84.4-97.6)	39.9 (30.4-50.3)	7.1 (2.5-20.4)	0.7 (0.6-0.9)
TL1	32.6 (22.4-44.9)	94.6 (87.8-97.7)	92.6 (83.5-96.9)	40.4 (30.7-50.8)	6.1 (2.4-15.6)	0.7 (0.6-0.9)
GCC parameters						
Average (µm)	48.2 (38.3-58.2)	98.9 (94.1-99.8)	98.9 (94.2-99.8)	47.6 (37.7-57.8)	44.3 (6.2-318.3)	0.5 (0.4-0.6)
Superior (µm)	43.5 (33.4-54.2)	98.9 (94.1-99.8)	98.8 (93.6-99.8)	45.5 (35.7-55.7)	40.0 (5.6-288.6)	0.6 (0.5-0.7)
Inferior (µm)	52.8 (43.2-62.3)	98.9 (94.1-99.8)	99.0 (94.7-99.8)	50.0 (39.9-60.1)	48.6 (6.8-348.2)	0.5 (0.4-0.6)
FLV (%)	62.7 (53.8-70.8)	89.1 (80.6-94.2)	92.4 (86.2-95.9)	53.2 (42.5-63.7)	5.8 (3.1-10.9)	0.4 (0.3-0.5)
ONH parameters						
Cup area (mm2)	72.0 (64.0-78.8)	76.3 (65.3-84.7)	86.3 (79.6-91.1)	56.8 (45.2-67.7)	3.0 (2.0-4.7)	0.4 (0.3-0.5)
Cup/disc area ratio	73.6 (65.8-80.1)	72.0 (60.3-81.4)	84.5 (77.7-89.6)	56.8 (44.9-68.0)	2.6 (4.7-3.9)	0.4 (0.3-0.5)
Rim area (mm2)	72.0 (64.0-78.8)	76.3 (65.3-84.7)	86.3 (79.6-91.1)	56.8 (45.2-67.7)	3.0 (2.0-4.7)	0.4 (0.3-0.5)

6.4 Comparison of clinical diagnostic usefulness of retinal nerve fiber layer thickness measurements made using the RTVue-100 Fourier-domain optical coherence tomograph and the GDx-VCC/ECC scanning laser polarimeter

The normal, OHT, preperimetric and perimetric glaucoma eyes represented 28.3 %, 15.8 %, 18.6 % and 37.3 % of the tested eyes, respectively (*Table 6*). Of the 66 glaucoma eyes 26 (39.4 %) had mild, 19 (28.8 %) moderate and 21 (31.8 %) advanced VF damage. Image acquisition was successful in all eyes, and with all methods image quality met the predetermined quality criteria. An ARP was seen in 50 eyes (28.3 %). Sensitivity and specificity calculated for the different parameters are shown in *Table 19* and *Table 20*. When the software-provided "borderline" and "outside normal limits" classifications were grouped together as pathological results against "within normal limits" classification (*Table 19*), the sensitivity and specificity values determined for average, superior and inferior RNFLT ranged 63.6 to 65.7 % and 97.4 to 98.7 % for RTVue-100 OCT, 49.5 to 58.6 % and 92.3 to 96.2 % for GDx-VCC, and 56.6 to 60.6 % and 94.9 to 97.4 % for GDx-ECC, respectively. For average RNFLT, RTVue-100 OCT was more sensitive than GDx-VCC ($p=0.002$). For the other comparisons no difference was found.

For the different localized nerve fiber bundle defect parameters, sensitivity varied between 67.7 % and 83.8 % with RTVue-100 OCT, 33.3 % and 55.6 % with GDx-VCC, and 28.3 % and 57.6 % with GDx-ECC ($p<0.001$ for all comparisons). The corresponding specificity values ranged 84.6 to 93.6 % for RTVue-100 OCT, 96.2 to 100 % for GDx-VCC, and 98.7 to 100 % for GDx-ECC, respectively. When glaucoma was defined with presence of any nerve fiber bundle defect, both GDx methods were more specific than RTVue-100 OCT ($p\leq0.004$). For the other nerve fiber bundle defect parameters no difference was found.

Table 19. Sensitivity and specificity calculated for the different corresponding RNFLT parameters determined with RTVue-100 OCT, GDx-VCC and GDx-ECC, respectively; for the analysis the instrument-provided "borderline" and "outside normal limits" classifications were grouped together and considered as glaucomatous, and were analyzed against the instrument-provided "within normal limits" classification

	Sensitivity (95 % CI) (%)			**p-value***		**Specificity (95 % CI) (%)**			**p-value***	
	RTVue-100 OCT (1)	*GDx-VCC (2)*	*GDx-ECC (3)*	*1 vs. 2*	*1 vs. 3*	*RTVue-100 OCT (1)*	*GDx-VCC (2)*	*GDx-ECC (3)*	*1 vs. 2*	*1 vs. 3*
Average RNFLT	65.7 (55.9-74.3)	49.5 (39.9-59.2)	60.6 (50.8-69.7)	0.002	0.267	98.7 (93.1-99.8)	96.2 (89.3-98.7)	96.2 (89.3-98.7)	0.500	0.500
Superior RNFLT	64.6 (54.9-73.4)	58.6 (48.7-67.8)	57.6 (47.7-66.9)	0.210	0.143	98.7 (93.1-99.8)	92.3 (84.2-96.4)	94.9 (87.5-98.0)	0.063	0.250
Inferior RNFLT	63.6 (53.8-72.4)	55.6 (45.8-65.0)	56.6 (46.7-65.9)	0.229	0.167	97.4 (91.1-99.3)	94.9 (87.5-98.0)	97.4 (91.1-99.3)	0.687	1.000
Superotemporal bundle defect	67.7 (58.0-76.1)	33.3 (24.8-43.1)	28.3 (20.4-37.8)	<0.001	<0.001	91.0 (82.6-95.6)	96.2 (89.3-98.7)	98.7 (93.1-99.8)	0.125	0.031
Inferotemporal bundle defect	78.8 (69.7-85.7)	43.4 (34.1-53.3)	48.5 (38.9-58.2)	<0.001	<0.001	93.6 (85.9-97.2)	100 (95.3-100)	100 (95.3-100)	0.063	0.063
Any bundle defect	83.8 (75.4-89.8)	55.6 (45.8-65.0)	57.6 (47.7-66.9)	<0.001	<0.001	84.6 (75.0-91.0)	96.2 (89.3-98.7)	98.7 (93.1-99.8)	0.004	0.001
Any bundle defect or decreased average RNFLT	84.8 (76.5-90.6)	62.6 (52.8-71.5)	72.7 (50.4-67.2)	<0.001	<0.001	84.6 (75.0-91.0)	94.9 (87.5-98.0)	96.2 (92.9-100)	0.021	0.012
Any bundle defect and decreased average RNFLT	64.6 (54.9-73.4)	42.4 (33.2-52.3)	45.5 (28.4-44.9)	<0.001	<0.001	98.7 (93.1-99.8)	97.4 (91.1-99.3)	98.7 (92.9-100)	1.000	1.000
NFI	-	68.7 (59.0-77.0)	64.3 (54.4-73.1)	-	-	-	97.4 (91.1-99.3)	98.7 (93.1-99.8)	-	-

* McNemar's (binomial) test

When glaucoma was defined as presence of any bundle defect or a decreased average RNFLT, for GDx-VCC and GDx-ECC specificity did not change but sensitivity increased to 62.6 % and 72.7 %, respectively. No increase of sensitivity or specificity was found with RTVue-100 OCT. For this parameter, RTVue-100 OCT was more sensitive than any GDx-method ($p<0.001$ for both comparisons) without being less specific than those. When glaucoma was defined as presence of any bundle defect and a decreased average RNFLT, all methods were similarly highly specific (97.4 to 98.7 %, $p=1.000$), but the sensitivity was higher (64.6 %) for RTVue-100 OCT than GDx-VCC (42.4 %) or GDx-ECC (45.5 %, $p<0.001$ for both comparisons). Sensitivity and specificity of GDx-VCC NFI and GDx-ECC NFI were similar to those found for average, superior and inferior RNFLT of RTVue-100 OCT.

Agreement of classification between the methods was investigated for parameters which showed favorable diagnostic performance in the current investigation, represent the health or damage of the global peripapillary RNFL, and are indicated on the standard instrument reports (average RNFLT for RTVue-100 OCT and NFI for GDx-VCC and GDx-ECC). Using these parameters, of the 99 preperimetric and perimetric glaucoma eyes 73 (73.7 %) were identified with at least one technique. Of these 73 eyes 57 (78.1 %) were detected by all methods, 64 (87.7 %) by at least one of the GDx techniques and RTVue-100 OCT, 1 (1.4 %) by RTVue-100 OCT only, and 8 (11.0 %) by at least one of the GDx methods only (*Figure 7*). The kappa measure of agreement between RTVue-100 OCT average RNFLT and NFI was 0.84 (95 % CI: 0.76 - 0.91) for GDx-VCC and 0.85 (95 % CI: 0.77 - 0.93) for GDx-ECC.

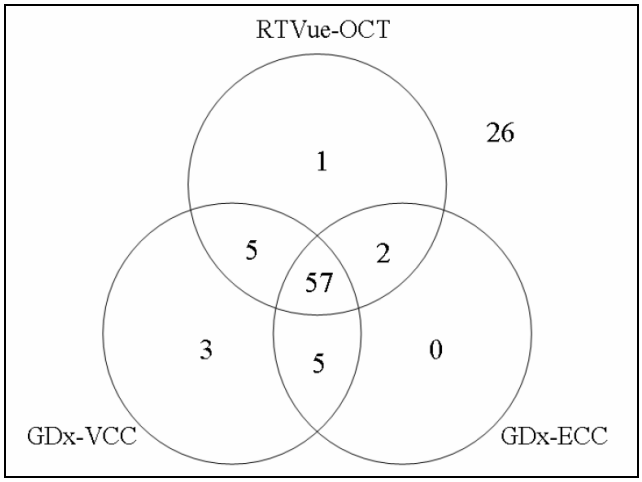

Figure 7. A Venn diagram showing the distribution of glaucomatous eyes classified as having RNFLT damage by average RNFLT of RTVue-100 OCT, and NFI of GDx-VCC and GDx-ECC, respectively

When the software-provided "within normal limits" and "borderline" classifications were grouped together against "outside normal limits" classification, for the main RNFLT sectors specificity was only minimally higher, but sensitivity was considerably lower than the corresponding values calculated for the other grouping, for all methods (*Table 20*).No significant difference between the methods was found for any parameter in this grouping.

Table 20. Sensitivity and specificity calculated for the corresponding main RNFLT parameters determined with RTVue-OCT, GDx-VCC and GDx-ECC, respectively, when the instrument-provided "within normal limits" and "borderline" classifications were grouped together and considered as healthy, and were analyzed against the instrument-provided "outside normal limits" classification.

	RTVue-100 OCT (1)	**GDx-VCC (2)**	**GDx-ECC (3)**	**p-value***	
				1 vs. 2	*1 vs. 3*
Sensitivity (95 % CI) (%)					
Average RNFLT	53.5 (43.8-63.1)	42.4 (33.2-52.3)	51.5 (41.8-61.1)	0.052	0.824
Superior RNFLT	48.5 (38.9-58.2)	50.5 (40.8-60.2)	48.5 (38.9-58.2)	0.824	1.000
Inferior RNFLT	50.5 (40.8-60.2)	41.4 (32.2-51.3)	44.4 (35.0-54.3)	0.122	0.307
Specificity (95 % CI) (%)					
Average RNFLT	98.7 (93.1-99.8)	97.4 (91.1-99.3)	98.7 (93.1-99.8)	1.000	1.000
Superior RNFLT	98.7 (93.1-99.8)	96.2 (89.3-98.7)	97.4 (91.1-99.3)	0.500	1.000
Inferior RNFLT	100 (95.3-100)	98.7 (93.1-99.8)	100 (95.3-100)	1.000	1.000

* McNemar's (binomial) test

6.5 Influence of age-related macular degeneration on inner macular thickness measurements made with RTVue-100 Fourier-domain optical coherence tomograph

Compared to the age-matched controls, no difference in any RNFLT and ONH parameter value was seen for any AMD group (*Table 21*). The software-provided classification was "within normal limits" for these parameters in almost all eyes. No significant difference in classification of these parameters was seen between any of the AMD groups and the normal group (Pearson's chi-square test, $p>0.05$ for all comparisons, detailed data are not shown).

Table 21. Comparison of RNFLT and ONH parameters between the control group and each of the AMD groups

	Control (0; n=25)	Drusen (1; n=19)	CNV (2; n=16)	CNV-anti-VEGF (3; n=19)	p-value
RNFLT parameters (µm, mean±SD)					
Superior	130.93±14.41	134.35±13.33	130.82±15.81	129.32±13.54	0.737*
Inferior	137.96±14.02	144.06±16.20	135.20±13.94	135.44±17.37	0.273*
Average	107.14±8.30	111.15±8.98	107.06±10.15	106.74±10.46	0.420*
Sector 1	71.29±9.53	72.77±11.29	68.04±9.74	71.50±11.56	0.603*
Sector 2	96.90±11.93	97.38±14.71	94.18±13.71	99.10±15.43	0.774*
Sector 3	131.95±15.51	132.04±17.86	131.61±19.45	131.40±17.93	0.999*
Sector 4	145.17±21.62	148.59±17.95	142.53±22.16	136.27±17.62	0.278*
Sector 5	121.99±19.26	128.98±17.77	127.16±21.10	122.70±20.20	0.609*
Sector 6	124.48±17.20	127.65±19.40	121.94±15.98	126.85±15.82	0.759*
Sector 7	96.92±15.47	104.12±12.80	96.25±14.34	100.37±17.30	0.355*
Sector 8	70.04±10.76	75.77±12.96	75.37±14.06	75.64±12.13	0.330*
Sector 9	66.32±9.38	71.58±14.17	72.62±13.81	70.95±12.11	0.338*
Sector 10	85.68±12.60	94.28±15.20	91.28±14.59	89.72±18.82	0.316*
Sector 11	119.00±16.79	127.23±20.68	119.44±19.66	119.95±27.42	0.580*
Sector 12	138.57±25.19	145.58±21.42	135.38±20.08	138.36±27.13	0.620*
Sector 13	158.66±17.79	164.56±22.86	151.06±13.85	152.21±19.91	0.122*
Sector 14	135.64±22.49	138.93±22.85	134.92±26.53	131.26±22.28	0.793*
Sector 15	87.16±17.77	85.68±15.55	89.06±19.97	81.46±15.36	0.587*
Sector 16	64.36±8.97	63.28±9.10	62.12±8.83	60.04±8.45	0.439*
ONH parameters					
Disc area (mm^2,mean±SD)	1.81±0.41	1.92±0.35	1.89±0.36	1.76±0.39	0.566*
Cup area (mm^2, mean±SD)	0.48±0.52	0.58±0.42	0.49±0.39	0.56±0.45	0.870*
Rim area (mm^2, mean±SD)	1.33±0.40	1.34±0.26	1.40±0.28	1.20±0.32	0.325*
Rim volume (mm^3, mean±SD)	0.21±0.13	0.19±0.09	0.20±0.08	0.17±0.11	0.598*
Nerve head volume (mm^3, mean±SD)	0.38±0.20	0.34±0.15	0.35±0.12	0.30±0.17	0.491*
Cup volume (mm^3, median (IQR))	0.01 (0.00 - 0.12)	0.07 (0.01 - 0.18)	0.05 (0.00 - 0.06)	0.10 (0.00 - 0.16)	0.519†

*ANOVA; † Kruskall-Wallis test

No macular retinal segmentation error was detected in the healthy control group. Inner retinal image segmentation errors were detected in 8 of the 19 eyes with drusen (42.1 %), all 16 CNV eyes (100 %) and 17 of the 19 eyes in the CNV-anti-VEGF group (89.5 %; Pearson's chi-square test with Bonferroni correction, $p<0.001$ for all comparisons, *Table 22*).

Table 22. Comparison of the frequency of GCC segmentation errors, and the software-provided classification of average and pattern-based GCC parameters between the control group and each of the AMD groups

	Control (0; n=25)	**Drusen (1; n=19)**	**CNV (2; n=16)**	**CNV-anti-VEGF (3; n=19)**	**p-value***		
					0 vs. 1	*0 vs. 2*	*0 vs. 3*
Segmentation error	0	8	16	17	<0.001	<0.001	<0.001
Classification W/B/O							
Superior GCC	25/0/0	17/2/0	11/1/4	18/0/1	0.097	0.036	0.246
Inferior GCC	25/0/0	19/0/0	12/2/2	15/1/3	NA	0.093	0.055
Average GCC	25/0/0	18/1/0	13/1/2	15/3/1	0.246	0.080	0.055
GCC FLV	25/0/0	13/4/2	1/0/15	2/3/14	0.030	<0.001	<0.001

W, Within normal limits; B, Borderline; O, Outside normal limits; * Pearson's chi-square test with Bonferroni correction

In the AMD groups, inner retinal segmentation errors were localized and topographically related to the outer retinal changes (*Figure 8*).

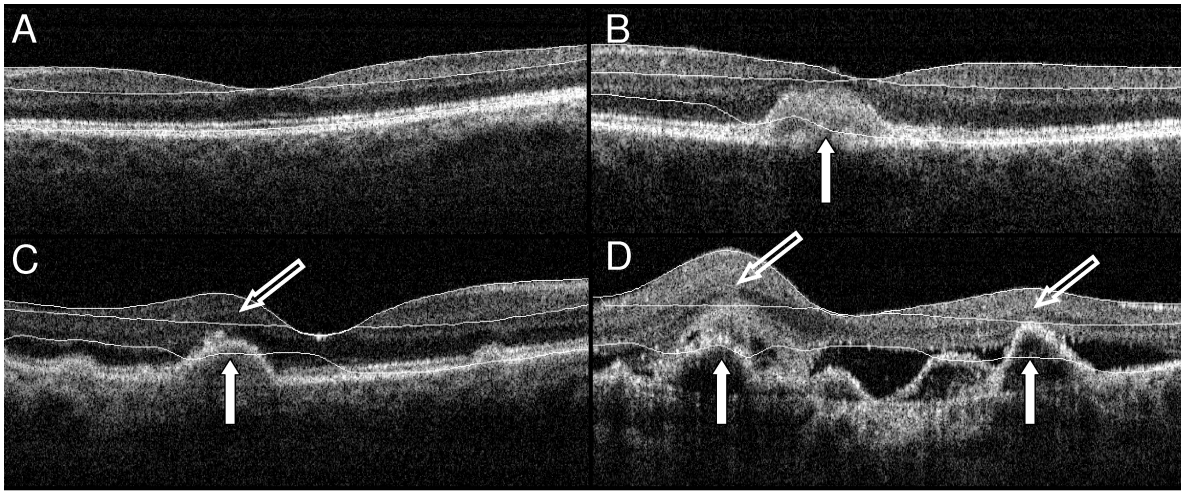

Figure 8. Typical examples of successful and erroneous segmentation for inner retinal thickness measurements (GCC scan)

A, Normal outer retinal layers and no inner retinal segmentation error in a healthy control eye; B, Soft macular drusen (white arrow) with no inner retinal segmentation error in the drusen group; C, A localized inner retinal segmentation error (empty arrow) adjacent to a soft macular drusen (white arrow) in the drusen group; D, A localized inner retinal segmentation error (empty arrow) adjacent to a CNV membrane (white arrow) in the CNV group. Outer retinal segmentation errors are also visible in all images with drusen and CNV (B, C and D), but these errors do not influence the GCC measurements.

The clinical significance of the segmentation errors was investigated with statistical comparisons of the measured values and the software-provided classifications between the healthy group and the AMD groups. Superior, inferior and average GCC did not differ significantly between the healthy control eyes and the various AMD groups (ANOVA, $p>0.05$ for all comparisons, *Table 23*). In contrast, GCC FLV, GLV and RMS were all

significantly greater (more abnormal) in the CNV and CNV-anti-VEGF group than in the control eyes (Mann-Whitney U-test with Bonferroni correction, p<0.001, *Table 23*). For GCC FLV, a similar, significant difference was found between the control eyes and the drusen group (p=0.048, *Table 23*).

Table 23. Comparison of average and pattern-based GCC parameters between the control group and each of the AMD groups

	Control (0; n=25)	**Drusen (1; n=19)**	**CNV (2;n=16)**	**CNV-anti-VEGF (3; n=19)**	**p-value**
Average parameters (µm, mean±SD)					
Superior GCC	98.90±5.85	94.67±8.87	90.22±19.83	93.88±9.34	0.123*
Inferior GCC	100.19±6.53	97.09±8.11	96.90±21.49	89.68±12.38	0.060*
Average GCC	99.54±5.92	95.88±8.03	93.52±17.39	91.78±9.93	0.094*
Pattern-based parameters					
GCC FLV (%, median (IQR))	0.51 (0.23-1.06)	1.19 (0.57-2.90)	11.91 (5.40-16.02)	4.71 (3.53-8.55)	0.048† (0 vs. 1) <0.001† (0 vs. 2) <0.001† (0 vs. 3)
GCC GLV (%, median (IQR))	1.53 (0.72-4.43)	3.58 (0.95-7.88)	13.23 (7.31-23.13)	8.29 (4.67-14.97)	0.068† (0 vs. 1) <0.001† (0 vs. 2) <0.001† (0 vs. 3)
GCC RMS (median (IQR))	0.08 (0.07-0.10)	0.10 (0.08-0.12)	0.35 (0.24-0.41)	0.19 (0.17-0.28)	0.054† (0 vs. 1) <0.001† (0 vs. 2) <0.001† (0 vs. 3)

* ANOVA; † Mann-Whitney U-test with Bonferroni correction

Of the four GCC parameters classified by the software, classification of superior, inferior and average GCC thickness did not differ significantly between the normal eyes and the different AMD groups for all but one comparison (*Table 22*). In contrast, for GCC FLV, the only pattern-based GCC parameter classified by the instrument, the frequency of "borderline" and "outside normal limits" classifications was significantly greater in each AMD group than in the control group (Pearson's chi-square test with Bonferroni correction, p≤0.03 for all comparisons, *Table 22*).

6.6 Nerve fiber layer and macular thinning measured with the RTVue-100 Fourier-domain optical coherence tomograph and the GDx-VCC/ECC scanning laser polarimeter during the course of acute optic neuritis

In all eyes, image acquisition was successful and image quality met the preset criteria with all methods, except for one GDx-VCC and one GDx-ECC image obtained on 2 different patients with MS (cases 1 and 6) in the acute phase of the disease, when poor fixation due to low visual acuity caused poor image quality. These images were excluded from the analysis. No eyes had a TSS score ≤80; thus all eyes showed a typical retardation pattern on GDx-VCC examination.

Time-dependent alteration of the peripapillary RNFLT measured with RTVue-100 OCT, GDx-VCC, and GDx-ECC, respectively, and average GCC are shown in *Figure 9* to *Figure 11*, for all ON eyes, separately. *Figure 9* shows that using the RTVue-100 OCT, in the first month of follow-up, average RNFLT increased considerably in all eyes with diffuse optic disc edema in the acute phase (cases 1, 4, and 9). Temporal RNFLT measured with RTVue-100 OCT increased in 2 of these eyes (cases 4 and 9).

For eyes with only nasal disc edema (cases 2, 6, and 8; *Figure 10*) or no disc edema (cases 3, 5, and 7; *Figure 11*), no clinically significant increase of RTVue-100 OCT RNFLT was seen. In contrast, peripapillary RNFLT measured both with GDx-VCC and GDx-ECC decreased in the acute phase of the disease, in all eyes. RNFLT values determined with GDx-VCC and GDx-ECC were similar during the follow-up period. Temporal sector RNFLT measured with either GDx method showed a large variability during the follow-up (data not shown). After the second month of follow-up, the initial increase of RTVue-100 OCT RNFLT disappeared, and peripapillary RNFLT decreased until a stable value was reached at 2 to 5 months. For the same eye, stability of peripapillary RNFLT appeared at the same time with all methods, in all cases. Average GCC decreased from the initial visit, for all eyes. Stability of average GCC appeared when stability of RNFLT appeared during the follow-up. Decrease of RNFLT and GCC continued after the development of the treatment-related improvement of VF MD in the first month.

The measured thickness changes are shown in *Table 24* and *Table 25*. In *Table 24*, the early increase of peripapillary RNFLT measured with RTVue-100 OCT and the lack of increase of the other parameters are presented. The changes are compared to the data of the corresponding healthy fellow eyes (which represent the normal status of the neuritis eyes

before the onset of ON) or the healthy status of the neuritis eyes (when measurements taken before the onset of acute ON were available). *Table 24* shows that for all 3 eyes (cases 1, 4, and 9) with diffuse optic disc edema, average RNFLT measured with the RTVue-100 OCT increased by 23.7 % to 82.5 % in the acute phase. For 2 of them, temporal sector RNFLT measured with the RTVue-100 OCT also showed a meaningful increase (54.2 % and 66.6 %, respectively). No such increase was found for any other parameter or eyes with only nasal disc edema or no disc edema.

In the ON eyes, relative thinning at the end of follow-up (expressed in percent of the highest value measured in the first month of follow-up) was different with the different measurement methods (*Table 25*). For eyes with diffuse optic disc edema (cases 1, 4, and 9), the relative decrease of RTVue-100 OCT average and temporal RNFLT was considerably greater than the other figures. For the other eyes, the percentage decrease of RTVue-100 OCT average RNFLT and average GCC were comparable. Decrease of GDx-VCC RNFLT and GDx-ECC RNFLT were similar for all eyes. For the healthy control eyes, no clinically significant alteration was seen for any parameter (*Figure 12* and *Table 24*).

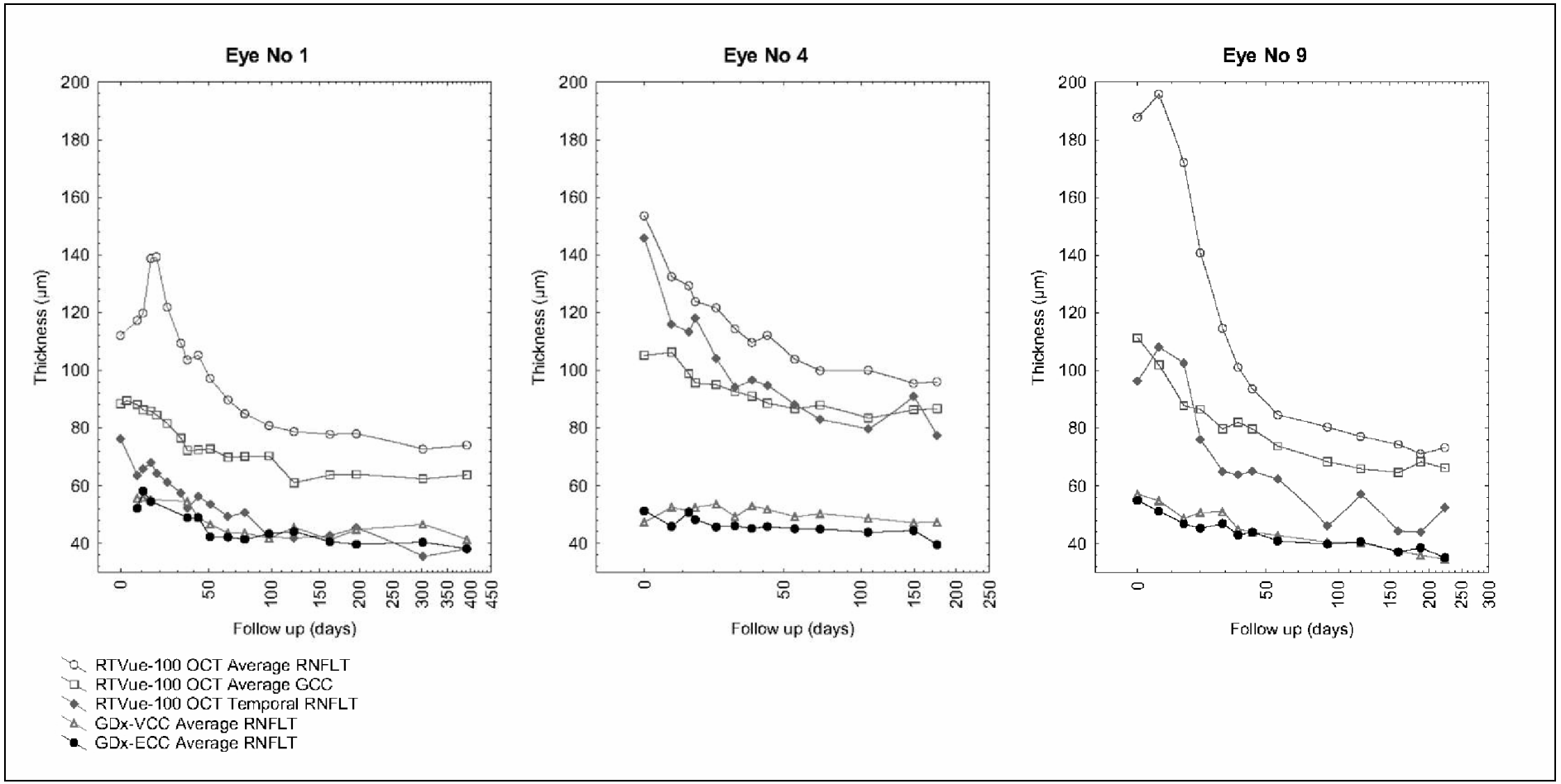

Figure 9. Alteration of RNFLT and average GCC in eyes presenting with diffuse optic disc edema in the early phase of the disease

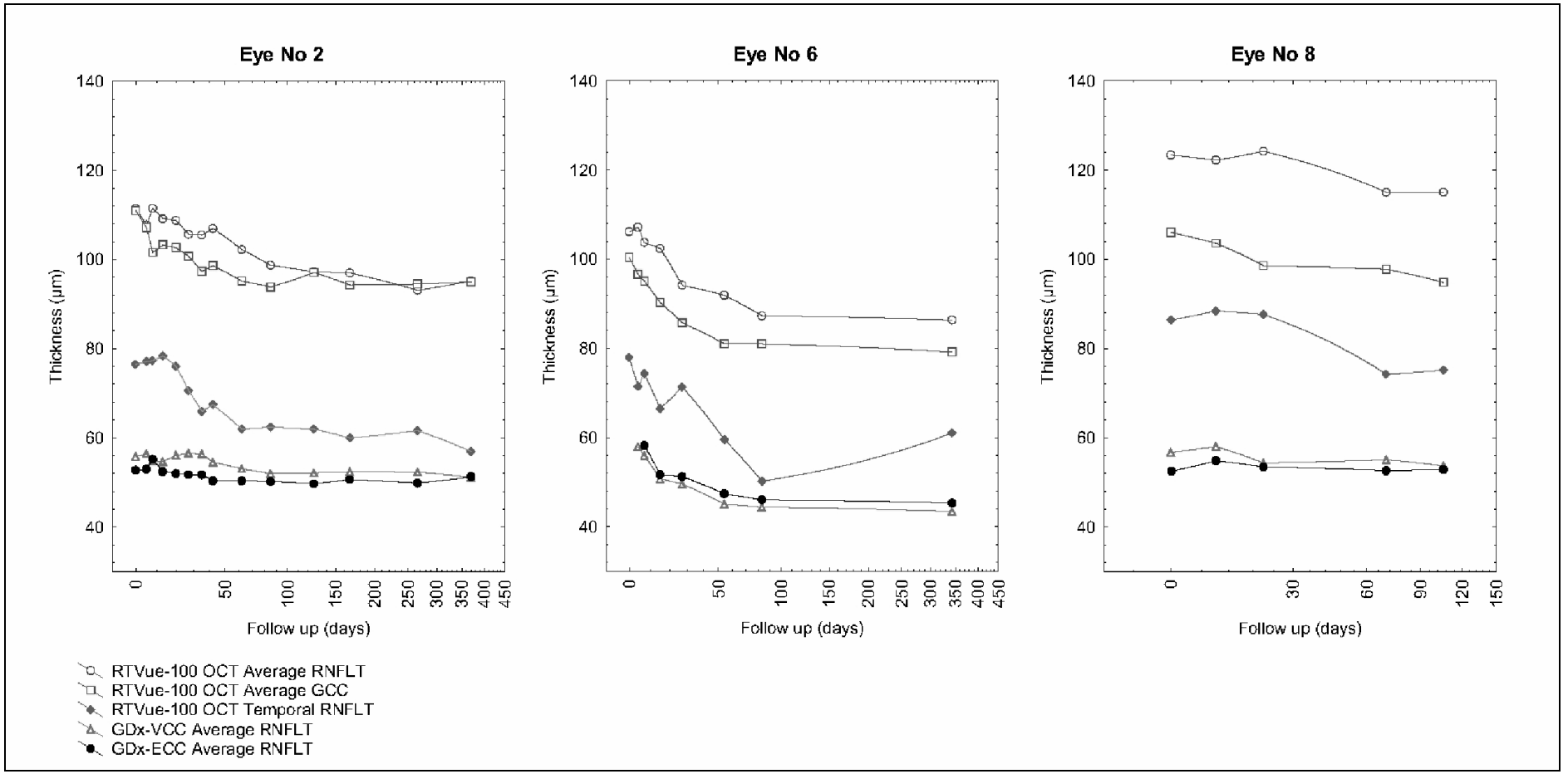

Figure 10. Alteration of RNFLT and average GCC in eyes presenting with nasal optic disc edema in the early phase of the disease

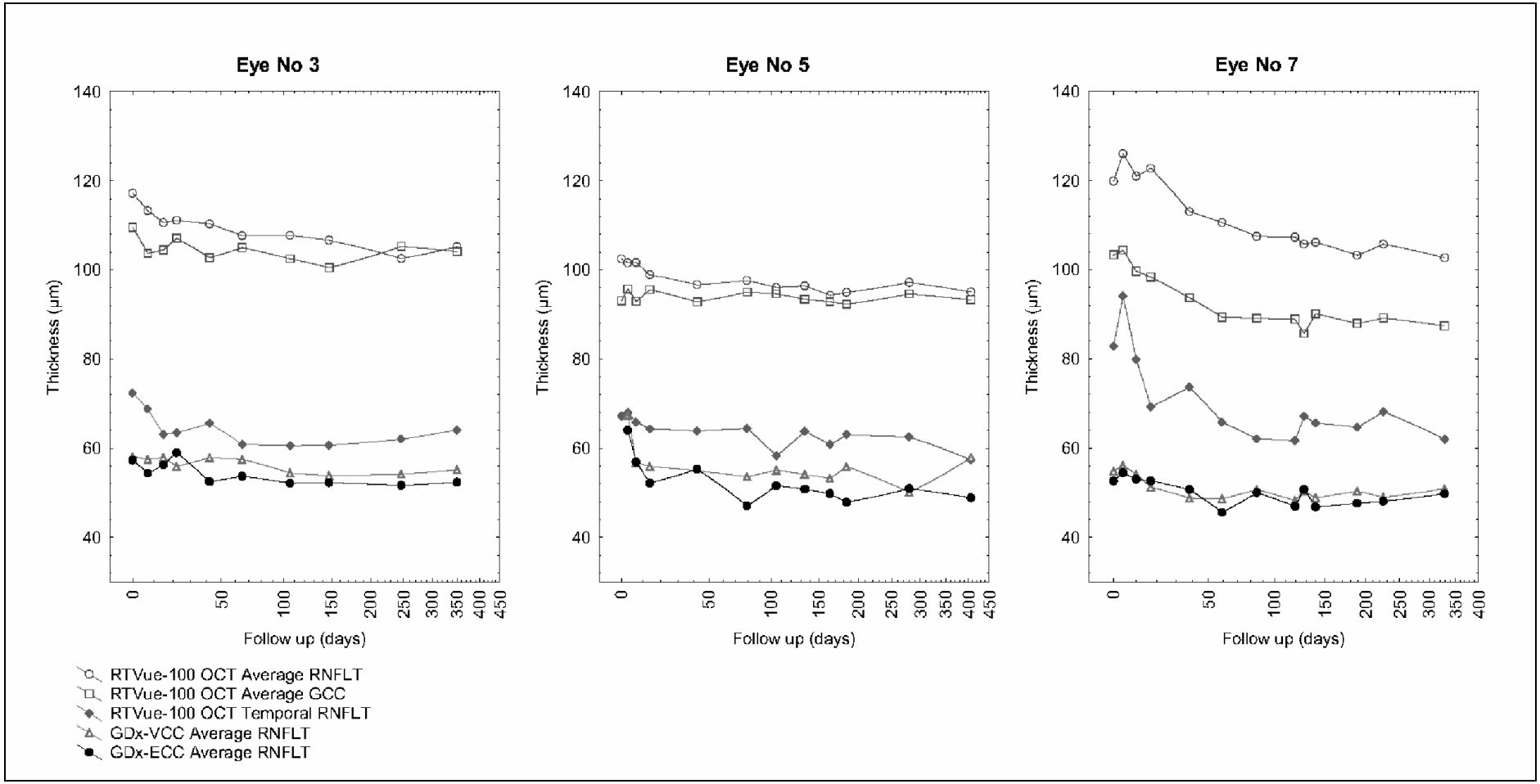

Figure 11. Alteration of RNFLT and average GCC in eyes presenting with no optic disc edema in the early phase of the disease

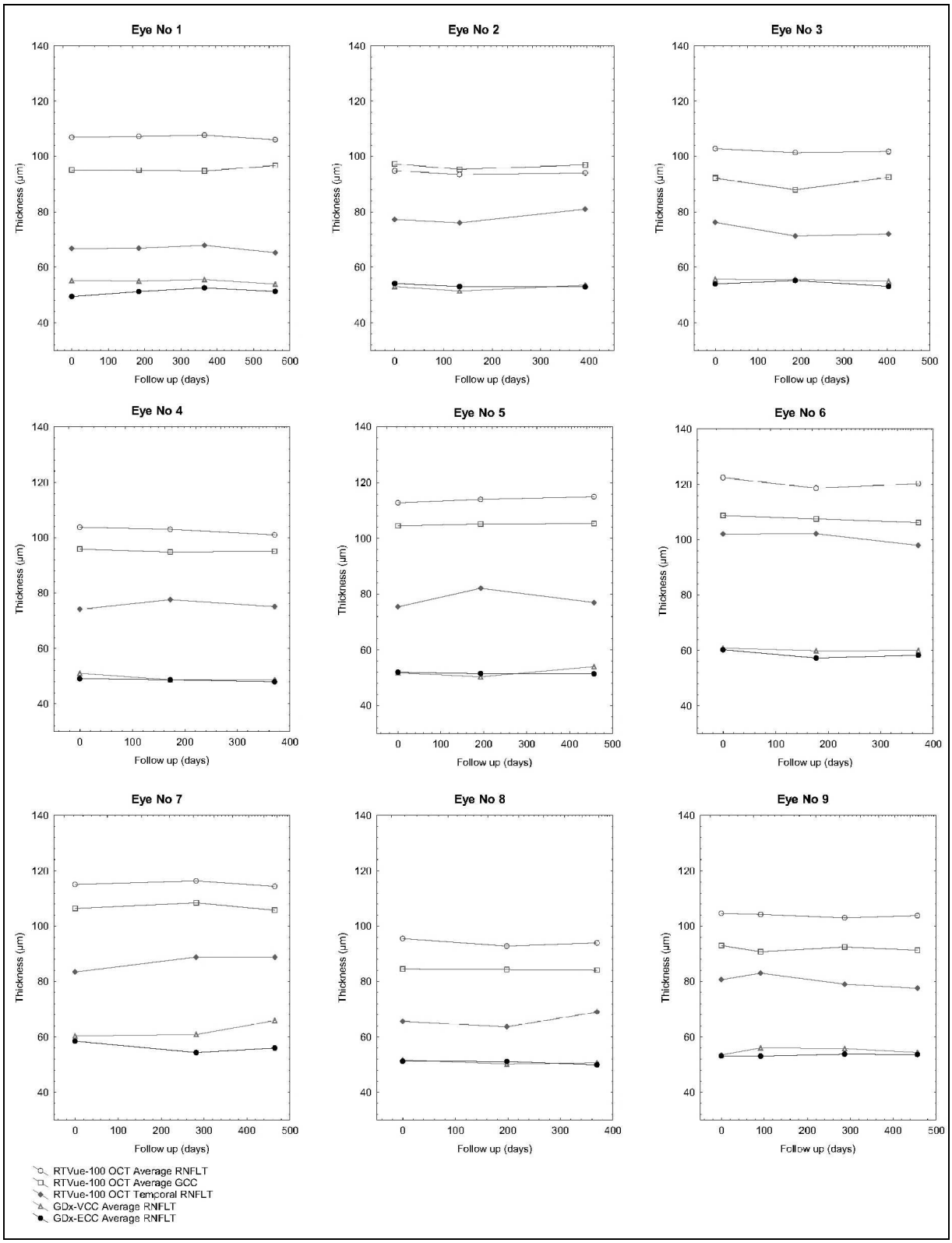

Figure 12. Alteration of RNFLT and average GCC in the healthy eyes of the control subjects

Table 24. Change of the different thickness parameters of the ON eyes in the early phase of neuritis compared to the corresponding parameters measured before the onset of ON, or in the healthy fellow eye

	No 1*	**No 2***	**No 3†**	**No 4***	**No 5***	**No 6***	**No 7***	**No 8†**	**No 9***
RTVue-100 OCT average RNFLT									
maximum (µm)	139.3	111.5	117.2	153.6	102.5	107.2	126.0	124.2	195.8
reference (µm)	112.6	117.0	117.0	118.0	122.0	98.3	121.1	121.1	107.3
difference (µm)	26.7	-5.5	0.2	35.6	-19.5	8.9	4.9	3.1	88.5
difference (%)	23.7	-4.7	0.1	30.2	-16.0	9.1	4.0	2.5	82.5
RTVue-100 OCT average GCC									
maximum (µm)	89.5	111.0	109.5	106.2	95.7	100.4	104.4	106.0	111.2
reference (µm)	90.6	109.6	109.6	103.0	108.2	96.0	106.6	106.6	97.5
difference (µm)	-1.1	1.4	-0.1	3.2	-12.5	4.4	-2.2	-0.6	13.7
difference (%)	-1.2	1.3	-0.1	3.1	-11.6	4.6	-2.1	-0.6	14.1
GDx-VCC average RNFLT									
maximum (µm)	55.8	56.6	58.1	53.6	67.4	57.9	56.2	58.0	57.0
reference (µm)	56.0	58.6	58.6	57.5	68.6	50.7	55.5	55.5	50.9
difference (µm)	-0.2	-2.0	-0.5	-3.9	-1.2	7.2	0.7	2.5	6.1
difference (%)	-0.4	-3.5	-0.9	-6.9	-1.7	14.2	1.2	4.4	12.0
GDx-ECC average RNFLT									
maximum (µm)	58.0	55.1	57.3	51.2	64.0	58.2	54.4	54.8	54.9
reference (µm)	51.9	54.5	54.5	55.6	58.9	49.4	51.9	51.9	49.6
difference (µm)	6.1	0.6	2.8	-4.4	5.1	8.8	2.5	2.9	5.3
difference (%)	11.8	1.1	5.2	-7.9	8.7	17.7	4.8	5.6	10.8
RTVue-100 OCT average temporal									
maximum (µm)	76.2	78.4	72.3	145.8	67.9	77.9	94.1	86.4	108.0
reference (µm)	67.8	75.7	75.7	87.5	94.4	68.8	92.2	92.2	70.1
difference (µm)	8.4	2.7	-3.4	58.3	-26.5	9.1	1.9	-5.8	37.9
difference (%)	12.5	3.5	-4.5	66.6	-28.1	13.2	2.0	-6.3	54.2

* Compared to the healthy fellow eye; † compared to the parameters of the same eye measured 1 to 4 months before the onset of the ON;
relative (%) difference = difference in µm / reference value in µm (%)

Table 25. Relative loss of RNFLT and average GCC at the end of the follow-up

	No 1	**No 2**	**No 3**	**No 4**	**No 5**	**No 6**	**No 7**	**No 8**	**No 9**
ON EYES									
RTVue-100 OCT average RNFLT									
max.; min. (µm)	139.3; 72.6	111.5; 93.1	117.2; 102.6	153.6; 95.4	102.5; 94.3	107.2; 86.4	126.0; 102.7	124.2; 112.6	195.8; 71.1
decrease (%)	47.8	16.5	12.5	37.9	8.0	19.4	18.5	9.4	63.7
RTVue-100 OCT average GCC									
max.; min. (µm)	89.5; 61.0	111.0; 93.8	109.5; 100.5	106.2; 83.4	95.7; 92.3	100.4; 79.1	104.4; 85.7	106.0; 94.8	111.2; 64.6
decrease (%)	31.9	15.4	8.2	21.5	3.6	21.2	17.9	10.6	41.9
GDx-VCC average RNFLT									
max.; min. (µm)	55.8; 41.2	56.6; 51.1	58.1; 53.8	53.6; 47.1	67.4; 50.1	57.9; 43.4	56.2; 48.2	58.0; 53.7	57.0; 34.5
decrease (%)	26.2	9.6	7.3	12.1	25.8	25.1	14.2	7.5	39.5
GDx-ECC average RNFLT									
max.; min. (µm)	58.0; 38.0	55.1; 49.7	57.3; 51.6	51.2; 39.4	64.0; 47.0	58.2; 45.3	54.4; 46.8	54.8; 52.5	54.9; 35.0
decrease (%)	34.5	9.9	9.9	23.0	26.5	22.2	14.0	4.3	36.3
RTVue-100 OCT average temporal									
max.; min. (µm)	76.2; 38.1	78.4; 56.9	72.3; 62.0	145.8; 77.3	67.9; 57.3	77.9; 61.0	94.1; 62.0	86.4; 75.2	108.0; 43.9
decrease (%)	50.0	27.4	14.2	47.0	15.6	21.7	34.1	13.0	59.4
HEALTHY CONTROL EYES									
RTVue-100 OCT average RNFLT									
max.; min. (µm)	107.7; 106.0	94.9; 93.6	102.8; 101.0	103.8; 101.0	115.0; 112.8	122.4; 118.7	116.4; 114.4	95.5; 92.8	104.6; 103.0
decrease (%)	1.6	1.4	1.7	2.6	1.9	3.1	1.7	2.8	1.5
RTVue-100 OCT average GCC									
max.; min. (µm)	96.8; 94.8	97.3; 95.4	92.6; 88.1	95.9; 94.8	105.3; 104.5	108.8; 106.2	108.5; 105.8	84.5; 84.1	93.0; 90.7
decrease (%)	2.0	2.0	4.9	1.1	0.8	2.3	2.5	0.5	2.4
GDx-VCC average RNFLT									
max.; min. (µm)	55.5; 53.9	53.5; 51.3	55.6; 54.9	51.0; 48.7	54.0; 50.3	60.9; 59.9	63.9; 60.4	51.7; 50.2	56.1; 53.5
decrease (%)	3.0	4.0	1.3	4.6	6.8	1.6	5.6	2.9	4.5
GDx-ECC average RNFLT									
max.; min. (µm)	52.5; 49.3	54.1; 52.9	55.1; 51.0	49.1; 48.0	52.0; 51.4	60.3; 57.3	58.5; 54.4	51.2; 49.9	53.8; 53.1
decrease (%)	6.0	2.2	7.5	2.3	1.1	5.0	7.1	2.5	1.3
RTVue-100 OCT average temporal									
max.; min. (µm)	67.9; 65.2	82.0; 76.1	76.2; 62.9	77.5; 74.1	85.0; 75.4	102.2; 98.0	88.8; 82.4	70.0; 63.7	83.0; 77.5
decrease (%)	4.0	7.3	17.5	4.5	11.4	4.1	7.2	9.0	6.6

7 DISCUSSION

7.1 Reproducibility of retinal nerve fiber layer and inner macular thickness measurements of the RTVue-100 Fourier-domain optical coherence tomograph

Our study is only the second investigation of the reproducibility of the RNFLT, and it is the first investigation of the reproducibility of GCC measurements with the RTVue-100 OCT system on healthy persons and glaucoma patients. Previous studies with the Stratus TD-OCT system have shown that reproducibility of the peripapillary RNFLT measurements is better in healthy eyes than in glaucomatous eyes;[45,114] pupil dilation [46,47] and variations of signal strength [48-50] influence the results and the reproducibility; RNFLT measurements for larger sectors are more reproducible than for narrower sectors;[51,52] and incorrect alignment of the measurement area can alter the measured RNFLT values.[53-56] With the RTVue-100 OCT, several technology-related factors were found improved compared with the TD-OCT technique. The short image acquisition time potentially reduces motion artifacts, and the operator-independent automatic image alignment of the RTVue-100 OCT system eliminates the problems resulting from operator-related improper alignment that have been reported for the Stratus OCT system, namely, measurement error and incorrect patient classification.[54-56,107] In addition, the resolution is twice as good as that of the Stratus TD-OCT system, which increases the reproducibility.[115,116] To investigate the clinical usefulness of these technical improvements, the reproducibility of the measurements was studied, as well as the influence of several patient-related factors on the reproducibility. Although change and asymmetry of the thickness of the macula region have been shown to be associated with glaucomatous retinal ganglion cell loss,[117-119] little information was available on the clinical value of GCC measurements in glaucoma diagnostics. Therefore, in addition to the RNFLT measurements, we also investigated the reproducibility of the GCC parameters.

The intrasession CV values found in the current study both for the normal and OHT subjects and the glaucoma patients are better than the corresponding figures reported for the Stratus TD-OCT [45,51,114] and are very similar to those reported by González-García et al for the RTVue-100 OCT.[65] Of all RNFLT parameters, the lowest CV was found for average RNFLT. For this parameter, the CV figures were 1.39 % for the hospital-based

normal and OHT persons, 1.65 % for the screening trial participants with no disease, and 2.38 % and 3.30 % for the 2 glaucoma groups with moderate and advanced glaucoma, respectively. The values for the inferior and superior RNFLT were 2.58 % and 2.76 %, respectively, in the normal and OHT group; 2.63 % and 3.18 %, respectively, in the screening trial participants; 4.42 % and 4.42 %, respectively, in the moderate glaucoma group; and 4.64 % and 7.14 %, respectively, in the severe glaucoma group. Most temporal and nasal CV values were somewhat higher than the corresponding inferior and superior RNFLT figures, but even in advanced glaucoma, the CV values for all quadrant RNFLT parameters were less than 8.3 %.

For all 37 hospital-based participants, the CV values calculated for the 16 peripapillary sectors varied between 4.90 % and 11.66 %; thus, they were higher than the corresponding figures for the retinal quadrants (3.61 % - 5.69 %) or for average RNFLT (2.20 %), suggesting that, similar to the results of studies made with the Stratus OCT,[51,114] the narrower the peripapillary area, the lower the reproducibility. Excellent intrasession ICC values were found for all RNFLT parameters, ranging between 81.2 % (sector 16) and 99.0 % (average RNFLT). For inferior and superior GCC, the CV values were 1.95 % and 2.36 % and the intrasession ICC values 99.0 % and 98.4 %, respectively. The CV values of the GCC parameters found in our study for the normal and glaucomatous eyes, respectively, are approximately half of the corresponding values reported for the Stratus OCT [118] and are similar to those found with a different FD-OCT system.[120] The above findings, in general, suggest that the reproducibility of the RNFLT and inner macula thickness measurements with the RTVue-100 OCT is high and is similar to that reported for other FD-OCT systems.[63,121,122]

For the Stratus OCT, pupil dilation was shown to improve image quality and to increase the measured RNFLT values in glaucoma;[46,47] therefore, it was recommended for the measurements.[45] Using the RTVue-100 OCT system, no clinically significant RNFLT or GCC change was found because of pupil dilation. Only 2 parameters (average RNFLT and sector 9 RNFLT) showed a statistically significant increase, but even for these, the change did not exceed 0.8 µm (1.5 %). No change resulting from pupil dilation was found for intratest variability, intrasession CV, or signal strength. These results show that pupil dilation is not necessary to achieve reproducible RNFLT and GCC measurements with the RTVue-100 OCT system.

To evaluate the potential influence of patient experience in imaging examinations on the measurement reproducibility, the intrasession CV for the normal and OHT subgroup of the

regularly imaged patients (mean age, 54.0 years) was compared with that for 40 healthy unselected consecutive glaucoma screening trial participants (mean age, 63.8 years) who lacked previous experience in imaging examination. No difference was seen either for intrasession reproducibility or for the thickness values. Age had no influence on the reproducibility in the healthy screening participants. These results show that no special patient training is necessary for reproducible RNFLT and GCC measurement with the RTVue-100 OCT and that the instrument is potentially suitable for use in the elderly population.

The same findings, however, also suggest that, similar to the Stratus OCT system,[48] the thinning of the RNFL influences the measurement reproducibility. The influence of glaucoma severity was confirmed for most parameters by a significant trend for increasingly higher CV with increasing glaucoma severity. This nevertheless may have little influence on the clinical applicability of the technique, because disease severity had no influence on intratest variability of the average and quadrant RNFLT values and GCC, which are used for comparison with the normative database for statistical classification. The intratest variability of the larger peripapillary areas applied for the statistical classification did not exceed 8.16 µm for the normal and OHT group and the eyes with moderate glaucoma and did not exceed 11.64 µm for advanced glaucoma.

Intersession reproducibility was assessed with the calculation of test-retest variability and intervisit CV between 2 measurement series 3 months apart. For the larger peripapillary areas, test-retest variability ranged from 4.25 µm (average RNFLT) to 9.57 µm (superior RNFLT) and intersession CV ranged between 2.64 % (average RNFLT) to 6.26 % (nasal RNFLT). These figures are better than the corresponding results published for the Stratus TD-OCT system.[51] For the GCC parameters, the corresponding figures did not exceed 4.51 µm and 2.81 %, respectively. Intratest variability represented 79.1 % to 98.6 % of test-retest variability, and intrasession CV represented 77.1 % to 95.0 % of intersession CV.

This study has limitations. Because all participants were white, caution is needed when conclusions from these results are applied to other ethnic groups. The results are not representative for eyes with clinically significant cataract or AMD, because corrected visual acuity of the participants was excellent and no macular degeneration was present.

7.2 Comparison of repeatability of retinal nerve fiber layer thickness measurements made using the RTVue-100 Fourier-domain optical coherence tomograph and the GDx-VCC/ECC scanning laser polarimeter

In this study, we compared repeatability of RNFLT measurements from the ONH scan of the RTVue-100 OCT system to that of GDx-VCC and GDx-ECC, all made on the same eyes. The motivation was that the RTVue-100 OCT,[104,123] being an example of the recently developed FD- OCT systems,[27,53,63,68,104,123] may in future be used in parallel with other widely used structural imaging methods with different working principles. Thus, it is of clinical importance to compare the characteristics of such systems.

In this study, GDx-VCC and GDx-ECC were used for comparisons with the new instrument. These methods are generally accepted as clinically useful glaucoma diagnostic tools, and have good repeatability.[23,26-32,124-127] To avoid bias due to ARP in SLP,[26,28,31] only eyes with typical retardation pattern were selected for study. As no published information on repeatability of RNFLT measurement with the ONH scan of the RTVue-100 OCT was available, we selected peripapillary measuring circle segments of different extents, and used eyes with either no damage, moderate damage, or severe glaucomatous damage for the comparisons.

As the working principles RTVue-100 OCT and GDx-VCC/ECC are different, it is not surprising that the corresponding RNFLT values all differed significantly between the methods. This basic finding is of practical importance, as it demonstrates that the measurement results are not directly comparable, even though those from both instruments are formally expressed in microns.

Variability of SLP measurements is relatively high on the temporal peripapillary quadrant, and the ability of GDx-VCC to detect localized nerve fiber bundle defects is limited.[52] Therefore, due to its potential clinical significance, we were specifically interested in repeatability of RTVue-100 OCT measurements for these areas. Thus, in addition to repeatability for the total 360º measuring circle and the superior and inferior quadrants (which are the most important areas to measure RNFLT and detect glaucoma), repeatability for the temporal quadrant, and the inferotemporal and superotemporal sectors (where most early localized glaucomatous RNFL defects occur), and the papillomacular sector (which is of clinical importance in several non-glaucomatous optic nerve diseases) was also compared between the systems. In the total study population, for the total

measuring circle an especially favorable repeatability (mean CV: 2.11 %) was found with RTVue-100 OCT. This was significantly better than the corresponding coefficient found for GDx-VCC (3.04 %), and tended to be better than that found for GDx-ECC (3.22 %). For the retinal quadrants no significant difference was seen except for the inferior quadrant, for which RTVue-100 OCT showed better repeatability than GDx-VCC, and the temporal quadrant, for which repeatability was significantly better with RTVue-100 OCT (4.88 %) than with GDx-ECC (7.40 %), and tended to be better than with GDx-VCC (6.81 %). This result shows that for the temporal retinal area the RTVue-100 OCT measurements are less variable than the GDx-VCC/ECC measurements. A similar difference was seen for the temporal quadrant for the normal and OHT subjects (group 1). As repeatability for the other quadrants did not differ systematically between RTVue-100 OCT and the GDx methods, our results suggest that the better repeatability seen with RTVue-100 OCT for the total measuring circle can mostly be attributed to the better results for the temporal quadrant.

Another finding for RTVue-100 OCT's repeatability was that for the total 360º circle and the quadrants, repeatability decreased statistically significantly with increasing glaucoma severity. This is not unique for RTVue-100 OCT,[48,128] and in a different study, we have found a similar pattern for GDx-VCC and GDx-ECC.[129] As the SD for most of the RNFLT parameters increased with increasing disease severity, this result cannot be attributed only to the lower mean RNFLT values in more severe glaucoma, and thus this finding cannot be a calculation-related technical artifact. It is interesting that for the 3 narrower sectors this pattern was not present. One may speculate that the relatively high CV for these narrower sectors may mask the influence of disease severity. This suggests that further investigation is necessary to clarify the significance of RTVue-100 OCT measurement variability for the narrower peripapillary sectors.

Classification ("normal" vs. "glaucomatous") was good for all 3 methods. The only discrepancy occurred for 1 eye in group 2 (glaucomatous eyes with moderate VF damage); both GDx reports classified the eye as "normal," but the RTVue-100 OCT report identified "borderline" RNFLT in the inferior quadrant and the inferotemporal sector. Clinically, an inferotemporal nerve fiber bundle defect and mild inferior neuroretinal rim loss were seen.

Our study has a number of limitations due to its design and the relatively small number of participants. In this study, we did not evaluate all aspects of measurement reproducibility with the RTVue-100 OCT system, but focused on only one aspect, namely the comparison of repeatability of the RNFLT measurements with those made using SLP. In the subject

groups with moderate and severe glaucoma (groups 2 and 3) no significant repeatability difference was found between the methods. This could be caused by the higher CV values in these groups, seen for all the methods used, or by the relatively small sample size, or both. As our participants were all Caucasian, no conclusions can be made in respect of other ethnic groups. Finally, in all our study eyes the optical media were clear (to ensure optimal imaging), therefore caution is needed in drawing conclusions regarding eyes with clinically significant cataract or other media opacities.

7.3 Diagnostic accuracy of retinal nerve fiber layer, inner macular thickness and optic disc measurements made with the RTVue-100 Fourier-domain optical coherence tomograph to detect glaucoma

As detection of glaucomatous ONH damage is frequently suboptimal,[130] evaluation of the diagnostic accuracy of the different imaging devices is of clinical importance. In the current study, we investigated the diagnostic capabilities of the RTVue-100 Fourier-domain OCT instrument on 286 Caucasian patients referred for glaucoma diagnostics to our center during 11 months. The RTVue-100 OCT is one of the recently developed Fourier-domain OCT systems that all have several technical advantages compared with the time-domain OCT technology.[65,70,131] Information on the clinical benefits provided by those technical improvements for detection of glaucoma and glaucoma progression, however, was limited before our investigations. In most diagnostic accuracy studies, a healthy normal group and an age-matched glaucoma group with pre-defined disease severity are compared.[61,66,69-71,132-135] In such investigations, for the best performing RNFLT and GCC parameters of the RTVue-100 OCT, the AUC varied between 0.900 and 0.971.[66,69,133-135] Other authors using other FD-OCT systems reported on similar values.[70,132] These results suggest that under pre-defined circumstances the diagnostic accuracy of FD-OCT technology is somewhat higher than that of TD-OCT technology.[61,66,70,132]

Though using the above approach information on diagnostic capabilities of an instrument under pre-defined conditions can be specified, the clinical usefulness of the same instrument in unselected patient populations remains undetermined. In contrast, using data of all eyes successfully imaged during our nearly 1-year study period allowed us to

evaluate diagnostic accuracy both for a general referral population and the different disease categories, separately. The significance of this approach is that disease severity may have an influence on the diagnostic capability of the FD-OCT instruments,[136] thus it needs to be considered in the evaluation. But for routine clinical purposes, diagnostic accuracy determined for the total referral patient population is the most useful information.

To evaluate the diagnostic capability of the instrument we used the software-provided classification, which is based on comparison between the measured values and the integrated normative database. As the RTVue-100 OCT has an age and disc size adjusted separate database for Caucasians,[106,107] which was used by us for our patients, the age-related RNFLT and GCC difference [137,138] between our healthy control and OHT subjects and the perimetric glaucoma patients was corrected for. We have previously shown that pupil dilation had no influence on the RNFLT and GCC measurements made with the RTVue-100 OCT.[129] Thus we did not dilate pupil for the measurements. This fits in with busy routine clinical practice, and increases the clinical applicability of the results.

As shown in *Table 16*, in the OHT group for most parameters the mean values suggested some damage, but the difference from the healthy group was significant only for two parameters. In contrast, for all other groups several parameters showed significant damage compared with the healthy eyes, and the measured values showed more damage for the more severe disease categories, respectively.

For the evaluation of the software-provided classification, “borderline” and “outside normal limits” classifications were grouped together as abnormal results. Prevalence of glaucoma exceeded 50 % in the study population (i.e. the number of eyes with and without glaucoma was comparable), thus it was meaningful to calculate the predictive values in addition to sensitivity, specificity and PLR. Specificity was consistently high (94.6 - 100 %); sensitivity was poor for detection of OHT and preperimetric glaucoma, and moderate to good (up to 92.8 %) for detection of perimetric glaucoma. For our total unselected study population, most RNFLT and GCC measurements had high specificity and PPV (92.4 - 100 %), and clinically useful PLR (>10 to infinite). No such favorable findings were obtained for the ONH parameters (cup area, cup/disc area ratio and rim area), which suggests that FD-OCT technology did not overcome the problems of ONH classification with the TD-OCT technology.[35,139,140]

Our results mean that in routine clinical practice a “borderline” or “outside normal limits” classification given for the main RNFLT parameters, RNFLT sectors (except for the

temporal sectors) or GCC parameters by the instrument's software, strongly suggests that the eye has lost retinal nerve fibers and macular ganglion cells. In contrast, because of the relatively low sensitivity and weak NLR, a "within normal limits" classification cannot exclude glaucoma.

Our study has limitations. As our patients were all Caucasians, our results cannot be applied to other ethnic groups, nor do our findings provide any information about the clinical value of the non-Caucasian normative database of the instrument.

7.4 Comparison of clinical diagnostic usefulness of retinal nerve fiber layer thickness measurements made using the RTVue-100 Fourier-domain optical coherence tomograph and the GDx-VCC/ECC scanning laser polarimeter

In the current investigation sensitivity and specificity of the RTVue-100 OCT were compared to those of GDx-VCC and GDx-ECC, for detection of glaucoma of glaucomatous RNFLT damage in a cross-sectional clinical decision making situation where all referred persons have to be classified as structurally undamaged or damaged. The comparison was based on measurements obtained from 177 consecutive patients referred to our glaucoma service for detection or exclusion of glaucoma, during ten months. The background of this comparison study is that the evaluated techniques have different working principles and age-corrected normative databases but comparable diagnostic reports, were recently developed, and both will probably be used for glaucoma detection in the following years. The FD-OCT instruments including the RTVue-100 OCT have several technical advantages over the TD-OCT systems.[63-68,104,141] GDx-ECC was consistently found superior to GDx-VCC for improving the signal-to-noise ratio.[22,23,25,26,29,31,32,78] As far as we know, the diagnostic capabilities of RTVue-OCT and GDx-ECC have not been compared.

To compare the diagnostic value of the different methods, we used parameters which are indicated on the standard instrument reports, comparable between the methods, and easily available for clinicians. The statistical classification, for each instrument, was based on the software-provided comparison with the corresponding integrated normative database. Such classification for average, superior and inferior RNFLT was available with all methods. However, for localized superotemporal and inferotemporal nerve fiber bundle defects,

which represent frequent and relatively early clinical signs of OAG, classification only for RTVue-100 OCT was available. In order to create a similar parameter for GDx-VCC and GDx-ECC, we used the GDx deviation map, where localized and statistically significant nerve fiber bundle type thinning adjacent to the superotemporal or inferotemporal edge of the ONH can be identified.[110,111] In a previous investigation by our group this parameter was successfully combined with the standard GDx-VCC/ECC parameters for glaucoma screening.[110,111] Since separation of "borderline" and "outside normal limits" classifications was not possible for this GDx parameter, the corresponding RTVue-100 OCT sectors with both "borderline" and "outside normal limits" classification results were considered as glaucomatous. To create corresponding sectors of similar size for RTVue-100 OCT and GDx-VCC/ECC, we combined the two software-provided superotemporal and inferotemporal RTVue-100 OCT sectors to one 45^{o}-sized superotemporal and inferotemporal sector, respectively.

Our patient population was suitable for a hospital-based diagnostic study, since the structurally normal (healthy and OHT) eyes represented 44.1 %, the preperimetric glaucoma eyes 18.6 %, and the perimetric glaucoma eyes 37.3 % of the population. In addition, of the perimetric glaucoma cases early glaucoma was present in 39.4 %, moderate glaucoma in 28.8 % and advanced glaucoma only in 31.8 %. Thus, eyes with early structural damage (preperimetric and early perimetric glaucoma cases) represented 60 % of the total glaucoma population. An ARP was seen in 28.3 % of the GDx-VCC images, which is similar to the figures reported in other diagnostic studies. [22,25-27,29,31,32,78,111]

All methods were similarly highly specific for the main RNFLT sectors (92.3 % to 98.7 %) as well as most nerve fiber bundle defect parameters and their combinations, though for one nerve fiber bundle defect parameter specificity was higher with GDx-VCC/ECC that with RTVue-100 OCT. Specificity was also high for NFI. These results confirm the findings of the previously published GDx-VCC/ECC diagnostic studies,[22,25-27] the results of our glaucoma screening investigations by our group with GDx-VCC and GDx-ECC,[110,111] and the limited data published on the diagnostic performance of RTVue-100 OCT.[66] In contrast, sensitivity of GDx-VCC/ECC ranged only between 28.3 % and 57.6 %, and was significantly, up to 35 % lower than that of RTVue-100 OCT, for all localized nerve fiber bundle defect parameters. Sensitivity of the different RTVue-100 OCT parameters varied between 63.6 % and 84.8 %. For average RNFLT sensitivity of RTVue-100 OCT was significantly higher than that of GDx-VCC. When sensitivity and

specificity of RTVue-100 OCT and GDx-ECC were compared, for the main RNFLT parameters (average, superior and inferior RNFLT) no significant difference was found. In addition, sensitivity of GDx-ECC NFI was similar to that of the above main parameters of RTVue-100 OCT. It is important that 87.7 % of the detected glaucoma cases were identified both by NFI of GDx-VCC/ECC and average RNFLT of RTVue-100 OCT, and the kappa measure of agreement between RTVue-100 OCT average RNFLT and NFI was similarly excellent using GDx-VCC (0.84) and GDx-ECC (0.85).

Our results show that in an unselected population characterized with high representation of preperimetric and early perimetric glaucoma eyes RTVue-100 OCT and GDx-ECC have similar diagnostic capabilities for the large RNFLT sectors, but RTVue-100 OCT is more sensitive for the narrow nerve fiber bundle defects. This finding is of clinical significance.

Our study has limitations. Since our patients were all Caucasians, caution is needed when this conclusion from our results is applied to patients belonging to other ethnic groups. In order to compare the cross-sectional diagnostic capability of RTVue-100 OCT and GDx-VCC/ECC on an unselected referral population we had to group the OHT eyes with the normal eyes (structurally undamaged eyes), and the preperimetric glaucoma eyes with the perimetric glaucoma eyes (structurally damaged eyes). This grouping may not be optimal when the exact diagnostic accuracy of a structural test is investigated, but it is essential when real life usefulness of different structural test is compared. The exact diagnostic accuracy of the different techniques compared by us has been clarified in other studies,[22,25-27,29-32,66,68-72,103] and our goal was to compare the real-life diagnostic capability on unselected patients. Thus, we think that the above grouping was useful for the current study. However, due to the cross-sectional design, the possibility of lack of future progression in some eyes in the preperimetric glaucoma group cannot be excluded, thus it is possible that some preperimetric glaucoma eyes were in fact normal.

7.5 Influence of age-related macular degeneration on inner macular thickness measurements made with RTVue-100 Fourier-domain optical coherence tomograph

In the current investigation we evaluated the influence of AMD on RNFLT, ONH and inner macular retinal thickness parameters measured with the RTVue-100 OCT, in non-glaucomatous eyes. The background of our study was that both glaucoma and AMD are frequent and frequently concomitant diseases of the elderly.[142-146] AMD may potentially influence macular thickness measurements and their software-provided classification for glaucoma and other optic neuropathies, even if all forms of AMD involve the outer retinal layers which are not investigated when inner macular retinal thickness is measured with the GCC scan of the RTVue-100 OCT.[66,69,112]

Our AMD patients were divided in three severity groups. Early and intermediate AMD was characterized with presence of subfoveal/juxtafoveal drusen and mild RPE changes and no severe deterioration of vision. In routine clinical practice, such eyes may easily be imaged for detection of glaucoma without their macular changes being detected. Untreated subfoveal CNV with severe decrease of visual acuity represented the advanced form of the disease. The potential influence of VEGF blockage on the CNV-induced RTVue-100 OCT changes was investigated in the third group comprising CNV eyes after intravitreal antiangiogenic treatment. All CNV eyes included in our study were either scheduled for intravitreal antiangiogenic treatment, or had already undergone such interventions, so no cases with large, end-stage CNV membranes (disciform scars) were investigated. Thus, our OCT findings were caused by relatively small CNV membranes, which do not make imaging for glaucoma impossible in clinical practice. Glaucoma and OHT were excluded through detailed clinical investigation of all participants, the age of the participants was similar in all groups and image quality was high for all measurements, so the differences found by us between the healthy control group and each of the AMD groups were attributed to the influence of macular pathology on the results.

As expected, we found no difference in RNFLT and ONH parameter values and their classification between the groups. Localized inner retinal image segmentation errors, topographically related to the AMD-induced outer retinal changes, were seen in all CNV eyes, most CNV-anti-VEGF eyes and 42.1 % of the soft drusen eyes. These segmentation errors had a clinically significant influence both on the measured GCC parameter values and their software-provided classification. Though no differences of the average inner

macular retinal thickness parameters (superior, inferior and average GCC) were found between the healthy eyes and the various AMD groups, all pattern-based GCC parameters (FLV, GLV and RMS) were significantly greater (more abnormal) in the CNV and CNV-anti-VEGF eyes than in the healthy group. The fact that the difference between the healthy control and early/moderate AMD eyes was significant only for one software-provided parameter (GCC FLV), does not mean that soft macular drusen have negligible influence on the pattern-based GCC parameters. This group was also significantly influenced, and in this respect did not differ from the other two groups with more advanced AMD, when the software-provided classification was analyzed. Of the four GCC parameters classified by the software, the three average thickness parameters (superior, inferior and average GCC) were similarly classified in the healthy group and the different AMD groups, except for one comparison. In contrast, GCC FLV, the only pattern-based parameter classified by the instrument, was significantly more frequently classified as "borderline" and "outside normal limits" in each of the AMD groups than in the control group.

Since in eyes with a healthy macula the structure-function relationship is similar for the GCC parameters and peripapillary RNFLT,[129,133,147,148] and diagnostic accuracy of the pattern-based GCC parameters is similar to or better than that of the RNFLT parameters,[69,140,148,150] it is of clinical importance to understand that even macular drusen can influence inner macular retinal thickness measurements. Though the effect of AMD on the inner macular average thickness parameters was not statistically significant, both the pattern-based GCC parameters and the software-provided classification of GCC FLV were significantly influenced. Such influence may lead to confusing measurement results when clinicians evaluate patients for glaucoma.

Our results suggest that a detailed examination of the macula is necessary before a GCC parameter classified as "borderline" or "outside normal limits" by the instrument's software is considered a sign of glaucoma or other optic neuropathies in the elderly, and corresponding RNFLT and GCC alterations are required to identify potential glaucoma cases with the RTVue-100 OCT, in clinical practice. Further studies are necessary to clarify whether inner macular retinal measurements made with other FD-OCT systems employing different segmentation softwares for diagnosis of glaucoma, are also influenced by the different severity forms of AMD.

7.6 Nerve fiber layer and macular thinning measured with the RTVue-100 Fourier-domain optical coherence tomograph and the GDx-VCC/ECC scanning laser polarimeter during the course of acute optic neuritis

The primary goal of the current study was to investigate the dynamics of RNFLT decrease and macular thinning, using different advanced imaging devices in acute ON in MS. Though RNFLT and macular thickness following acute ON were studied by several groups,[149,151-168] to our knowledge no prospective follow-up study on eyes with acute ON in MS has been published. Our secondary goal was to evaluate and compare the usefulness of the recently developed RTVue-100 OCT and the GDx-ECC, for the detection of thickness changes during the follow-up. These new generation instruments and software versions, which have major advantages for image acquisition, image quality, and signal-to-noise ratio compared to the corresponding earlier versions,[25,26,28,29,63,69,141] have not been used for quantification of RNFLT and macular thickness changes in MS.

Since the working principles employed in FD-OCT technology and SLP are different, the measured thickness values are not interchangeable, even if for clinical purposes they are both expressed in micrometers.[169] The relative changes (%), however, can be compared between the different methods. In our healthy control eyes, the measured values remained stable with all measurement techniques during the follow-up period. This confirms the previously published data [28,169] which showed that all methods used in the current investigation have small long-term variability on healthy eyes.

For those ON eyes that presented with diffuse optic disc edema, as a consequence of the initial edema of the peripapillary retina, average and temporal sector peripapillary RNFLT measured with the RTVue-100 OCT were higher in the first weeks than the corresponding values measured before the onset of the ON, or the values found for the healthy fellow eye. Then the values decreased until stability was reached during the follow-up. Thus, temporal sector RNFLT did not provide more useful follow-up information than average RNFLT, though axonal damage is frequently predominant for the temporal fibers. In contrast, RNFLT measured with GDx-VCC and GDx- ECC decreased already in the early follow-up period, for all eyes. This result is not unexpected, since SLP is based on retardation of the illuminating laser light by the intracellular structure of the ganglion cell axon,[25,26,28,29] thus polarimetric RNFLT cannot increase when the structure of the ganglion cell axon is damaged. No eye had an ARP,[28] thus it was possible to compare the usefulness of

GDx-ECC and GDx-VCC, without any bias. Though the GDx-ECC software improves the signal-to-noise ratio,[28,29] the corresponding values were similar with both GDx techniques. This suggests that GDx-ECC provides no clinically significant benefit over GDx-VCC for follow-up of RNFLT in ON if the retardation pattern is typical. The thickness of those inner macular layers that are directly influenced by ganglion cell loss was characterized with average GCC of the RTVue-100 OCT. Average GCC decreased from the onset of the ON including the early follow-up weeks.

The clinical usefulness of the various measurements was different. Temporal sector RNFLT showed large fluctuation during the follow-up with both GDx methods, thus separate evaluation of this sector was not possible with SLP. RNFLT measured with the RTVue-100 OCT showed an increase in the first weeks of the follow-up, due to optic disc and peripapillary edema. An increase of the measured RNFLT in ON can be misleading, and masks the true loss of retinal nerve fiber. The polarimetric RNFLT measurements were not always technically successful in the early weeks, when fixation was poor due to low visual acuity and severe VF damage. Compared to the short image acquisition time of the RTVue-100 OCT (0.39 sec), image acquisition with either GDx technique is relatively long (1 sec). As a consequence, poor fixation due to severely impaired visual function did not influence image quality of the RTVue-100 OCT, but had a negative influence on image quality of SLP. We do not think that poor image quality with GDx-VCC/ECC in the early phase of ON (which occurred in 2 of the 9 cases) was caused by loss of axonal microstructure. Peripapillary RNFLT showed a continuous decrease with both GDx techniques until it stabilized several months later. Thus, if poor GDx image quality was caused by loss of signal in the early weeks, and the thinning continued for several months, GDx image quality could have not returned to the optimal range during the follow-up. The GCC scan of the macula was free from artifacts during the whole follow-up, and due to its anatomic location it was not influenced by optic disc and peripapillary edema in the early phase of ON. Since automatic image segmentation of the FD-OCT technology is advanced, the GCC thickness is closely related to the ganglion cell quantity of the macula, and the GCC measurements are highly reproducible,[69,129] average GCC may represent an especially useful parameter for monitoring ganglion cell loss in acute ON. For the same eye, the decrease of the different thickness parameters ended at the same time during the follow-up in each case, which suggests that all tested methods are suitable to characterize stable chronic ON.

It is important that the dynamics of the alteration were different for RNFLT and all other parameters of the RTVue-100 OCT, showing that the measured structural change in acute ON strongly depends on the measurement method. We also found that at the end of the follow-up (at 6 to 12 months after the onset of ON) the relative loss of thickness was different with the different methods. These features may have a role in the suboptimal structure-function relationship found for ON in MS.[151,152,166,167] Our findings suggest that a standardized imaging method is needed for ophthalmologic evaluation of structural changes in acute ON.

Our study has limitations. Our patients were all white; thus no conclusion on patients with other ethnicity can be made from our results. Our sample size was small, which is due to the limited number of new patients with MS presenting with the first episode of acute ON in 12 months. Since the length of the follow-up did not exceed 12 months, and we did not evaluate eyes with more than one acute ON episode, our findings are not necessarily representative for eyes with chronic recurrent ON.

8 SUMMARY OF NEW RESULTS AND THEIR CLINICAL RELEVANCE

As far as we know each of our studies presented in the current PhD thesis represents novelty in international ophthalmological research.

8.1 Reproducibility of retinal nerve fiber layer and inner macular thickness measurements of the RTVue-100 Fourier-domain optical coherence tomograph

We have shown that reproducibility of the RNFLT and GCC measurements with the RTVue-100 OCT is better than that reported for the Stratus TD-OCT, and is similar to that reported for the RTVue-100 OCT by a different research group. The reproducibility is satisfactory for clinical diagnostic purposes both in healthy and glaucomatous eyes with moderate to severe damage. The measurement variability increases for narrower peripapillary areas and for increasing disease severity. Previous experience in imaging examinations is not required of patients to achieve reproducible measurements. Pupil dilation has no clinically significant influence on the measured thickness values or on their intrasession reproducibility. Although the reproducibility of the measurements decreases with increasing glaucoma severity, nevertheless, the intratest measurement variability of average RNFLT, superior quadrant RNFLT, and inferior quadrant RNFLT (the most important parameters used for statistical comparison with the normative database) did not depend significantly on disease severity in this study. The 3-month intersession variability is accounted for mostly by the short-term intrasession variability. This is potentially valuable for progression analysis, because between-visit variability is not much greater than within-visit variability.

8.2 Comparison of repeatability of retinal nerve fiber layer thickness measurements made using the RTVue-100 Fourier-domain optical coherence tomograph and the GDx-VCC/ECC scanning laser polarimeter

We have shown that for the total 360º measuring circle and for the temporal quadrant, RTVue-100 OCT's repeatability is better than that with either GDx-VCC or GDx-ECC. For the other quadrants the repeatability was similar to that of GDx-VCC and GDx-ECC, whether with variable compensation or ECC. Repeatability of the ONH scan of the RTVue-100 OCT decreases with increasing glaucoma severity, but even in advanced glaucoma the mean CV values are favorable, less than 7.30 % for all retinal quadrants, which is adequate for clinical measurements.

8.3 Diagnostic accuracy of retinal nerve fiber layer, inner macular thickness and optic disc measurements made with the RTVue-100 Fourier-domain optical coherence tomograph to detect glaucoma

We have shown that in a Caucasian referral population comprising healthy, OHT, preperimetric and perimetric glaucoma patients referred for detection or exclusion of glaucoma, the RTVue-100 OCT and its Caucasian normative database are highly specific to detect glaucoma. The sensitivity to detect preperimetric glaucoma, however, is moderate. The overall best-performing parameter was average RNFLT, but several other RNFLT and GCC parameters had similarly favorable diagnostic accuracy. Diagnostic performance for the different ONH parameters was not as high as that for the RNFLT and GCC parameters. This suggests that RNFLT and GCC parameters should be preferred for clinical decision making over ONH parameters for diagnostics of glaucoma.

8.4 Comparison of clinical diagnostic usefulness of retinal nerve fiber layer thickness measurements made using the RTVue-100 Fourier-domain optical coherence tomograph and the GDx-VCC/ECC scanning laser polarimeter

We have shown that a "borderline" or "outside normal limits" classification on the RTVue-100 OCT, GDx-VCC or GDx-ECC report represents clinically important and similarly specific information on RNFL damage, when a patient referred for glaucoma diagnostics is investigated. However, for localized nerve fiber bundle defects the sensitivity of RTVue-100 OCT is superior to that of either GDx technique. The diagnostic accuracy of NFI (the summary parameter indicating the probability of glaucoma on the GDx-VCC and GDx-ECC report) is similar to that of average RNFLT indicated on the RTVue-100 OCT report. These findings suggest that both GDx-VCC/ECC and RTVue-100 OCT are useful tools for glaucoma diagnostics, but the RTVue-100 OCT is more sensitive for early localized RNFL damage.

8.5 Influence of age-related macular degeneration on inner macular thickness measurements made with RTVue-100 Fourier-domain optical coherence tomograph

We have shown that even macular drusen may cause localized image segmentation errors in the GCC scan of the RTVue-100 OCT, which erroneously influence the software-provided classification of the result. This suggests that a detailed examination of the macula is necessary before a GCC parameter classified as "borderline" or "outside normal limits" by the instrument's software is considered a sign of glaucoma or other optic neuropathies in the elderly. Corresponding RNFLT and GCC alterations are required to identify potential glaucoma cases with the RTVue-100 OCT, in clinical practice. Our results also show that FD-OCT needs further development of segmentation algorithm.

8.6 Nerve fiber layer and macular thinning measured with the RTVue-100 Fourier-domain optical coherence tomograph and the GDx-VCC/ECC scanning laser polarimeter during the course of acute optic neuritis

We have shown in a prospective longitudinal study on eyes with acute ON due to MS that the relative structural loss and the dynamics of the RNFL and macular thinning are different with different ophthalmological imaging methods. Inner macular thickness, as measured with the GCC scan of the RTVue-100 OCT, is the clinically most useful parameter for monitoring the structural changes during the total follow-up period. It was not influenced either by initial optic disc edema or poor fixation due to severe VF and visual acuity damage in the acute phase of the disease. Therefore, the use of this parameter is recommended for longitudinal characterization of structural damage in ON.

9 SUMMARY

Glaucoma is caused by progressive apoptotic loss of the retinal ganglion cells, that result in the irreversible damage of the retinal nerve fiber layer (RNFL) and the optic nerve head. Development of visual field defect is usually preceded by thinning of the RNFL. Thus structural investigation methods of the retinal nerve fiber thickness (RNFLT) represent an important part of modern glaucoma diagnostics.

In the last decade, time-domain optical coherence tomography (OCT) and scanning laser polarimetry (GDx-VCC) have become a standard investigating method in glaucoma diagnostics. The recently developed Fourier-domain OCT technology provides several technical innovations. The RTVue-100 OCT is one of this new commercially available Fourier-domain OCT instruments. The recently released GDx-ECC software was developed to improve image quality in case of atypical retardation pattern. The possible role of the RTVue-100 OCT in glaucoma diagnostics has not yet been evaluated in detail, thus the aim of this research was to analyze the clinical usefulness of the device, and to compare it to that of the GDx-VCC/ECC technologies.

Our results showed that the reproducibility of the RTVue-100 OCT is favorable for clinical diagnostic purposes both in healthy and glaucomatous eyes; for some peripapillary areas it is better than that of the GDx-VCC/ECC; specificity of the RTVue-100 OCT is high to detect perimetric glaucoma, though the sensitivity to detect preperimetric glaucoma is only moderate; for localized nerve fiber bundle defects the sensitivity of RTVue-100 OCT is superior to that of either GDx technique; AMD may cause localized image segmentation errors in the GCC scan of the RTVue-100 OCT, which may cause improper software-provided classification of the result; and in acute optic neuritis in multiple sclerosis inner macular thickness, as measured with the GCC scan of the RTVue-100 OCT, is more suitable to longitudinal characterization of structural damage than RNFLT parameters measured either with RTVue-100 OCT or the GDx-VCC/ECC methods.

10 ÖSSZEFOGLALÁS

A glaucoma a retinális ganglionsejtek progresszív pusztulásával járó betegség, ami a retinális idegrostréteg (RNFL) és a papilla irreverzibilis károsodásához vezethet. Mivel a látótér defektus megjelenését időben általában megelőzi a retinális idegrostréteg vastagság (RNFLT) csökkenése, a glaucoma korszerű diagnosztikájához az RNFLT-t mérő különböző morfometriai vizsgálatok ma már szervesen hozzátartoznak.

A time-domain optikai koherencia tomográfia (OCT) és a scanning lézer polarimetria (GDx-VCC) az elmúlt évtizedben standard szemészeti vizsgálómódszerré vált. A közelmúltban kifejlesztett Fourier-domain OCT technológia azonban számos technológiai fejlesztéssel rendelkezik; ezen az elven működik az RTVue-100 OCT készülék is.

A közelmúltban forgalomba hozott GDx-ECC szoftvert az atípusos polarizációs minta miatt nehezen klasszifikálható regisztrátumok képminőségének javítására fejlesztették ki. Mivel a Fourier-domain OCT technikának a glaucoma diagnosztikájában betölthető szerepét még alig vizsgálták, munkám során a módszer klinikai alkalmazhatóságának elemzését, valamint a GDx-VCC/ECC módszerrel való összehasonlítását végeztem el.

Eredményeink alapján megállapítottuk, hogy az RTVue-100 OCT mérési reprodukálhatósága igen kedvező mind egészséges, mind glaucomás szemeken; hasonló, sőt egyes peripapillaris területek esetében kedvezőbb, mint a GDx-VCC/ECC módszeré; specificitása magas, ám preperimetriás glaucomás szemeken szenzitivitása mérsékelt; lokalizált RNFLT kiesés esetében az RTVue-100 OCT szenzitivitása magasabb, mint a GDx-VCC/ECC módszeré; az AMD szegmentációs hibát okozhat az RTVue-100 OCT esetében, ami téves klasszifikációt eredményezhet; végül a sclerosis multiplex eredetű acut opticus neuritis lefolyása során fellépő strukturális károsodás követésére az RTVue-100 OCT belső macula vastagság paramétere (GCC) alkalmasabb, mint a GDx-VCC/ECC módszerrel és az RTVue-100 OCT készülékkel mért RNFLT paraméterek.

11 REFERENCES

1. Holló G, Vargha P, Follmann P, Süveges I. (1998) Frekvenciakettőzött perimetria: új és sokat ígérő módszer a glaucomás látótérkiesés korai felismerésére. Szemészet, 135: 245-249.

2. European Glaucoma Society. Terminology and guidelines for glaucoma. 2nd ed. Dogma s.r.l., Savona 2003.

3. Quigley HA. (1996) Number of people with glaucoma worldwide. Br J Ophthalmol, 80: 389-393.

4. Quigley HA, Broman AT. (2006) The number of people with glaucoma worldwide in 2010 and 2020. Br J Ophthalmol, 90: 262-267.

5. Németh J, Frigyik A, Vastag O, Göcze P, Pető T, Elek I. (2005) Vaksági okok Magyarországon 1996 és 2000 között. Szemészet, 142: 126-132.

6. Topouzis F, Coleman AL, Harris A, Koskosas A, Founti P, Gong G, Yu F, Anastasopoulos E, Pappas T, Wilson MR. (2008) Factors associated with undiagnosed open-angle glaucoma: the Thessaloniki Eye Study. Am J Ophthalmol, 145: 327-335.

7. The Eye Diseases Prevalence Research Group. (2004) Prevalence of open-angle glaucoma among adults in the United States. Arch Ophthalmol, 122: 532-538.

8. Bonomi L, Marchini G, Marraffa M, Bernardi P, De Franco I, Perfetti S, Varotto A, Tenna V. (1998) Prevalence of glaucoma and intraocular pressure distribution in a defined population: The Egna-Neumarkt study. Ophthalmology, 105: 209-215.

9. Tielsch JM, Sommer A, Katz J, Royall RM, Quigley HA, Javitt J. (1991) Racial variations in the prevalence of primary open-angle glaucoma: The Baltimore Eye survey. JAMA, 266: 369-374.

10. Wolfs RC, Borger PH, Ramrattan RS, Klaver CC, Hulsman CA, Hofman A, Vingerling JR, Hitchings RA, de Jong PT. (2000) Changing views on open-angle glaucoma: definitions and prevalences – The Rotterdam study. Invest Ophthalmol Vis Sci, 41: 3309-3321.

11. Antón A, Andrada MT, Mujica V, Calle MA, Portela J, Mayo A. (2004) Prevalence of primary open-angle glaucoma in a Spanish population: The Segovia study. J Glaucoma, 13: 371-376.

12. Nizankowska MH, Kaczmarek R. (2005) Prevalence of glaucoma in the Wroclaw population. The Wroclaw epidemiological study. Ophthalmic Epidemiol, 12: 363-371.

13. Holló G. (1997) Glaucoma: kórtan és klinikum. Inthera, Budapest.

14. Süveges I. (1999) A glaukóma pathomechanizmusa, konzervatív terápiája. Orv Hetil, 140: 2211-2214.

15. Heijl A, Leske MC, Bengtsson B, Hyman L, Bengtssson B, Hussein M, for the Early Manifest Glaucoma Trial Group. (2002) Reduction of intraocular pressure and glaucoma progression: results from the Early Manifest Glaucoma Trial. Arch Ophthalmol, 120: 1268-1279.

16. Carpineto P, Ciancaglini M, Mastropasqua L. (2005) Optical coherence tomography: validity as a diagnostic tool. In: Iester M, Garway-Heath D, Lemij H (szerk): Optic nerve head and retinal nerve fibre layer analysis. Dogma S.r.l., 135-138, Savona, Italy.

17. Somfai GM, Salacz G. (2005) Optical biopsy of the retina in vivo: on optical coherence tomography and its clinical use in ophthalmology. Orv Hetil, 146: 1157-1163.

18. Miglior S, Riva I, Guareschi M, Di Matteo F, Romanazzi F, Buffagni L, Rulli E. (2007) Retinal sensitivity and retinal nerve fiber layer thickness measured by optical coherence tomography in glaucoma. Am J Ophthalmol, 144: 733-740.

19. Holló G, Nagymihály A, Vargha P. (1997) A retinális idegrostréteg vizsgálata scanning lézer polarimetriával. Szemészet, 134: 17-22.

20. Holló G, Süveges I, Nagymihály A, Vargha P. (1997) Scanning laser polarimetry of the retinal nerve fiber layer in primary open-angle and capsular glaucoma. Br J Ophthalmol, 81: 857-861.

21. Zhou Q, Knighton RW. (1997) Light scattering and form birefringence of parallel cylindrical arrays that represent cellular organelles of the retinal nerve fiber layer. Appl Opt, 36: 2273-2285.

22. Mai TA, Reus NJ, Lemij HG. (2007) Structure-function relationship is stronger with enhanced corneal compensation than with variable corneal compensation in scanning laser polarimetry. Invest Ophthalmol Vis Sci, 48: 1651-1658.

23. Garas A, Tóth M, Vargha P, Holló G. (2010) Influence of pupil dilation on repeatability of scanning laser polarimetry with variable and enhanced corneal compensation in different stages of glaucoma. J Glaucoma, 19: 142-148.

24. Garas A, Simó M, Holló G. (2010) Nerve fiber layer and macular thinning measured with different imaging methods during the course of acute optic neuritis. Eur J Ophthalmol, early online publication, PII: C24F7753-9C5F-4B13-AF56-61EDD66783D3.

25. Mai TA, Reus NJ, Lemij HG. (2007) Diagnostic accuracy of scanning laser polarimetry with enhanced versus variable corneal compensation. Ophthalmology, 114: 1988-1993.

26. Sehi M, Guaqueta DC, Feuer WJ, Greenfield DS; Advanced Imaging in Glaucoma Study Group. (2007) Scanning laser polarimetry with variable and enhanced corneal compensation in normal and glaucomatous eyes. Am J Ophthalmol, 143: 272-279.

27. Bowd C, Tavares IM, Medeiros FA, Zangwill LM, Sample PA, Weinreb RN. (2007) Retinal nerve fiber layer thickness and visual sensitivity using scanning laser polarimetry with variable and enhanced corneal compensation. Ophthalmology, 114: 1259-1265.

28. Tóth M, Holló G. (2008) Increased long-term measurement variability with scanning laser polarimetry employing enhanced corneal compensation: an early sign of glaucoma progression. J Glaucoma, 17: 571-577.

29. Tóth M, Holló G. (2005) Enhanced corneal compensation for scanning laser polarimetry on eyes with atypical polarisation pattern. Br J Ophthalmol, 89: 1139-1142.

30. Reus NJ, Zhou QY, Lemij HG. (2006) Enhanced imaging algorithm for scanning laser polarimetry with variable corneal compensation. Invest Ophthalmol Vis Sci, 47: 3870-3877.

31. Medeiros FA, Bowd C, Zangwill LM, Patel C, Weinreb RN. (2007) Detection of glaucoma using scanning laser polarimetry with enhanced corneal compensation. Invest Ophthalmol Vis Sci, 48: 3146-3153.

32. Saito H, Tomidokoro A, Yanagisawa M, Aihara M, Tomita G, Araie M. (2008) Scanning laser polarimetry with enhanced corneal compensation in patients with open-angle glaucoma. J Glaucoma, 17: 24-29.

33. Huang D, Swanson EA, Lin CP, Schuman JS, Stinson WG, Chang W, Hee MR, Flotte T, Gregory K, Puliafito CA, Fujimoto JG. (1991) Optical coherence tomography. Science, 254: 1178-1181.

34. Geitzenauer W, Hitzenberger CK, Schmidt-Erfurth UM. (2011) Retinal optical coherence tomography: past, present and future perspectives. Br J Ophthalmol, 95: 171-177.

35. Li G, Fansi AK, Boivin JF, Joseph L, Harasymowycz P. (2010) Screening for glaucoma in high-risk populations using optical coherence tomography. Ophthalmology, 117: 453-461.

36. Huang J, Liu X, Wu Z, Guo X, Xu H, Dustin L, Sadda S. (2011) Macular and retinal nerve fiber layer thickness measurements in normal eyes with the Stratus OCT, the Cirrus HD-OCT, and the Topcon 3D OCT-1000. J Glaucoma, 20: 118-125.

37. Fercher AF. (2010) Optical coherence tomography - development, principles, applications. Z Med Phys, 20: 251-276.

38. Sakata LM, Deleon-Ortega J, Sakata V, Girkin CA. (2009) Optical coherence tomography of the retina and optic nerve - a review. Clin Experiment Ophthalmol, 37: 90-99.

39. Parikh RS, Parikh S, Sekhar GC, Kumar RS, Prabakaran S, Babu JG, Thomas R. (2007) Diagnostic capability of optical coherence tomography (Stratus OCT 3) in early glaucoma. Ophthalmology, 114: 2238-2243.

40. Nouri-Mahdavi K, Nikkhou K, Hoffman DC, Law SK, Caprioli J. (2008) Detection of early glaucoma with optical coherence tomography (StratusOCT). J Glaucoma, 17: 183-188.

41. Hougaard JL, Heijl A, Bengtsson B. (2008) Glaucomatous retinal nerve fibre layer defects may be identified in Stratus OCT images classified as normal. Acta Ophthalmol, 86: 569-575.

42. Hougaard JL, Heijl A, Bengtsson B. (2007) Glaucoma detection by Stratus OCT. J Glaucoma, 16: 302-306.

43. Ajtony C, Balla Z, Somoskeoy S, Kovacs B. (2007) Relationship between visual field sensitivity and retinal nerve fiber layer thickness as measured by optical coherence tomography. Invest Ophthalmol Vis Sci, 48: 258-263.

44. Perneczky T, Milibák T. (2009) A peripapillaris idegrostréteg-vastagság, a maculavastagság és -volumen vizsgálata optikai koherencia tomográffal primer nyitott zugú glaucomában. Ophthalmologia Hungarica, 146: 65-70.

45. Budenz DL, Chang RT, Huang X, Knighton RW, Tielsch JM. (2005) Reproducibility of retinal nerve fiber thickness measurements using the Stratus OCT in normal and glaucomatous eyes. Invest Ophthalmol Vis Sci, 46: 2440-2443.

46. Smith M, Frost A, Graham CM, Shaw S. (2007) Effect of pupillary dilatation on glaucoma assessments using optical coherence tomography. Br J Ophthalmol, 91: 1686-1690.

47. Paunescu LA, Schuman JS, Price LL, Stark PC, Beaton S, Ishikawa H, Wollstein G, Fujimoto JG. (2004) Reproducibility of nerve fiber thickness, macular thickness, and optic nerve head measurements using Stratus OCT. Invest Ophthalmol Vis Sci, 45: 1716-1724.

48. Wu Z, Vazeen M, Varma R, Chopra V, Walsh AC, LaBree LD, Sadda SR. (2007) Factors associated with variability in retinal nerve fiber layer thickness measurements obtained by optical coherence tomography. Ophthalmology, 114: 1505-1512.

49. Barkana Y, Burgansky-Eliash Z, Gerber Y, Melamed S, Neudorfer M, Avni I, Bartov E, Morad Y. (2009) Inter-device variability of the Stratus optical coherence tomography. Am J Ophthalmol, 147: 260-266.

50. Cheung CY, Leung CK, Lin D, Pang CP, Lam DS. (2008) Relationship between retinal nerve fiber layer measurement and signal strength in optical coherence tomography. Ophthalmology, 115: 1347-1351.

51. Budenz DL, Fredette MJ, Feuer WJ, Anderson DR. (2008) Reproducibility of peripapillary retinal nerve fiber thickness measurements with Stratus OCT in glaucomatous eyes. Ophthalmology, 115: 661-666.

52. Vizzeri G, Bowd C, Medeiros FA, Weinreb RN, Zangwill LM. (2009) Scan tracking coordinates for improved centering of Stratus OCT scan pattern. J Glaucoma, 18: 81-87.

53. Vizzeri G, Bowd C, Medeiros FA, Weinreb RN, Zangwill LM. (2008) Effect of improper scan alignment on retinal nerve fiber layer thickness measurements using Stratus optical coherence tomograph. J Glaucoma, 17: 341-349.

54. Cheung CY, Yiu CK, Weinreb RN, Lin D, Li H, Yung AY, Pang CP, Lam DS, Leung CK. (2009) Effects of scan circle displacement in optical coherence tomography retinal nerve fibre layer thickness measurement: a RNFL modelling study. Eye, 23: 1436-1441.

55. Vizzeri G, Bowd C, Medeiros FA, Weinreb RN, Zangwill LM. (2009) Effect of signal strength and improper alignment on the variability of Stratus optical coherence tomography retinal nerve fiber layer measurements. Am J Ophthalmol, 148: 229-255.

56. Yoo C, Sun IH, Kim YY. (2009) The influence of eccentric scanning of optical coherence tomography on retinal nerve fiber layer analysis in normal subjects. Ophthalmologica, 223: 326-332.

57. Guedes V, Schuman JS, Hertzmark E, Wollstein G, Correnti A, Mancini R, Lederer D, Voskanian S, Velazquez L, Pakter HM,Pedut-Kloizman T, Fujimoto JG, Mattox C. (2003) Optical coherence tomography measurement of macular and nerve fiber layer thickness in normal and glaucomatous human eyes. Ophthalmology, 110: 177-189.

58. Wollstein G, Schuman JS, Price LL, Aydin A, Beaton SA, Stark PC, Fujimoto JG, Ishikawa H. (2004) Optical coherence tomography (OCT) macular and peripapillary retinal nerve fiber layer measurements and automated visual fields. Am J Ophthalmol, 138: 218-225.

59. Burgansky-Eliash Z, Wollstein G, Chu T, Ramsey JD, Glymour C, Noecker RJ, Ishikawa H, Schuman JS. (2005) Optical coherence tomography machine learning classifiers for glaucoma detection: a preliminary study. Invest Ophthalmol Vis Sci, 46: 4147-4152.

60. Medeiros FA, Zangwill LM, Bowd C, Vessani RM, Susanna R Jr, Weinreb RN. (2005) Evaluation of retinal nerve fiber layer, optic nerve head, and macular thickness measurements for glaucoma detection using optical coherence tomography. Am J Ophthalmol, 139: 44-55.

61. Wollstein G, Ishikawa H, Wang J, Beaton SA, Schuman JS. (2005) Comparison of three optical coherence tomography scanning areas for detection of glaucomatous damage. Am J Ophthalmol, 139: 39-43.

62. van Velthoven ME, Faber DJ, Verbraak FD, van Leeuwen TG, de Smet MD. (2007) Recent developments in optical coherence tomography for imaging the retina. Prog Retin Eye Res, 26: 57-77.

63. Menke MN, Knecht P, Sturm V, Dabov S, Funk J. (2008) Reproducibility of nerve fiber layer thickness measurements using 3D Fourier-domain OCT. Invest Ophthalmol Vis Sci, 49: 5386-5391.

64. Sung KR, Kim DY, Park SB, Kook MS. (2009) Comparison of retinal nerve fiber layer thickness measured by Cirrhus HD and Stratus optical coherence tomography. Ophthalmology, 116: 1264-1270.

65. González-García AO, Vizzeri G, Bowd C, Medeiros FA, Zangwill LM, Weinreb RN. (2009) Reproducibility of RTVue retinal nerve fiber layer thickness and optic disc measurements and agreement with Stratus optical coherence tomography measurements. Am J Ophthalmol, 147: 1067-1074.

66. Sehi M, Grewal DS, Sheets CW, Greenfield DS. (2009) Diagnostic ability of Fourier-domain vs time domain optical coherence tomography for glaucoma detection. Am J Ophthalmol, 148: 597-605.

67. Han IC, Jaffe GJ. (2009) Comparison of spectral and time domain optical coherence tomography for retinal thickness measurement in healthy and diseased eyes. Am J Ophthalmol, 147: 847-858.

68. Costa-Cunha LV, Cunha LP, Malta RF, Monteiro ML. (2009) Comparison of Fourier-domain and time-domain optical coherence tomography in the detection of band atrophy of the optic nerve. Am J Ophthalmol, 147: 56-63.

69. Tan O, Chopra V, Lu AT, Schuman JS, Ishikawa H, Wollstein G, Varma R, Huang D. (2009) Detection of macular ganglion cell loss in glaucoma by Fourier-domain optical coherence tomography. Ophthalmology, 116: 2305-2314.

70. Leung CK, Cheung CY, Weinreb RN, Qiu Q, Liu S, Li H, Xu G, Fan N, Huang L, Pang CP, Lam DS. (2009) Retinal nerve fiber layer imaging with spectral-domain optical coherence tomography: a variability and diagnostic performance study. Ophthalmology, 116: 1257-1263.

71. Chang RT, Knight OJ, Feuer WJ, Budenz DL. (2009) Sensitivity and specificity of time-domain versus spectral-domain optical coherence tomography in diagnosing early to moderate glaucoma. Ophthalmology, 116: 2294-2299.

72. Jeoung J W, Park KH. (2010) Comparison of Cirrus and Stratus OCT on the ability to detect localized retinal nerve fiber layer defects in preperimetric glaucoma. Invest Ophthalmol Vis Sci, 51: 938-945.

73. Huang JY, Pekmezci M, Mesiwala N, Kao A, Lin S. (2011) Diagnostic power of optic disc morphology, peripapillary retinal nerve fiber layer thickness, and macular inner retinal layer thickness in glaucoma diagnosis with Fourier-domain optical coherence tomography. J Glaucoma, 20: 87-94.

74. Schulze A, Lamparter J, Pfeiffer N, Berisha F, Schmidtmann I, Hoffmann EM. (2011) Diagnostic ability of retinal ganglion cell complex, retinal nerve fiber layer, and optic nerve head measurements by Fourier-domain optical coherence tomography. Graefes Arch Clin Exp Ophthalmol, early online publication, DOI:10.1007/s00417-010-1585-5.

75. Wang G, Qiu KL, Lu XH, Sun LX, Liao XJ, Chen HL, Zhang MZ. (2011) The effect of myopia on retinal nerve fibre layer measurement: a comparative study of spectral-domain optical coherence tomography and scanning laser polarimetry. Br J Ophthalmol, 95: 255-260.

76. Townsend KA, Wollstein G, Schuman JS. (2009) Imaging of the retinal nerve fibre layer for glaucoma. Br J Ophthalmol, 93: 139-143.

77. Zhou Q. (2006) Retinal scanning laser polarimetry and methods to compensate for corneal birefringence. Bull Soc belge Ophtalmol, 302: 89-106.

78. Greenfield DS, Knighton RW, Huang XR. (2000) Effect of corneal polarization axis on assessment of retinal nerve fiber layer thickness by scanning laser polarimetry. Am J Ophthalmol, 129: 715-722.

79. Weinreb RN, Bowd C, Greenfield DS, Zangwill LM. (2002) Measurement of the magnitude and axis of corneal polarization with scanning laser polarimetry. Arch Ophthalmol, 120: 901-906.

80. Colen TP, Tang NE, Mulder PG, Lemij HG. (2004) Sensitivity and specificity of new GDx parameters. J Glaucoma, 13: 28-33.

81. Munkwitz S, Funk J, Loeffler KU, Harbarth U, Kremmer S. (2004) Sensitivity and specificity of scanning laser polarimetry using the GDx. Br J Ophthalmol, 88: 1142-1145.

82. Greenfield DS, Knighton RW, Feuer WJ, Schiffman JC, Zangwill L, Weinreb RN. (2002) Correction for corneal polarization axis improves the discriminating power of scanning laser polarimetry. Am J Ophthalmol, 134: 27-33.

83. Gürses-Özden R, Liebmann JM, Schuffner D, Buxton DF, Soloway BD, Ritch R. (2001) Retinal nerve fiber layer thickness remains unchanged following laser-assisted in situ keratomileusis. Am J Ophthalmol, 132: 512-516.

84. Angeles R, Abunto T, Bowd C, Zangwill LM, Schanzlin DJ, Weinreb RN. (2004) Corneal changes after laser in situ keratomileusis: measurement of corneal polarization magnitude and axis. Am J Ophthalmol, 137: 697-703.

85. Holló G, Katsanos A, Kóthy P, Kerek A, Süveges I. (2003) Influence of LASIK on scanning laser polarimetric measurement of the retinal nerve fibre layer with fixed angle and customised corneal polarisation compensation. Br J Ophthalmol, 87: 1241-1246.

86. Bowd C, Medeiros FA, Weinreb RN, Zangwill LM. (2007) The effect of atypical birefringence patterns on glaucoma detection using scanning laser polarimetry with variable corneal compensation. Invest Ophthalmol Vis Sci, 48: 223-227.

87. Garway-Heath DF, Greaney MJ, Caprioli J. (2002) Correction for the erroneous compensation of anterior segment birefringence with the scanning laser polarimeter for glaucoma diagnosis. Invest Ophthalmol Vis Sci, 43: 1465-1474.

88. Zhou Q, Weinreb RN. (2002) Individualized compensation of anterior segment birefringence during scanning laser polarimetry. Invest Ophthalmol Vis Sci, 43: 2221-2228.

89. Choplin NT, Zhou Q, Knighton RW. (2003) Effect of individualized compensation for anterior segment birefringence on retinal nerve fiber layer assessments as determined by scanning laser polarimetry. Ophthalmology, 110: 719-725.

90. Greenfield DS, Knighton RW. (2001) Stability of corneal polarization axis measurements for scanning laser polarimetry. Ophthalmology, 108: 1065-1069.

91. Bowd C, Zangwill LM, Medeiros FA, Tavares IM, Hoffmann EM, Bourne RR, Sample PA, Weinreb RN. (2006) Structure-function relationships using confocal scanning laser ophthalmoscopy, optical coherence tomography, and scanning laser polarimetry. Invest Ophthalmol Vis Sci, 47: 2889-2895.

92. Bagga H, Greenfield DS, Feuer W, Knighton RW. (2003) Scanning laser polarimetry with variable corneal compensation and optical coherence tomography in normal and glaucomatous eyes. Am J Ophthalmol, 135: 521-529.

93. Tannenbaum DP, Hoffman D, Lemij HG, Garway-Heath DF, Greenfield DS, Caprioli J. (2004) Variable corneal compensation improves discrimination between normal and glaucomatous eyes with the scanning laser polarimeter. Ophthalmology, 111: 259-264.

94. Badala F, Nouri-Mahdavi K, Raoof DA, Leeprechanon N, Law SK, Caprioli J. (2007) Optic disk and nerve fiber layer imaging to detect glaucoma. Am J Ophthalmol, 144: 724-732.

95. Reus NJ, de Graaf M, Lemij HG. (2007) Accuracy of GDx VCC, HRT I, and clinical assessment of stereoscopic optic nerve head photographs for diagnosing glaucoma. Br J Ophthalmol, 91: 313-318.

96. Medeiros FA, Vizzeri G, Zangwill LM, Alencar LM, Sample PA, Weinreb RN. (2008) Comparison of retinal nerve fiber layer and optic disc imaging for diagnosing glaucoma in patients suspected of having the disease. Ophthalmology, 115: 1340-1346.

97. Bagga H, Greenfield DS, Feuer WJ. (2005) Quantitative assessment of atypical birefringence images using scanning laser polarimetry with variable corneal compensation. Am J Ophthalmol, 139: 437-446.

98. Yanagisawa M, Tomidokoro A, Saito H, Mayama C, Aihara M, Tomita G, Shoji N, Araie M. (2009) Atypical retardation pattern in measurements of scanning laser polarimetry and its relating factors. Eye, 23: 1796-1780.

99. Sehi M, Ume S, Greenfield DS. (2007) Scanning laser polarimetry with enhanced corneal compensation and optical coherence tomography in normal and glaucomatous eyes. Invest Ophthalmol Vis Sci, 48: 2099-2104.

100. Morishita S, Tanabe T, Yu S, Hangai M, Ojima T, Aikawa H, Yoshimura N. (2008) Retinal nerve fibre layer assessment in myopic glaucomatous eyes: comparison of GDx variable corneal compensation with GDx enhanced corneal compensation. Br J Ophthalmol, 92: 1377-1381.

101. Schrems WA, Laemmer R, Hoesl LM, Horn FK, Mardin CY, Kruse FE, Tornow RP. (2011) Influence of atypical retardation pattern on the peripapillary retinal nerve fibre distribution assessed by scanning laser polarimetry and optical coherence tomography. Br J Ophthalmol, early online publication, DOI:10.1136/bjo. 2010.190074.

102. Monteiro ML, Moura FC, Medeiros FA. (2008) Scanning laser polarimetry with enhanced corneal compensation for detection of axonal loss in band atrophy of the optic nerve. Am J Ophthalmol, 145: 747-754.

103. Windisch BK, Harasymowycz PJ, See JL, Chauhan BC, Belliveau AC, Hutchison DM, Nicolela MT. (2009) Comparison between confocal scanning laser tomography, scanning laser polarimetry and optical coherence tomography on the ability to detect localised retinal nerve fibre layer defects in glaucoma patients. Br J Ophthalmol, 93: 225-230.

104. Bagci AM, Shahidi M, Ansari R, Blair M, Blair NP, Zelkha R. (2008) Thickness profiles of retinal layers by optical coherence tomography image segmentation. Am J Ophthalmol, 146: 679-687.

105. Sinai MJ, Garway-Heath DF, Greenfield D, Fingeret M, Varma R, Liebmann J, Schuman JS, Huang D, Optovue Normative Database Study Group. (2008) The effects of age, optic disc size, and signal strength on Fourier-domain optical coherence tomography measurements of the nerve fiber layer, optic disc, and ganglion cell complex. Invest Ophthalmol Vis Sci, 49: E-abstract 4636.

106. Sinai MJ, Garway-Heath DF, Fingeret M, Varma R, Liebmann JM, Greenfield DS, Girkin CA, Schuman JS. (2009) The role of ethnicity on the retinal nerve fiber layer and optic disc area measured with Fourier domain optical coherence tomography. Invest Ophthalmol Vis Sci, 50: E-abstract 4785.

107. Garas A, Vargha P, Holló G. (2011) Automatic, operator-adjusted, and manual disc-definition for optic nerve head and retinal nerve fiber layer measurements with the RTVue-100 optical coherence tomograph. J Glaucoma, 20: 80-86.

108. Laser Diagnostic Technologies I.n.c. (2004) RNFL analysis with GDx VCC: a primer and clinical guide. Laser Diagnostic Technologies, Inc., San Diego. www.meditec.zeiss.com (accessed 20 September 2008).

109. Mills RP, Budenz DL, Lee PP, Noecker RJ, Walt JG, Siegartel LR, Evans SJ, Doyle JJ. (2006) Categorizing the stage of glaucoma from pre-diagnosis to end-stage disease. Am J Ophthalmol, 141: 24-30.

110. Tóth M, Kóthy P, Vargha P, Holló G. (2007) Accuracy of combined GDx-VCC and Matrix FDT in a glaucoma screening trial. J Glaucoma, 16: 462-470.

111. Tóth M, Kóthy P, Holló G. (2008) Accuracy of scanning laser polarimetry, scanning laser tomography and their combination in a glaucoma screening trial. J Glaucoma, 17: 639-646.

112. American Academy of Ophthalmology Retina Panel. (2009) Age-related macular degeneration, Preferred practice pattern guidelines. American Academy of Ophthalmology, San Francisco. www.aao.org/ppp (accessed 22 January 2011).

113. Polman CH, Reingold SC, Edan G, Filippi M, Hartung HP, Kappos L, Lublin FD, Metz LM, McFarland HF, O'Connor PW, Sandberg-Wollheim M, Thompson AJ, Weinshenker BG, Wolinsky JS. (2005) Diagnostic criteria for multiple sclerosis: 2005 revisions to the "McDonald Criteria". Ann Neurol, 58: 840-846.

114. Tzamalis A, Kynigopoulos M, Schlote T, Haefliger I. (2009) Improved reproducibility of retinal nerve fiber layer thickness measurements with the repeat-scan protocol using the Stratus OCT in normal and glaucomatous eyes. Graefes Arch Clin Exp Ophthalmol, 247: 245-252

115. Gurses-Ozden R, Ishikawa H, Hoh ST, Liebmann JM, Mistlberger A, Greenfield DS, Dou HL, Ritch R. (1999) Increasing sampling density improves reproducibility of optical coherence tomography measurements. J Glaucoma, 8: 238-241.

116. Mok KH, Lee VW, So KF. (2004) Increasing scans per examination improves the reproducibility on retinal nerve fiber layer measurements by optical coherence tomography. Optom Vis Sci, 81: 268-271.

117. Bagga H, Greenfield DS, Knighton RW. (2005) Macular symmetry testing for glaucoma detection. J Glaucoma, 14: 358-363.

118. Tan O, Li G, Lu AT, Varma R, Huang D, Advanced Imaging for Glaucoma Study Group. (2008) Mapping of macular substructures with optical coherence tomography for glaucoma diagnosis. Ophthalmology, 115: 949-956.

119. Nakamura H, Hangai M, Mori S, Hirose F, Yoshimura N. (2011) Hemispherical focal macular photopic negative response and macular inner retinal thickness in open-angle glaucoma. Am J Ophthalmol, 151: 494-506.

120. Leung CK, Cheung CY, Weinreb RN, Lee G, Lin D, Pang CP, Lam DS. (2008) Comparison of macular thickness measurements between time domain and spectral domain optical coherence tomography. Invest Ophthalmol Vis Sci, 49: 4893-4897.

121. Vizzeri G, Weinreb RN, Gonzalez-Garcia AO, Bowd C, Medeiros FA, Sample PA, Zangwill LM. (2009) Agreement between spectral-domain and time-domain OCT for measuring RNFL thickness. Br J Ophthalmol, 93: 775-781.

122. Wolf-Schnurrbusch UE, Ceklic L, Brinkmann CK, Iliev ME, Frey M, Rothenbuehler SP, Enzmann V, Wolf S. (2009) Macular thickness measurements in healthy eyes using six different optical coherence tomography instruments. Invest Ophthalmol Vis Sci, 50: 3432-3437.

123. Lim JI, Tan O, Fawzi AA, Hopkins JJ, Gil-Flamer JH, Huang D. (2008) A pilot study of Fourier-domain optical coherence tomography of retinal dystrophy patients. Am J Ophthalmol, 146: 417-426.

124. Leung CK, Cheung CY, Lin D, Pang CP, Lam DS, Weinreb RN. (2008) Longitudinal variability of optic disc and retinal nerve fiber layer measurements. Invest Ophthalmol Vis Sci, 49: 4886-4892.

125. Mai TA, Reus NJ, Lemij HG. (2008) Retinal nerve fiber layer measurement repeatability in scanning laser polarimetry with enhanced corneal compensation. J Glaucoma, 17: 269-274.

126. Choi J, Kim KH, Lee CH, Cho H, Sung KR, Choi JY, Cho BJ, Kook MS. (2008) Relationship between retinal nerve fibre layer measurements and retinal sensitivity by scanning laser polarimetry with variable and enhanced corneal compensation. Br J Ophthalmol, 92: 906-911.

127. Monteiro ML, Moura FC. (2008) Comparison of the GDx VCC scanning laser polarimeter and the stratus optical coherence tomograph in the detection of band atrophy of the optic nerve. Eye, 22: 641-648.

128. DeLeón Ortega JE, Sakata LM, Kakati B, McGwin G Jr, Monheit BE, Arthur SN, Girkin CA. (2007) Effect of glaucomatous damage on repeatability of confocal scanning laser ophthalmoscope, scanning laser polarimetry, and optical coherence tomography. Invest Ophthalmol Vis Sci, 48: 1156-1163.

129. Garas A, Vargha P, Holló G. (2010) Reproducibility of retinal nerve fiber layer and macular thickness measurement with the RTVue-100 optical coherence tomograph. Ophthalmology, 117: 738-746.

130. Reus NJ, Lemij HG, Garway-Heath DF, Airaksinen PJ, Anton A, Bron AM, Faschinger C, Holló G, Iester M, Jonas JB, Mistlberger A, Topouzis F, Zeyen TG. (2010) Clinical assessment of stereoscopic optic disc photographs for glaucoma: the European optic disc assessment trial. Ophthalmology, 117: 717-723.

131. Moreno-Montañés J, Olmo N, Alvarez A, García N, Zarranz-Ventura J. (2010) Cirrus high-definition optical coherence tomography compared with Stratus optical coherence tomography in glaucoma diagnosis. Invest Ophthalmol Vis Sci, 51: 335-343.

132. Park SB, Sung KR, Kang SY, Kim KR, Kook MS. (2009) Comparison of glaucoma diagnostic capabilities of Cirrus HD and Stratus optical coherence tomography. Arch Ophthalmol, 127: 1603-1609.

133. Mori S, Hangai M, Sakamoto A, Yoshimura N. (2010) Spectral-domain optical coherence tomography measurement of macular volume for diagnosing glaucoma. J Glaucoma, 19: 528-534.

134. Seong M, Sung KR, Choi EH, Kang SY, Cho JW, Um TW, Kim YJ, Park SB, Hong HE, Kook MS. (2010) Macular and peripapillary retinal nerve fibre layer measurements by spectral domain optical coherence tomography in normal-tension glaucoma. Invest Ophthalmol Vis Sci, 51: 1446-1452.

135. Li S, Wang X, Wu G, Wang N. (2010) Evaluation of optic nerve head and retinal nerve fibre layer in early and advance glaucoma using frequency-domain optical coherence tomography. Graefes Arch Clin Exp Ophthalmol, 248: 429-434.

136. Leite MT, Zangwill LM, Weinreb RN, Rao HL, Alencar LM, Sample PA, Medeiros FA. (2010) Effect of disease severity on the performance of Cirrus spectral-domain OCT for glaucoma diagnosis. Invest Ophthalmol Vis Sci, 51: 4104-4109.

137. Budenz DL, Anderson DR, Varma R, Schuman J, Cantor L, Savell J, Greenfield DS, Patella VM, Quigley HA, Tielsch J. (2007) Determinants of normal retinal nerve fibre layer thickness measured by Stratus OCT. Ophthalmology, 114: 1046-1052.

138. Sung KR, Wollstein G, Bilonick RA, Townsend KA, Ishikawa H, Kagemann L, Noecker RJ, Fujimoto JG, Schuman JS. (2009) Effects of age on optical coherence tomography measurements of healthy retinal nerve fibre layer, macula, and optic nerve head. Ophthalmology, 116: 1119-1124.

139. Hong S, Ahn H, Ha SJ, Yeom HY, Seong GJ, Hong YJ. (2007) Early glaucoma detection using the Humphrey Matrix Perimeter, GDx VCC, Stratus OCT, and retinal nerve fibre layer photography. Ophthalmology, 114: 210-215.

140. Rao HL, Zangwill LM, Weinreb RN, Sample PA, Alencar LM, Medeiros FA. (2010) Comparison of different spectral domain optical coherence tomography scanning areas for glaucoma diagnosis. Ophthalmology, 117: 1692-1699.

141. Kim JS, Ishikawa H, Sung KR, Xu J, Wollstein G, Bilonick RA, Gabriele ML, Kagemann L, Duker JS, Fujimoto JG, Schuman JS. (2009) Retinal nerve fibre layer thickness measurement reproducibility improved with spectral domain optical coherence tomography. Br J Ophthalmol, 93: 1057-1063.

142. Pauleikhoff D. (2005) Neovascular age-related macular degeneration: natural history and treatment outcomes. Retina, 25: 1065-1084.

143. Attebo K, Mitchell P, Smith W. (1996) Visual acuity and the causes of visual loss in Australia. The Blue Mountains Eye Study. Ophthalmology, 103: 357-364.

144. Klaver CC, Wolfs RC, Vingerling JR, Hofman A, de Jong PT. (1998) Age-specific prevalence and causes of blindness and visual impairment in an older population: the Rotterdam Study. Arch Ophthalmol, 116: 653-658.

145. Klein R, Wang Q, Klein BE, Moss SE, Meuer SM. (1995) The relationship of age-related maculopathy, cataract, and glaucoma to visual acuity. Invest Ophthalmol Vis Sci, 36: 182-191.

146. Kawasaki R, Yasuda M, Song SJ, Chen SJ, Jonas JB, Wang JJ, Mitchell P, Wong TY. (2010) The prevalence of age-related macular degeneration in Asians: a systematic review and meta-analysis. Ophthalmology, 117: 921-927.

147. Cho JW, Sung KR, Lee S, Yun SC, Kang SY, Choi J, Na JH, Lee Y, Kook MS. (2010) Relationship between visual field sensitivity and macular ganglion cell complex thickness as measured by spectral domain optical coherence tomography (RTVue-100 SD OCT). Invest Ophthalmol Vis Sci, 51: 6401-6407.

148. Kim NR, Lee ES, Seong GJ, Kim JH, An HG, Kim CY. (2010) Structure-function relationship and diagnostic value of macular ganglion cell complex measurement using Fourier-domain OCT in glaucoma. Invest Ophthalmol Vis Sci, 51: 4646-4651.

149. Bertuzzi F, Suzani M, Tagliabue E, Cavaletti G, Angeli R, Balgera R, Rulli E, Ferrarese C, Miglior S. (2010) Diagnostic validity of optic disc and retinal nerve fiber layer evaluations in detecting structural changes after optic neuritis. Ophthalmology, 117: 1256-1264.

150. Garas A, Vargha P, Holló G. (2011) Diagnostic accuracy of nerve fibre layer, macular thickness and optic disc measurements made with the RTVue-100 optical coherence tomograph to detect glaucoma. Eye, 25: 57-65.

151. Danesh-Meyer HV, Carroll SC, Ku JY, Hsiang J, Gaskin B, Gamble GG, Savino PJ. (2006) Correlation of retinal nerve fiber layer measured by scanning laser polarimeter to visual field in ischemic optic neuropathy. Arch Ophthalmol, 124: 1720-1726.

152. DeLeón-Ortega J, Carroll KE, Arthur SN, Girkin CA. (2007) Correlations between retinal nerve fiber layer and visual field in eyes with nonarteritic anterior ischemic optic neuropathy. Am J Ophthalmol, 143: 288-294.

153. Garcia-Martin E, Pueyo V, Martin J, Almarcegui C, Ara JR, Dolz I, Honrubia FM, Fernandez FJ. (2010) Progressive changes in the retinal nerve fiber layer in patients with multiple sclerosis. Eur J Ophthalmol, 20: 167-173.

154. Trip SA, Schlottmann PG, Jones SJ, Altmann DR, Garway-Heath DF, Thompson AJ, Plant GT, Miller DH. (2005) Retinal nerve fiber layer axonal loss and visual dysfunction in optic neuritis. Ann Neurol, 58: 383-391.

155. Gugleta K, Mehling M, Kochkorov A, Grieshaber M, Katamay R, Flammer J, Orgül S, Kappos L. (2008) Pattern of macular thickness changes measured by ocular coherence tomography in patients with multiple sclerosis. Klin Monbl Augenheilkd, 225: 408-412.

156. Pulicken M, Gordon-Lipkin E, Balcer LJ, Frohman E, Cutter G, Calabresi PA. (2007) Optical coherence tomography and disease subtype in multiple sclerosis. Neurology, 69: 2085-2092.

157. Cheng H, Laron M, Schiffman JS, Tang RA, Frishman LJ. (2007) The relationship between visual field and retinal nerve fiber layer measurements in patients with multiple sclerosis. Invest Ophthalmol Vis Sci, 48: 5798-5805.

158. Siger M, Dziegielewski K, Jasek L, Bieniek M, Nicpan A, Nawrocki J, Selmaj K. (2008) Optical coherence tomography in multiple sclerosis: thickness of the retinal nerve fiber layer as a potential measure of axonal loss and brain atrophy. J Neurol, 255: 1555-1560.

159. Ratchford JN, Quigg ME, Conger A, Frohman T, Frohman E, Balcer LJ, Calabresi PA, Kerr DA. (2009) Optical coherence tomography helps differentiate neuromyelitis optica and MS optic neuropathies. Neurology, 73: 302-308.

160. Zaveri MS, Conger A, Salter A, Frohman TC, Galetta SL, Markowitz CE, Jacobs DA, Cutter GR, Ying GS, Maguire MG, Calabresi PA, Balcer LJ, Frohman EM. (2008) Retinal imaging by laser polarimetry and optical coherence tomography evidence of axonal degeneration in multiple sclerosis. Arch Neurol, 65: 924-928.

161. Cettomai D, Pulicken M, Gordon-Lipkin E, Salter A, Frohman TC, Conger A, Zhang X, Cutter G, Balcer LJ, Frohman EM, Calabresi PA. (2008) Reproducibility of optical coherence tomography in multiple sclerosis. Arch Neurol, 65: 1218-1222.

162. Savini G, Bellusci C, Carbonelli M, Zanini M, Carelli V, Sadun AA, Barboni P. (2006) Detection and quantification of retinal nerve fiber layer thickness in optic disc edema using Stratus OCT. Arch Ophthalmol, 124: 1111-1117.

163. Kallenbach K, Simonsen H, Sander B, Wanscher B, Larsson H, Larsen M, Frederiksen JL. (2010) Retinal nerve fiber layer thickness is associated with lesion length in acute optic neuritis. Neurology, 74: 252-258.

164. Merle H, Olindo S, Donnio A, Richer R, Smadja D, Cabre P. (2008) Retinal peripapillary nerve fiber layer thickness in neuromyelitis optica. Invest Ophthalmol Vis Sci, 49: 4412-4417.

165. de Seze J, Blanc F, Jeanjean L, Zéphir H, Labauge P, Bouyon M, Ballonzoli L, Castelnovo G, Fleury M, Defoort S, Vermersch P,Speeg C. (2008) Optical coherence tomography in neuromyelitis optica. Arch Neurol, 65: 920-923.

166. Merle H, Olindo S, Donnio A, Beral L, Richer R, Smadja D, Cabre P. (2010) Retinal nerve fiber layer thickness and spatial and temporal contrast sensitivity in multiple sclerosis. Eur J Ophthalmol, 20: 158-166.

167. Gundogan FC, Demirkaya S, Sobaci G. (2007) Is optical coherence tomography really a new biomarker candidate in multiple sclerosis? - A structural and functional evaluation. Invest Ophthalmol Vis Sci, 48: 5773-5781.

168. Henderson AP, Trip SA, Schlottmann PG, Altmann DR, Garway-Heath DF, Plant GT, Miller DH. (2008) An investigation of the retinal nerve fibre layer in progressive multiple sclerosis using optical coherence tomography. Brain, 131: 277-287.

169. Garas A, Tóth M, Vargha P, Holló G. (2010) Comparison of repeatability of retinal nerve fiber layer thickness measurement made using the RTVue Fourier-domain optical coherence tomograph and the GDx scanning laser polarimeter with variable or enhanced corneal compensation. J Glaucoma, 19: 412-417.

12 LIST OF PUBLICATIONS

12.1 Peer-reviewed publications

1. **Garas A**, Vargha P, Holló G. (2010) Reproducibility of retinal nerve fiber layer and macular thickness measurement with the RTVue-100 optical coherence tomograph. **Ophthalmology,** 117: 738-746. **IF: 5.491**

2. **Garas A**, Vargha P, Holló G. (2011) Diagnostic accuracy of nerve fibre layer, macular thickness and optic disc measurements made with the RTVue-100 optical coherence tomograph to detect glaucoma. **Eye,** 25: 57-65. **IF: 1.974**

3. **Garas A**, Vargha P, Holló G. (2011) Automatic, operator-adjusted, and manual disc-definition for optic nerve head and retinal nerve fiber layer measurements with the RTVue-100 optical coherence tomograph. **J Glaucoma,** 20: 80-86. **IF: 1.744**

4. **Garas A**, Tóth M, Vargha P, Holló G. (2010) Comparison of repeatability of retinal nerve fiber layer thickness measurement made using the RTVue Fourier-domain optical coherence tomograph and the GDx scanning laser polarimeter with variable or enhanced corneal compensation. **J Glaucoma,** 19: 412-417. **IF: 1.744**

5. **Garas A**, Tóth M, Vargha P, Holló G. (2010) Influence of pupil dilation on repeatability of scanning laser polarimetry with variable and enhanced corneal compensation in different stages of glaucoma. **J Glaucoma,** 19: 142-148. **IF: 1.744**

6. Holló G, Kóthy P, **Garas A,** Géczy Anna, Vargha P. (2011) Non-population-based glaucoma screening exercise in an osteoporosis patient organization: can elderly persons with advanced health awareness identify their risk for glaucoma? **J Glaucoma,** early online publication, DOI: 10.1097/IJG.0b013e3182208a48. **IF: 1.744**

7. **Garas A**, Simó M, Holló G. (2011) Nerve fiber layer and macular thinning measured with different imaging methods during the course of acute optic neuritis. **Eur J Ophthalmol,** 21: 473-483. **IF: 0.887**

8. **Garas A**, Vargha P, Holló G. (2011) Comparison of diagnostic accuracy of the RTVue Fourier-domain OCT and the GDx-VCC/ECC polarimeter to detect glaucoma. **Eur J Ophthalmol,** accepted for publication. **IF: 0.887**

9. **Garas A,** Kóthy P, Holló G. (2011) Accuracy of the RTVue-100 Fourier-domain optical coherence tomograph in an optic neuropathy screening trial. **Int Ophthalmol,** 31: 175-182.

10. **Garas A**, Holló G. (2009) Fourier-domain optical coherence tomography for glaucoma diagnostics: reproducibility of measurements with the RTVue-100 OCT. **Ophthalmologia Hungarica,** 146: 97-103.

12.2 Book chapter

1. Holló G, Tóth M, **Garas A**. A retinalis idegrostréteg vizsgálata. In: Németh J (szerk.), Szemészeti diagnosztikus képalkotó eljárások. Semmelweis Kiadó, Budapest, **2011:**137-145.

13 ACKNOWLEDGEMENTS

I am owing to render thanks first of all for my tutor Prof. Dr. Gábor Holló for his continuous and irreplaceable support and for providing several idea and advice during my work.

I would like to thank Prof. Dr. Ildikó Süveges for giving me the chance to study in the Programme of Ophthalmology, and Prof. Dr. János Németh for ensuring me the possibility to carry out my studies at the Department of Ophthalmology and for his valuable support as well.

I am especially grateful to Mr. Péter Vargha for performing the statistical analysis for our studies and for his precious advices.

I would also wish to thank Dr. Márta Tóth and Dr. Péter Kóthy, members of the Glaucoma Group, and my co-authors for their valuable help.

I also acknowledge Mrs. Veronika Tóth, Mrs. Zsuzsanna Schönléber, Ms. Nóra Kállai and Ms. Orsolya Kutni, the technicians of the Glaucoma and Perimetry Service for their kind assistance, and Anna Wyszoczky and Katalin Farkas medical students for technically helping my work.

I thank Mr. Dániel Somfalvi and Mr. Róbert Deutsch for their skilled technical support.

Last but not least I am thankful to my family for the persistent support which I have continuously received.